PB94134335

(2)

DOT/FAA/CT-93/69.I
DOT-VNTSC-FAA-93-13.I

FAA Technical Center
Atlantic City Airport,
NJ 08405

Damage Tolerance Assessment Handbook

Volume I: Introduction
Fracture Mechanics
Fatigue Crack Propagation

Research and
Special Programs
Administration
John A. Volpe National
Transportation Systems Center
Cambridge, MA 02142-1093

Final Report
October 1993

This document is available to the public
through the National Technical Information
Service Springfield, Virginia 22161

U.S. Department of Transportation
Federal Aviation Administration

REPORT DOCUMENTATION PAGE

Form Approved
OMB No. 0704-0188

1. AGENCY USE ONLY (Leave blank)

2. REPORT DATE
October 1993

3. REPORT TYPE AND DATES COVERED
June 1990 - Dec. 1992

4. TITLE AND SUBTITLE
Damage Tolerance Assessment Handbook
Volume I: Introduction
Fracture Mechanics
Fatigue Crack Propagation

5. FUNDING NUMBERS
FA3H2/A3128

6. AUTHOR(S)

7. PERFORMING ORGANIZATION NAME(S) AND ADDRESS(ES)
U.S. Department of Transportation
Research and Special Programs Administration
Volpe National Transportation Systems Center
Kendall Square, Cambridge, MA 02142

8. PERFORMING ORGANIZATION REPORT NUMBER
DOT-VNTSC-FAA-93-13.I

9. SPONSORING/MONITORING AGENCY NAME(S) AND ADDRESS(ES)
Federal Aviation Administration
Technical Center
Atlantic City Airport
NJ 08405

10. SPONSORING/MONITORING AGENCY REPORT NUMBER
DOT/FAA/CT-93/69.I

11. SUPPLEMENTARY NOTES

12a. DISTRIBUTION/AVAILABILITY STATEMENT
This document is available to the public through the National Technical Information Service, Springfield, VA 22161

12b. DISTRIBUTION CODE

13. ABSTRACT (Maximum 200 words)

This "Damage Tolerance Assessment Handbook" consists of two volumes:

Volume I introduces the damage tolerance concept with a historical perspective followed by the fundamentals of fracture mechanics and fatigue crack propagation. Various fracture criteria and crack growth rules are studied.

Volume II treats exclusively the subject of damage tolerance evaluation of airframes.

14. SUBJECT TERMS
Damage Tolerance, Fracture Mechanics, Crack Initiation, Fracture Toughness, Stress Intensity Factor, Residual Strength, Crack Propagation, Fatigue, Inspection.

15. NUMBER OF PAGES
168

16. PRICE CODE

17. SECURITY CLASSIFICATION OF REPORT
Unclassified

18. SECURITY CLASSIFICATION OF THIS PAGE
Unclassified

19. SECURITY CLASSIFICATION OF ABSTRACT
Unclassified

20. LIMITATION OF ABSTRACT

PREFACE

The preparation of this Handbook has required the cooperation of numerous individuals from the U.S. Government, universities, and industry. It is the outcome of one of the research programs on the Structural Integrity of Aging Aircraft supported by the Federal Aviation Administration Technical Center and performed at the Volpe Center of the Department of Transportation.

The contributions from the Federal Aviation Administration, the FAA Technical Center, the Department of Defense, and the staff of the Volpe Center are greatly acknowledged.

Please forward all comments and suggestions to :

U.S. Department of Transportation
Office of Systems Engineering, DTS-74
Volpe National Transportation Systems Center
Cambridge, MA 02142

METRIC/ENGLISH CONVERSION FACTORS

ENGLISH TO METRIC

LENGTH (APPROXIMATE)

1 inch (in.) = 2.5 centimeters (cm)
1 foot (ft) = 30 centimeters (cm)
1 yard (yd) = 0.9 meter (m)
1 mile (mi) = 1.6 kilometers (km)

AREA (APPROXIMATE)

1 square inch (sq in, in^2) = 6.5 square centimeters (cm^2)
1 square foot (sq ft, ft^2) = 0.09 square meter (m^2)
1 square yard (sq yd, yd^2) = 0.8 square meter (m^2)
1 square mile (sq mi, mi^2) = 2.6 square kilometers (km^2)
1 acre = 0.4 hectares (he) = 4,000 square meters (m^2)

MASS - WEIGHT (APPROXIMATE)

1 ounce (oz) = 28 grams (gr)
1 pound (lb) = .45 kilogram (kg)
1 short ton = 2,000 pounds (lb) = 0.9 tonne (t)

VOLUME (APPROXIMATE)

1 teaspoon (tsp) = 5 milliliters (ml)
1 tablespoon (tbsp) = 15 milliliters (ml)
1 fluid ounce (fl oz) = 30 milliliters (ml)
1 cup (c) = 0.24 liter (l)
1 pint (pt) = 0.47 liter (l)
1 quart (qt) = 0.96 liter (l)
1 gallon (gal) = 3.8 liters (l)
1 cubic foot (cu ft, ft^3) = 0.03 cubic meter (m^3)
1 cubic yard (cu yd, yd^3) = 0.76 cubic meter (m^3)

TEMPERATURE (EXACT)

$[(x - 32)(5/9)]$ °F = y°C

METRIC TO ENGLISH

LENGTH (APPROXIMATE)

1 millimeter (mm) = 0.04 inch (in)
1 centimeter (cm) = 0.4 inch (in)
1 meter (m) = 3.3 feet (ft)
1 meter (m) = 1.1 yards (yd)
1 kilometer (km) = 0.6 mile (mi)

AREA (APPROXIMATE)

1 square centimeter (cm^2) = 0.16 square inch (sq in, in^2)
1 square meter (m^2) = 1.2 square yards (sq yd, yd^2)
1 square kilometer (kn^2) = 0.4 square mile (sq mi, mi^2)
1 hectare (he) = 10,000 square meters (m^2) = 2.5 acres

MASS - WEIGHT (APPROXIMATE)

1 gram (gr) = 0.036 ounce (oz)
1 kilogram (kg) = 2.2 pounds (lb)
1 tonne (t) = 1,000 kilograms (kg) = 1.1 short tons

VOLUME (APPROXIMATE)

1 milliliter (ml) = 0.03 fluid ounce (fl oz)
1 liter (l) = 2.1 pints (pt)
1 liter (l) = 1.06 quarts (qt)
1 liter (l) = 0.26 gallon (gal)
1 cubic meter (m^3) = 36 cubic feet (cu ft, ft^3)
1 cubic meter (m^3) = 1.3 cubic yards (cu yd, yd^3)

TEMPERATURE (EXACT)

$[(9/5)y + 32]$ °C = x °F

QUICK INCH-CENTIMETER LENGTH CONVERSION

INCHES	0			1			2			3			4			5			6			7			8		
CENTIMETERS	0	1	2	3	4	5	6	7	8	9	10	11	12	13	14	15	16	17	18	19	20	21	22	23	24	25

INCHES: 0, 1, 2, 3, 4, 5, 6, 7, 8, 9, 10

CENTIMETERS: 0 1 2 3 4 5 6 7 8 9 10 11 12 13 14 15 16 17 18 19 20 21 22 23 24 25

25.40

QUICK FAHRENHEIT-CELSIUS TEMPERATURE CONVERSION

°F	-40°	-22°	-4°	14°	32°	50°	68°	86°	104°	122°	140°	158°	176°	194°	212°
°C	-40°	-30°	-20°	-10°	0°	10°	20°	30°	40°	50°	60°	70°	80°	90°	100°

For more exact and or other conversion factors, see NBS Miscellaneous Publication 286, Units of Weights and Measures. Price $2.50. SD Catalog No. C13 10286.

TABLE OF CONTENTS

TABLE OF CONTENTS (continued)

TABLE OF CONTENTS (continued)

LIST OF ILLUSTRATIONS

LIST OF ILLUSTRATIONS (continued)

LIST OF ILLUSTRATIONS (continued)

LIST OF ILLUSTRATIONS (continued)

LIST OF ILLUSTRATIONS (continued)

LIST OF ILLUSTRATIONS (continued)

LIST OF TABLES

CHAPTER 1:

INTRODUCTION

1. INTRODUCTION

Present airworthiness standards, FAR 25.571 [1-1], and advisory guidance [1-2] require the evaluation of damage tolerance for transport category airframe designs. Broadly speaking, damage tolerance refers to the ability of the design to prevent structural cracks from precipitating catastrophic fracture when the airframe is subjected to flight or ground loads. Transport category airframe structure is generally made damage tolerant by means of redundant ("fail-safe") designs for which the inspection intervals are set to provide at least two inspection opportunities per number of flights or flight hours it would take for a visually detectable crack to grow large enough to cause a failure in flight.

As part of the certification process, an aircraft manufacturer performs tests and analyses to demonstrate compliance with FAR 25.571. These tests and analyses are generally based upon an implicit assumption of isolated cracking, i.e., the effect of a single crack is considered with respect to the issues of detectable or initial size, fracture-critical size, and rate of growth. The same general approach has been adopted for military airplanes [1-3].

Findings from a recent accident [1-4] and subsequent inspections of some older transport category airplanes have shown that multiple site damage (MSD) can occur in the transport category fleet. Fatigue (possibly exacerbated by corrosion) may act to form a large colony of similar cracks at adjacent details in older airframes. Such cracks, while still too small to be visually detectable, can suddenly link together to form a single crack large enough to cause a failure in flight. Moreover, the time between MSD formation can be shorter than a typical inspection interval designed to control isolated cracking. Tolerance to MSD is an implied requirement of FAR 25.571, but compliance enforcement is generally reserved to the continuing airworthiness program for older aircraft in those cases where a risk of MSD is suspected or has been established.

Inspection is an important subject in its own right. Especially when the potential for MSD exists, means of nondestructive crack detection better than visual inspection must be considered. A comprehensive review of advanced inspection methods is outside the scope of this handbook, but some discussion is required on the topic of inspection performance. In the present context, "performance" means the ability of a method or procedure to detect a crack, as a function of the size of that crack when the structure is inspected.

1.1 HISTORICAL PERSPECTIVE

Experience with structural failures has precipitated significant change in aircraft structural design procedures. Attention is now focused on propagation of cracks and the ability to arrest a fracture in the place of previous emphasis on initiation of cracks. The basis for this new approach was known by the1960s, but technology development has been driven by dramatic events. These events can be appreciated in terms of case histories, presented below, that describe the context for the activity stimulated by these events. Most of these examples have been extracted from the text of a seminar entitled: "Damage Tolerance Technology - A Course in Stress Analysis Oriented Fracture Mechanics" by Mr. Thomas Swift, FAA National Resource Specialist, Fracture Mechanics and Metallurgy.

Liberty Ship Failures

Brittle fractures were observed in about twenty-five percent of the welded Liberty ships constructed in the United States. Of the 4694 ships constructed, 1289 experienced brittle fracture of the hull and 233 of these were catastrophic, resulting in either loss of the ship or the structure being declared unsafe. Figure 1-1 shows one such fracture which occurred in the T-2 tanker Schenectady, which failed at dockside without warning in mild weather. The ship broke in half in a matter of seconds. Investigation revealed that the maximum bending moments at the time of failure were one-half the bending moments allowed for in the design. During this time, the Navy Research Laboratories (NRL) became interested in fracture mechanics and much of the early work on this subject in the United States was conducted at NRL.

Comet

On January 10, 1954, a Comet I aircraft (DH 106-1) serial number G-ALYP known as Yoke Peter disintegrated in the air at approximately 30,000 feet and crashed into the Mediterranean Sea off Elba. The aircraft was on a flight from Rome to London. At the time of the crash the aircraft had flown 3680 hours and experienced 1286 pressurized flights (Figures 1-2 and 1-3).

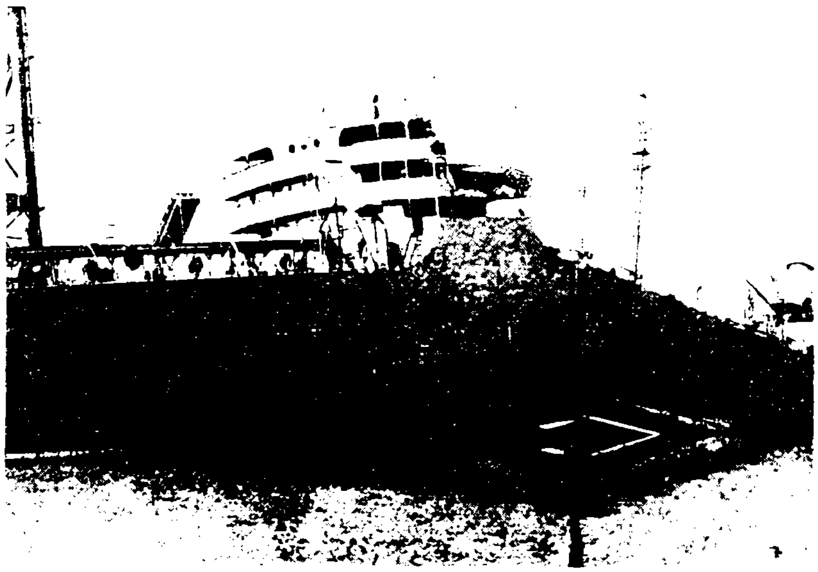

Figure 1-1. Photograph of tanker Schenectady.

[Reprinted with permission of the National Academy of Sciences from Brittle Behavior of Engineering Structures, National Research Council, Wiley, New York 1957.]

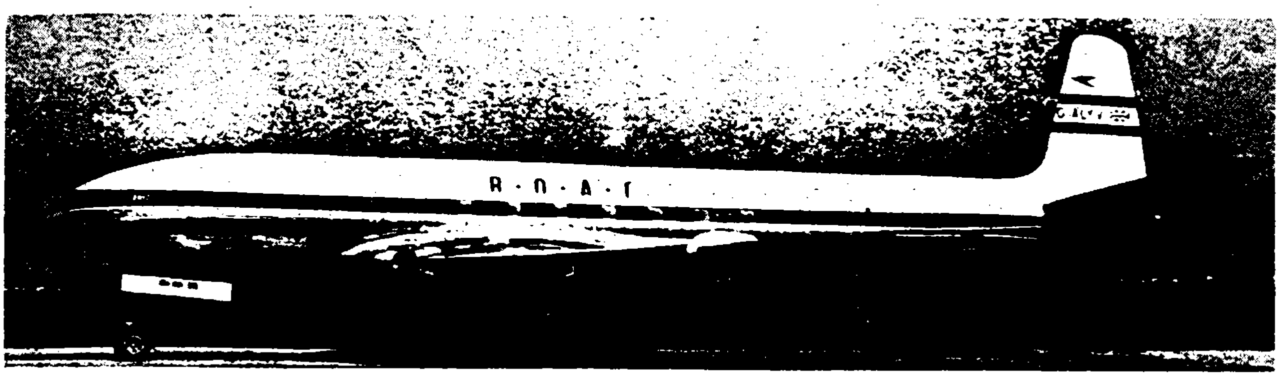

Figure 1-2. Comet I aircraft, circa 1952.

[Reprinted from Jane's All the World's Aircraft, 1953-54, p. 63, by permission of Jane's Information Group.]

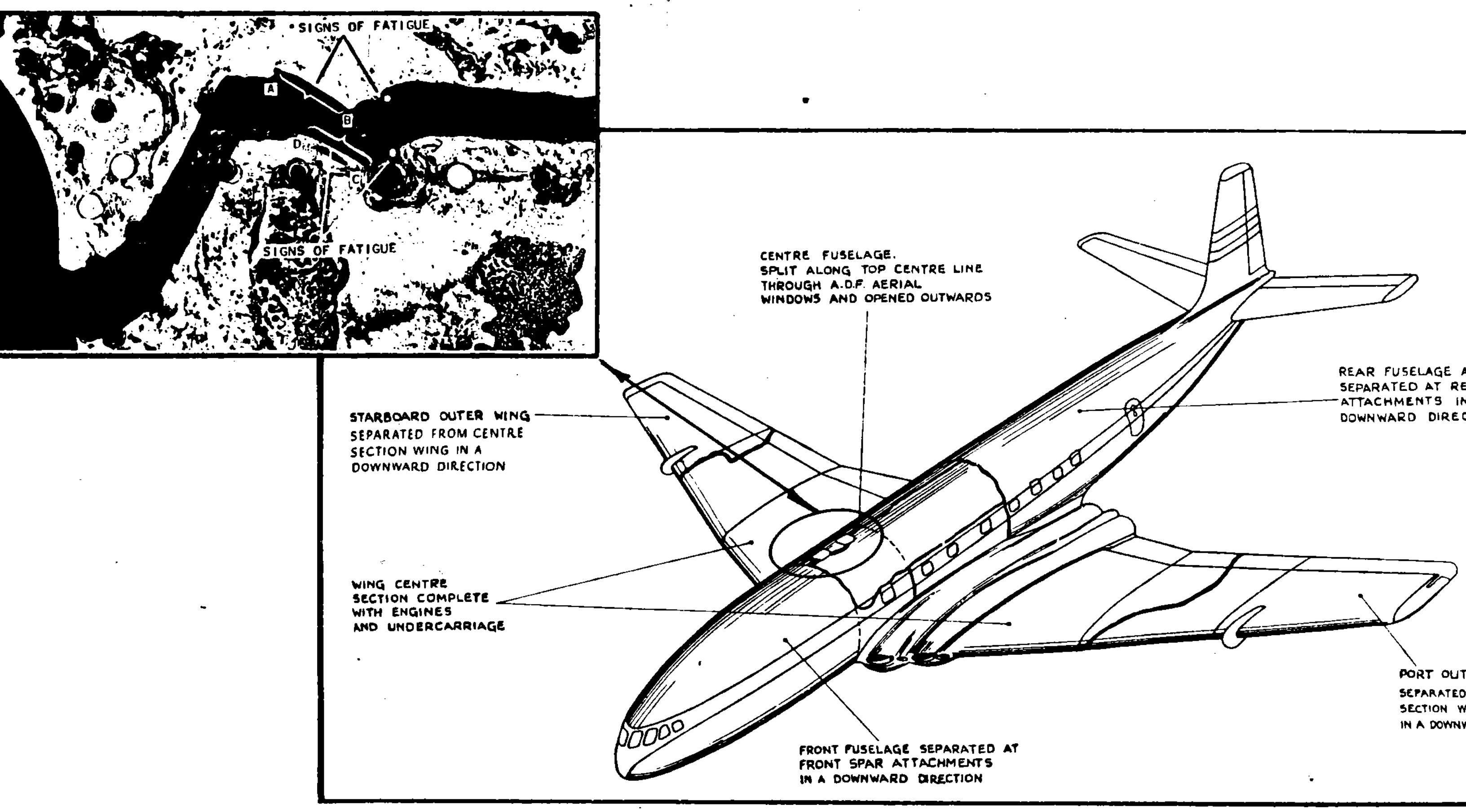

Figure 1-3. Probable Comet failure initiation site.

[From T. Swift, FAA]

The design of the Comet aircraft commenced in September 1946. The first prototype flew on July 27, 1949. Yoke Peter first flew on January 9, 1951, and was granted a Certificate of Registration on September 18, 1951. A certificate of airworthiness was granted on March 22, 1952. The aircraft was delivered to B.O.A.C. on March 13, 1952, and entered into scheduled passenger service on May 2, 1952, after having accumulated 339 hours. Yoke Peter was the first jet-propelled passenger-carrying aircraft in the world to enter scheduled service. The Comets were removed from service on January 11, 1954. A number of modifications were made to the fleet to rectify some of the items which were thought to have caused the accident. Service was resumed on March 23, 1954.

On April 8, 1954, only sixteen days after the resumption of service, another Comet aircraft G-ALYY known as Yoke Yoke disintegrated in the air at 35,000 feet and crashed into the ocean near Naples. The aircraft was on a flight from Rome to Cairo. At the time of the crash the aircraft had flown 2703 hours and experienced 903 pressurized flights.

Prior to these two accidents, on May 2, 1953, another Comet, G-ALYV had crashed in a tropical storm of exceptional severity near Calcutta. An inquiry, directed by the Central Government of India, determined that this accident was caused by structural failure which resulted from either:

a) Severe gusts encountered during a thunderstorm.
b) Overcontrolling or loss of control by the pilot when flying through a thunderstorm.

After the Naples crash on April 8, 1954, B.O.A.C. immediately suspended all services. On April 12, 1954, the Chairman of the Airworthiness Review Board withdrew the certificate of airworthiness.

The UK Minister of Supply instructed Sir Arnold Hall, Director of the Royal Aeronautical Establishment, to complete an investigation into the cause of the accidents. On April 18, 1954, Sir Arnold decided that a repeated loading test of the pressure cabin was needed. It was decided to conduct the test in a tank under water. In June 1954, the test started on aircraft G-ALYU, known as Yoke Uncle. The aircraft had accumulated 1230 pressurized flights prior to the test. After 1830 further pressurizations, for a total of 3060, the pressure cabin failed. The starting point of the failure was at the corner of a passenger window. The cabin cyclic pressure was 8.25 psi but a proof cycle of 1.33P was applied at approximately 1,000 pressure cycle intervals. It was during the application of one of these cycles that the cabin failed. Examination of the failure provided evidence of fatigue.

Further investigation of Yoke Peter on structure recovered near Elba also confirmed that the primary cause of the failure was pressure cabin failure due to fatigue. The origin in this case was at the corner of the Automatic Direction Finding (ADF) windows on the top centerline of the cabin.

Yoke Uncle was repaired and the fuselage skin was strain gauged near the window corners. The peak stresses measured were 43,100 psi for 8.25 psi cabin pressure plus 650 psi for 1g flight and 1950 psi for a 10 ft/sec gust for a total of 45,700 psi. The material was DTD 546 having an ultimate strength of 65,000 psi. Therefore, the 1P + 1g stress was 70% of the material ultimate strength.

Thus, the cause of the failures was determined to be fatigue due to high stresses at the window corners in the pressure cabin. This investigation resulted in considerable attention to detail design in all future pressure cabins and demonstrated the need for full-scale fuselage fatigue tests. The Comet failures sent a clear message to aircraft designers that the fatigue effects should not be ignored.

F-111 wing pivot fitting failure

On December 22, 1969, the left wing pivot forging of a U.S. Air Force F-111 aircraft failed during a 4.0g steady maneuver even though the aircraft was designed for a load factor of 11.0g. The failure, resulting in the loss of the aircraft, was attributed to the presence of a defect in the D6ac steel fitting which had propagated to a critical size at tension stresses induced by the 4.0g maneuver.

The aircraft had accumulated only 105 flight hours at the time of the failure. The fracture surface of the outboard portion of the left wing is shown in the Figure 1-4, illustrating the size of the defect (it gives a good feel for the size of a defect which can cause catastrophic failure). The failure, at such a small crack size, was attributed by many to be a function of the low fracture toughness of the D6ac steel caused by salt bath quenching. This incident resulted in the largest single investigation of a structural alloy ever undertaken. It precipitated investigations into the history of U.S. Air Force accidents related to fatigue. The results of these investigations culminated in a complete change in design criteria for Air Force aircraft. Many of the design specifications were changed and others introduced. The most important document to be issued was MIL-A-83444 "Airplane Damage Tolerance Requirements" [1-3]. This document requires that structure be designed using fracture mechanics principles. The document was issued on July 2, 1974, after considerable review by industry. At the time of issue, the manufacturers did not believe they had the analytical tools or experience to meet the criteria. The Air Force, with this in mind, funded a large number of research and development programs to provide data and fracture mechanics analytical methods. These programs were conducted by the industry which provided aircraft to the Air Force. Thus, the F-111 failure provided the necessary boost to fracture mechanics development in the United States. This incident also provided evidence that a fatigue test of a single "good" aircraft was insufficient protection against the possibility of the rogue flaw.

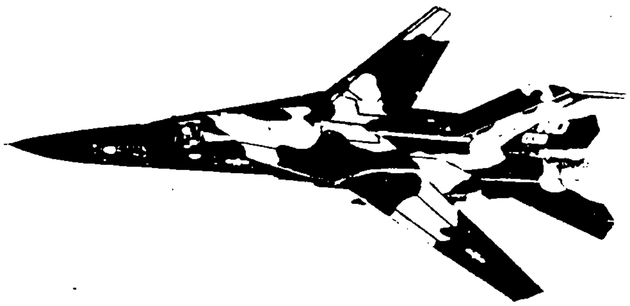

(a) F-111 in flight.

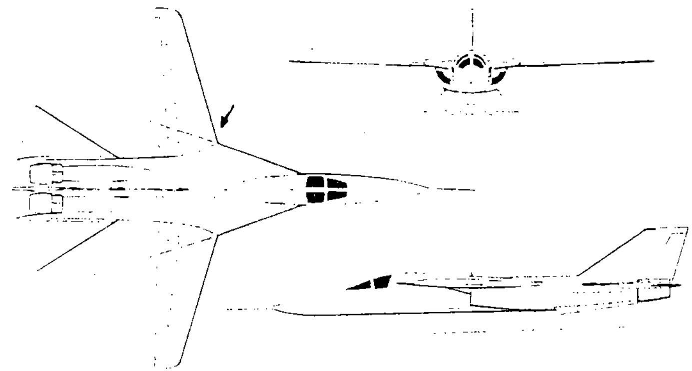

(b) F-111, plan view showing probable failure initiation site

[Reprinted from Jane's All the World's Aircraft, 1969-70, p. 329, by permission of Jane's Information Group.]

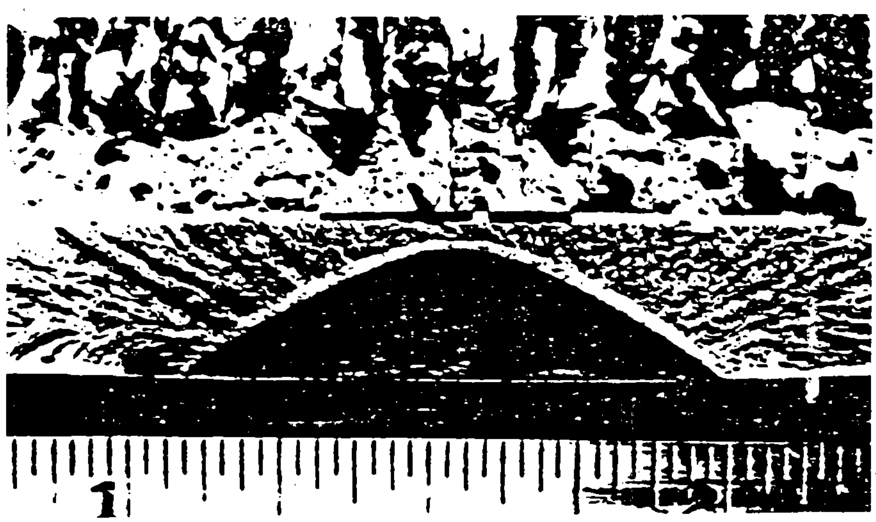

(c) Crack in left wing pivot forging of F-111 aircraft.

Figure 1-4. USAF Tactical Air Command F-111A circa 1969.

[Reprinted from Case Studies in Fracture Mechanics, AMMRC MS 77-5, June 1977, Fig. 2, with permission of General Dynamics Corporation for use of their data.]

Failure initiating at rivet holes

In 1988, a commercial transport aircraft experienced an explosive decompression when approximately 18 feet of the upper crown skin and structure separated from the fuselage while in flight at 24,000 feet (Figures 1-5a and 1-5b). A flight attendant was swept overboard, but the crew managed an emergency landing [1-4].

An examination of the remaining structure surrounding the separated area confirmed the existence of small cracks in the vicinity of several rivet holes in lap joints prior to the failure of the fuselage structure. Areas of corrosion and disbonding of glued aluminum skin panels were observed in lap joints in locations adjacent to the fracture surface. The airplane was manufactured in 1969. At the time of the accident, it had accumulated 35,496 flight hours and 89,680 landings.

This failure was attributed to multiple site damage (MSD). Many small fatigue cracks along a rivet line joined suddenly to form one or more large cracks. This process defeated the crack arrest design that was based on growth of a single isolated crack. A catastrophic failure occurred since the crack did not turn to produce fail-safe "flapping" of the skin as had been intended.

Concern with the cumulative effects of metal fatigue in aging airframes as a source of MSD became a priority following this incident. The MSD in the above aircraft is believed to have resulted from corrosion, but MSD has been found in other circumstances. Isolated cracks generally continue to grow slowly when they are long enough to constitute "obvious partial damage" that can be found visually or discovered by means of fuel or cabin leaks. Individual MSD cracks may be too small to be found by these means.

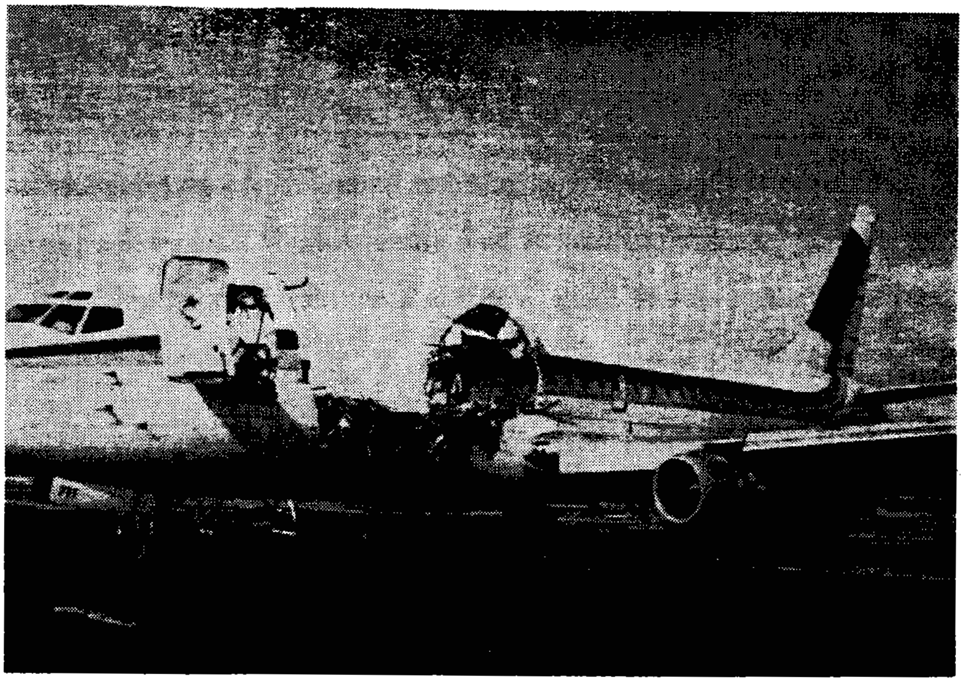

(a) General view, left side of forward fuselage.

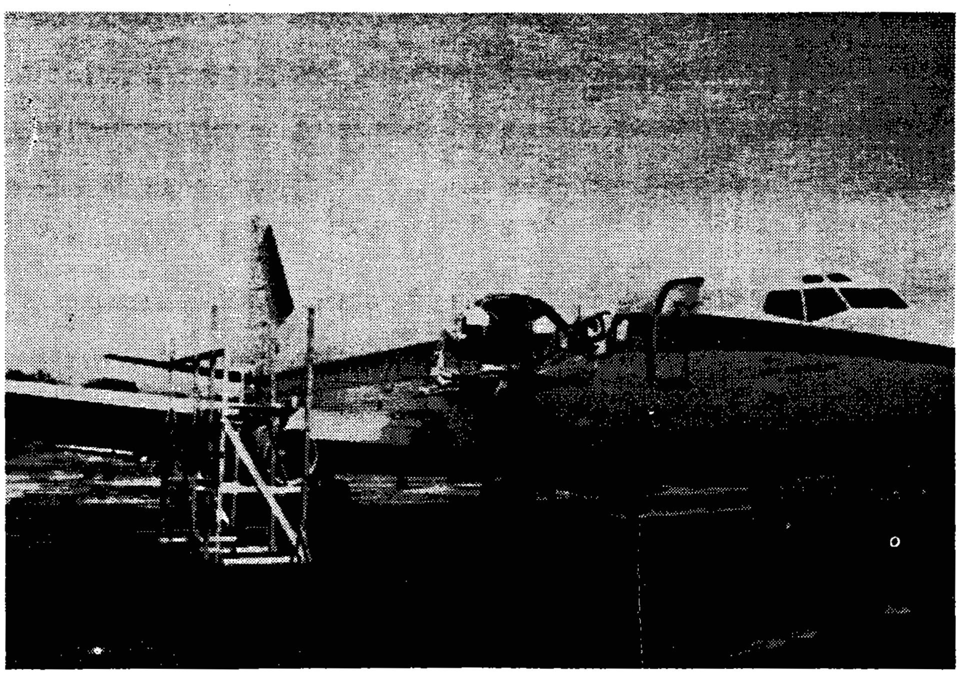

(b) General view, right side of forward fuselage.

Figure 1-5. An aircraft fuselage failure.

[From T. Swift, FAA]

These three case histories mark the evolution of attitudes toward aircraft structural design from one based on safe-life procedures to the correct emphasis on damage tolerance evaluation. While no quantitative surveys of transport aircraft failures have concentrated on this issue, there is considerable additional experience to support this change in attitude. Several examples are summarized in the following paragraphs.

Hawker Siddley

In Argentina, a Hawker Siddley AVRO 748 suffered an in-flight separation of a wing due to fatigue on April 14, 1976. This had been the first AVRO aircraft to be designed on fail-safe principles where wing bending structure had been separated into multiple elements. Previous AVRO designs, such as the Manchester and Lancaster bombers, had been designed with all wing bending material concentrated in front and rear spar caps. The change to fail-safe design concept in the 748 did not prevent catastrophic failure which was precipitated by fatigue cracking at multiple uninspectable sites. The current damage tolerance design philosophy includes in-service inspections specifically based on expected crack growth scenarios.

Dan-Air

A Dan-Air aircraft horizontal stabilizer failure in Zambia (1976) occurred after only 400 hours of flight following 800 hours of service to Pan American Airways. Stainless steel skin had been installed to relieve a buffeting problem. As a result, a stress concentration was created at the steel/aluminum interface. While maintenance was performed 6 inches from the location of the crack that precipitated the failure, there was no planned inspection. The fail-safe design did not prevent a failure. This type of crack was found in dozens of aircraft inspected after the accident.

Propeller blades

In one case, a propeller blade was thrown while flying at 20,000 feet with the cabin fully pressurized. No damage tolerance had been incorporated in the design of this particular aircraft. The cabin pressure of 4.6 psi (corresponding to a nominal skin stress, PR/t = 13 ksi) produced 17 feet of damage to the fuselage. The crew of the aircraft managed a safe landing. The fuselage material was 7075-T6 aluminum. This material has low fracture toughness, so it has little crack stopping ability and generally small critical crack lengths.

Passenger door corners.

All passenger aircraft have problems with the concentration of stress at details such as doors and windows. In one case, an operator found a corner crack and repaired it. At that time, the engineering involved was restricted to a static strength analysis of the repair; fatigue was not considered. Such patches did not always fix the problem since they were often too stiff and adversely affected the stress distribution local to the patch. This type of detail has poor fatigue/damage tolerance.

The main problem posed by door corners is out-of-plane bending. The maximum principal stress is at 45° across the detail. A subsequent finite element analysis of this configuration predicted that the stress at the door corner was approximately 2.5 times the design stress.

1.2 RESULTS OF AIR FORCE SURVEY

Some sense of the sensitivity of structural elements to cracking problems and how often they occur can be deduced from surveys conducted by the Air Force.[1]

[1] Additional experience is also documented in Technical Report AFFDL-TR-79-3118, Volume III, titled Durability Methods Development - Structural Durability Survey: State-of-the-Art Assessment.

Figure 1-6 shows the distribution and magnitude of service cracking problems in Air Force aircraft. There are a total of 31,429 major and minor cracking problems recorded on twelve types of military aircraft. The distribution shows that the majority of incidents were in the fuselage and wing with about the same number in each.

Figures 1-7(*a*) and (*b*) illustrate examples of two Air Force surveys of major cracking incidents. During a 21-month period, in one study (Figure 1-7(*a*)), 1226 major cracking/failure incidents were reported. The majority of these were fatigue initiated, with corrosion fatigue second, followed by stress corrosion. In another study (Figure 1-7(*b*)), out of 64 major cracking incidents reported, the majority were due to stress corrosion followed by corrosion fatigue and fatigue in about equal numbers. It is noted that some failures were attributed to overload. This is rare in commercial transport history.

Figure 1-8 shows the distribution of origins of those failures reported in Figure 1-7(*b*). The majority of failures were due to poor quality where cracks initiated at holes. Material flaws, defects, and scratches were second, followed by poor design details. This magnitude of cracking incidents also contributed to an Air Force decision to change the design philosophy of their structures. Prior to this time, the main philosophy had been a safe-life approach where the design was based on a full scale fatigue test to four lifetimes.

1.3 COMPARISON OF OLD AND NEW APPROACHES

This section describes the elements of the older safe-life method (fatigue design) and contrasts it with the concepts of fracture mechanics and crack propagation that are central to the current damage tolerance approach. Even though the safe-life approach is not allowed as a basis for certification of most major transport airframe components, AC 25.571-1 does permit exceptions in certain cases, and in any case it is still important to understand the fatigue performance of structure.

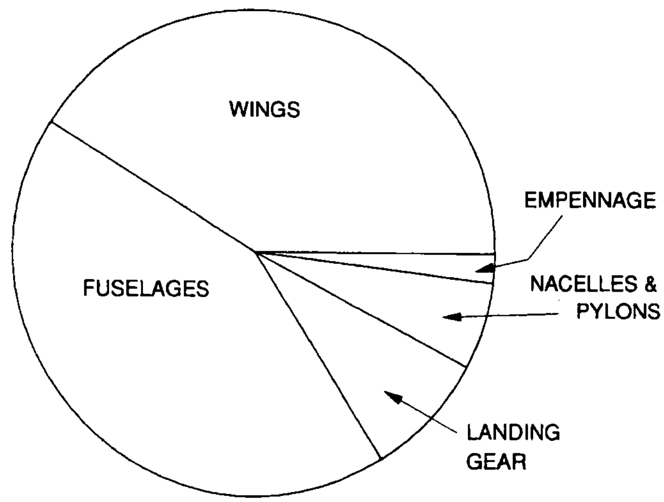

Figure 1-6. Examples of distribution and magnitude of service cracking problems.

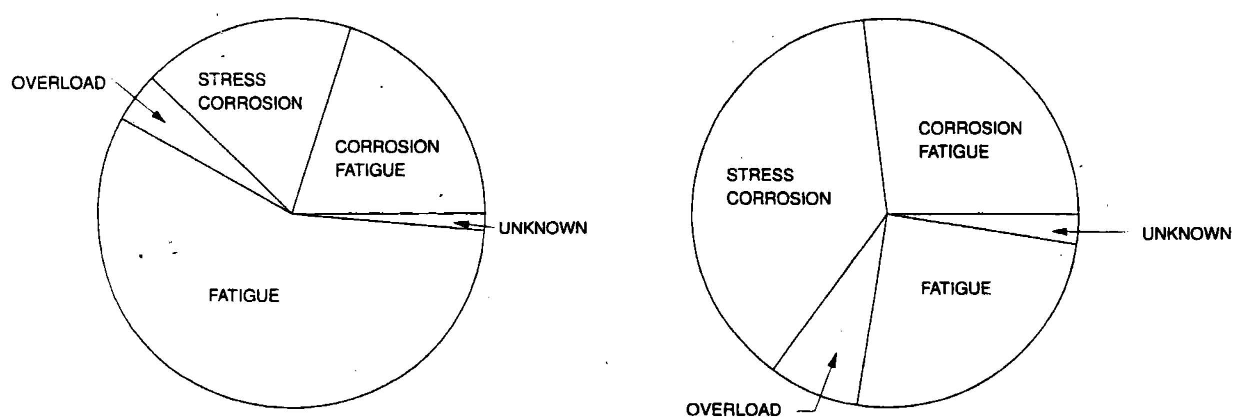

(a) 1226 major cracking/failure incidents
(21-month period)
(Ref. USAF report on study of aircraft
structural integrity).

(b) 64 major cracking/failure incidents
(Ref. AFFDL TR-70-149).

Figure 1-7. Crack initiation/growth and failure mechanisms.

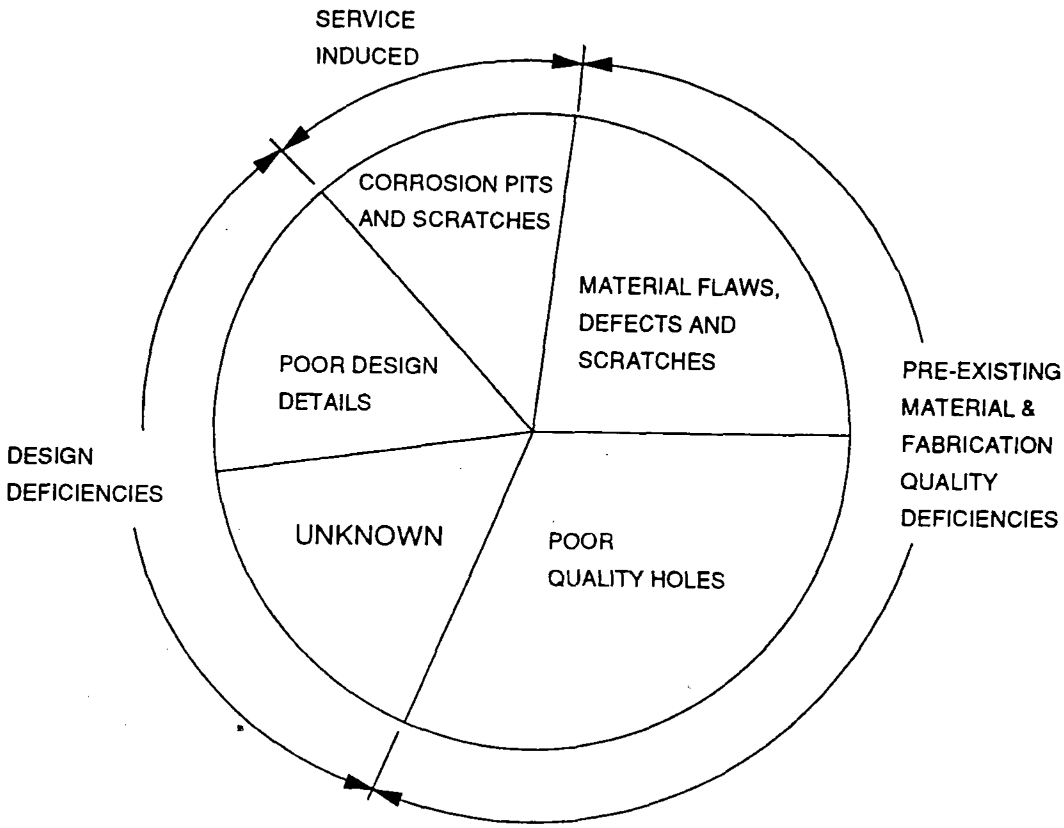

Figure 1-8. Cracking and failure origins.

A wholly empirical idea is fundamental to the old method, whereas the new approach deals with the physics of the problem. For safe-life, the design objective was to make the time needed to form a crack longer than the operational life of the structure. Variability in observations of time that characterizes crack formation (scatter) required the use of factors of safety to ensure a conservative design. Damage tolerant designs differ in that they have a physical basis, i.e., the size of a crack. Factors of safety are still required (e.g., on inspection intervals), but they are generally smaller than fatigue scatter factors because there is less uncertainty in damage tolerance assessment.

1.3.1 Fatigue Safe-Life Approach

Metal fatigue was first recognized as an engineering problem over a century ago, when the German railways encountered a series of axle failures which could not be explained from past experience. The concept of fatigue as the result of repeated loading was proposed, and a fatigue-resistant axle design was developed after several years of empirical study by means of full scale axle fatigue tests [1-5]. The relationship between fatigue and cyclic stress could be easily visualized for axles, where the material was alternately subjected to tension and compression as the axle rotated under the static loads imposed through its bearings. As a result, the rotating bending fatigue test at laboratory scale became the standard in the field for more than half a century (Figure 1-9), with the fatigue life defined as the number of cycles to specimen failure.[2] The cyclic fatigue stress concept has since been extended to more complicated cases; early

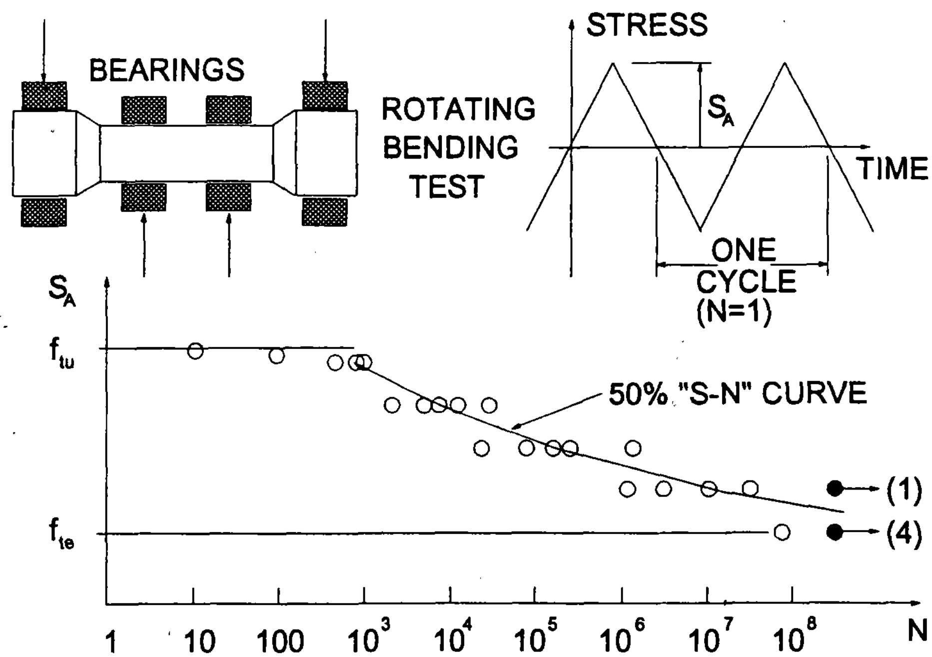

Figure 1-9. Results of a typical fatigue experiment.

[2] For typical laboratory size specimens, about 95% of this life is consumed by crack formation, and only 5% by slow crack propagation.

developments are briefly summarized in Timoshenko's history [1-6]. A good summary of recent (circa 1950 to 1970) fatigue design practices is given by Osgood [1-7], and a detailed description of European airframe fatigue design practices has been prepared by Barrois [1-8].

Basic material properties in fatigue can be summarized by an "S-N" curve and a modified Goodman diagram. The S-N curve (Figure 1-9) is an empirical description of fatigue life based on rotating bending or similar tests, where S_A is the amplitude of the applied stress cycle and N is the expected number of cycles to failure. The S-N curve describes the material behavior only under the condition of zero mean stress. For design purposes, the material is tested over a range of stresses corresponding to lives of one cycle at ultimate strength f_{tu} to one equivalent to unlimited duration at the endurance strength f_{te}.

There is actually no unique S-N curve for any material. If several nominally identical specimens are tested at the same stress amplitude, the number of cycles to failure is generally different for each specimen, as indicated by the open-circle symbols representing individual data points in Figure 1-9. The shortest and longest individual life may differ by as much as a factor of 10 in some cases. The data points at each stress amplitude are averaged to produce the 50th percentile S-N curve shown in the figure.

As the tests are repeated at lower stress amplitude, the individual lives begin to spread out, and "run-outs" are obtained in some tests. A run-out is a specimen that has not failed after the longest time one is willing to wait. In Figure 1-9, the run-outs are represented by solid circles with arrows plotted at $N = 2 \times 10^8$ cycles (the maximum waiting time in this case). As the stress amplitude is further decreased, the proportion of run-outs increases, and a material "endurance strength" f_{te} is sometimes defined as the stress amplitude where the run-out proportion reaches 100 percent. Fatigue life is sometimes said to be unlimited at stress amplitudes below f_{te}, but, strictly speaking, all one can say is that the life at these low stress amplitudes exceeds the test time.

The effect of non-zero mean stress is schematically illustrated in Figure 1-10. Stresses in service such as those resulting from aircraft maneuvers are cycles more complex than the ideal laboratory pure alternating wave. The effect of mean stresses contained in these complex cycles shifts the average lives from the values expected from S-N data. A modified Goodman diagram is used to extend the description to cases in which the material is subjected to alternating stress superimposed upon a mean stress. The usual presentation is in the nondimensional form shown in Figure 1-11, where both the alternating stress amplitude S_A and mean stress S_M are expressed as fractions of the material's ultimate static strength f_{tu}. Both S-N curve data and experimentally determined Goodman diagrams for aircraft structural alloys are well documented (see ref. [1-9]). Figure 1-12 illustrates the Goodman diagram (using unscaled stresses) for 2024-T4 aluminum.

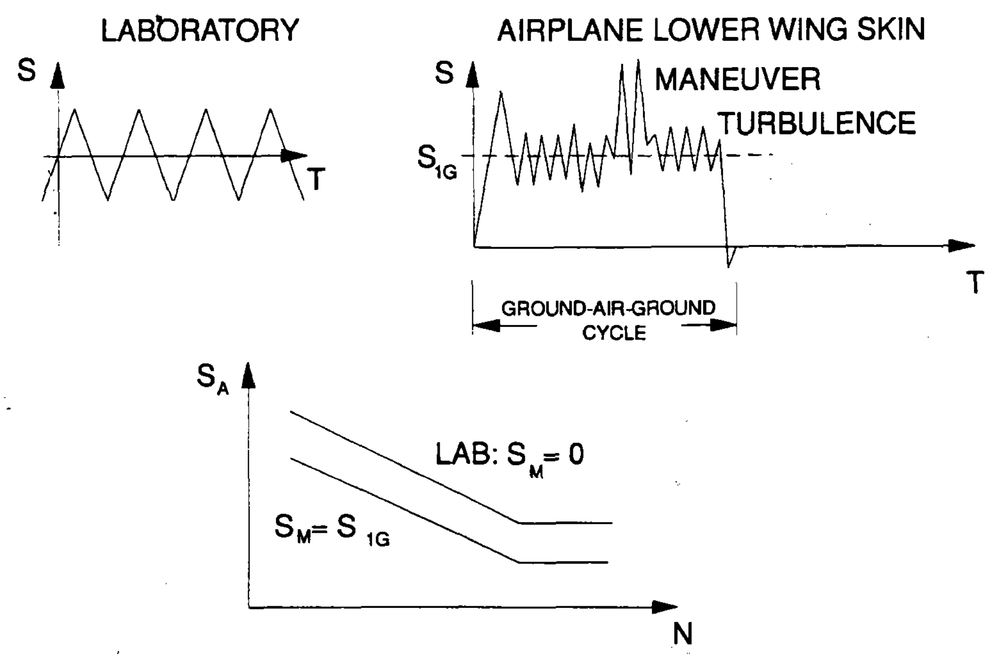

Figure 1-10. Effect of mean stress.

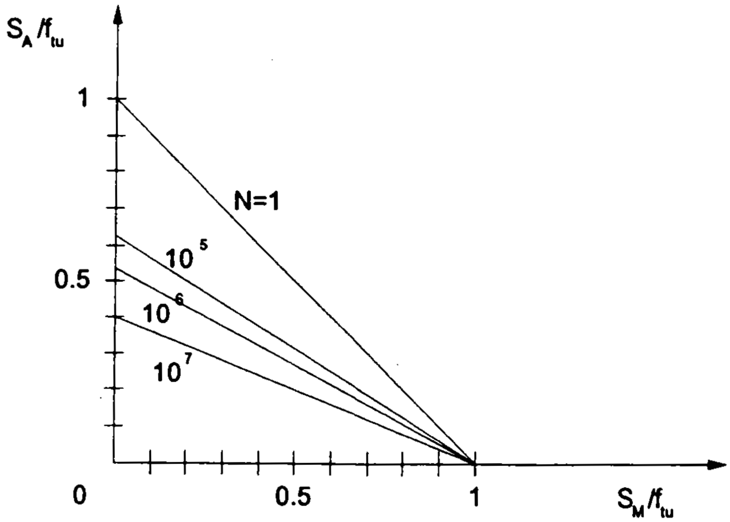

Figure 1-11. Modified Goodman diagram.

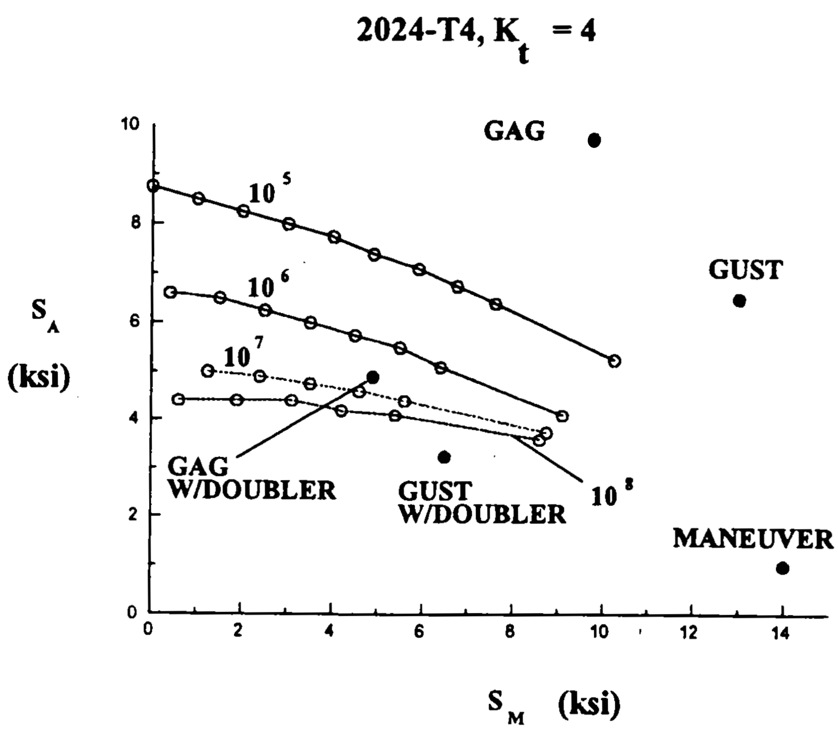

Figure 1-12. Goodman diagram for 2024-T4 aluminum.
Source: ALCOA Structural Handbook.

The foregoing description refers to average fatigue life. In reality, the fatigue life of a given material subjected to given stresses is not a unique property. Each test specimen has a life which results from random arrangements of material defects at the atomic scale. This effect is suggested by the scatter in the data of Figure 1-9. A complete description of the material fatigue life properties thus requires a specification of the life distribution (probability function) as well as the average (50% S-N curve). Although the average information documented in reference [1-9] is based on numerous individual specimen tests, life distributions are generally not reported. One exception is the work done by Weibull, in which the probabilistic approach to fatigue life description is developed in detail [1-10]. Weibull's book includes examples of life distribution data for a number of aircraft alloys.

Structural component fatigue lives can be estimated by combining a service stress description with basic material properties. The easiest and most widely used estimation method is linear damage summation [1-11, 1-12].[3] Both the popularity and limitations of Miner's Rule stem from its simplicity:

- For an alternating stress above the endurance strength, damage is linearly proportional to the number of stress cycles.

- The fully reversed bending (zero mean stress) fatigue curve determines the relative rates of material damage caused by alternating stresses with different amplitudes.

- The damage rate is adjusted by means of a modified Goodman or similar diagram for cycles with non-zero mean stress.

- The rate of damage accumulation does not depend upon the sequence of different stress cycles.

[3] The method is also referred to as Miner's rule by engineers engaged in fatigue life estimation in the United States.

Figure 1-13 is a schematic representation of how the linear damage technique is applied. The stresses encountered in service are classified in terms of cycles of mean and alternating stress pairs and the corresponding number n_i of such occurrences. The fractional damage inflicted by these stresses is the ratio of n_i to N_i, the number of occurrences to initiate a crack corresponding to the stress pair (read as a point in the modified Goodman diagram for the appropriate fatigue quality index). This fraction is added to those of the remaining stress pairs to calculate the total damage for a load sequence ("spectrum"), for example, a single aircraft flight.

The design objective of such calculations is usually a prediction of the number of spectra permitted before formation of a crack, i.e., the reciprocal of the total damage fraction. Adjustment of the damage fraction to account for engineering uncertainties (safety factor) is included in the estimate as shown in Figure 1-13.

This method has been extended to the routine derivation of life estimates for random stress spectra with Gaussian properties [1-13, 1-14]. Linear damage summation is based on the

STRESS SPECTRUM FOR ONE FLIGHT			Material Properties based on FQI	Damage Ratios
Alternating Stress	Mean Stress	Occurrences per Flight		
S_{A1}	S_{M1}	n_1	N_1	n_1/N_1
S_{A2}	S_{M2}	n_2	N_2	n_2/N_2
S_{A3}	S_{M3}	n_3	N_3	n_3/N_3
S_{A4}	S_{M4}	n_4	N_4	n_4/N_4
				$\sum n/N$

$$\text{FLIGHTS TO CRACK NUCLEATION} = \frac{1}{(SF) \times \left(\sum n/N\right)}$$

SF = Safety factor
FQI = Fatigue quality index

Figure 1-13. How the Palmgren-Miner rule is applied.

assumptions that each stress cycle affects the material independently, and that the spectrum at a stress raiser is linearly scaled from the nominal stress spectrum. Neither assumption is true in most service situations, however. Even laboratory experiments have shown that actual life can be changed simply by rearranging the order of stress cycles in the spectrum, or that life estimates scaled from nominal stresses do not agree with the experimental results when the test specimen contains a notch or a hole [1-15].

Simulated service testing or field experience is required to obtain an accurate estimate of the life distribution. When similar structural details are employed in evolving designs (e.g., the evolution of transport airframes in an individual manufacturer's product line), the results of tests and field experience are usually fed back to adjust the estimation procedure. Most such adjustments are in the form of a fatigue quality index (FQI) and factor of safety or the use of an S-N curve more conservative than the average, although in some cases aerospace companies have developed elaborate empirical nonlinear damage summation procedures to replace Miner's rule. Such special procedures may be well calibrated for details similar to that from which they were derived, but extrapolation to other details can generally be expected to give poor results.

The FQI is used to account for the effects of local stress, by reference to S-N curves obtained from specimens with standard notches. Each such specimen has a known elastic stress concentration factor, K_t, at the root of the notch, as determined by the notch geometry. Since these specimens fail at the notch root, a plot on a scale of the nominal stress amplitude S_A is considered to characterize the S-N curve for the stress concentration factor K_t. (Notched-specimen S-N curves are generally obtained for $K_t = 2, 3, 4$, and 5.)

Figure 1-14 outlines how the FQI is derived from notched-specimen S-N curves. The schematic represents two replicas of a double-shear connection detail which is being tested in fatigue. The data points, which represent the results of these tests, are compared graphically with the family of notched-specimen S-N curves for the material. In general, the detail will not precisely follow any one S-N curve, but an "effective" K_t for the range of stress amplitudes expected in service can be estimated from the comparison.

Similar comparisons of data from a full scale fatigue test of an airframe provide effective K_t values for typical fastener details. These values are referred to as fatigue quality indices because they reflect the effects of detail design and fabrication quality, as well as geometric stress concentration. For example, $K_t = 3$ for the stress at the edge of an open circular hole in a skin under tension, but the FQI ranges from 3.5 to 4.5 for filled fastener holes in typical transport airframe details.

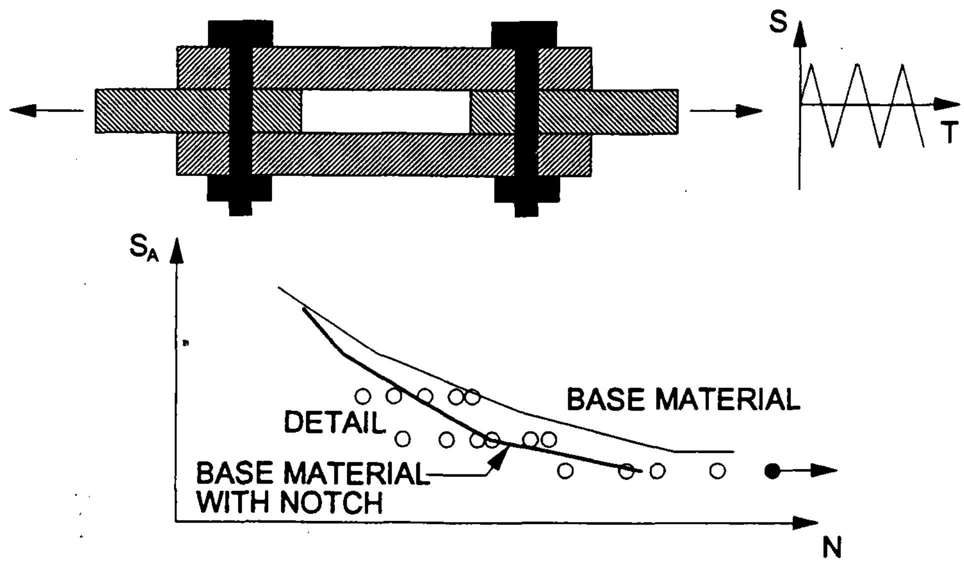

FQI = 3.5 to 4.5 for typical airframe fastener details

Figure 1-14. Fatigue quality index.

The FQI accounts for what is known about the average effect of fatigue when combined with realistic quality. A factor of safety (sometimes also called a "scatter factor") is applied to estimates of average fatigue life to account for the uncertainties. These include the previously mentioned random effects of material behavior and differences of actual service loads from the loads assumed for the purpose of estimating fatigue life (Figure 1-15). Fatigue factors of safety from 3 to 5 (but in some cases as high as 8) have historically been used to estimate airframe safe life.

When the FQI and factor of safety are properly applied, the calculated safe-life is usually a conservative estimate of the airframe's useful economic life. What this means is that, within the safe-life, most of the details in the airframe will not have had enough time to form cracks. If the safe-life is exceeded, the rate of crack formation can be expected to rise, and (usually well before the unfactored 50th percentile lifetime) enough cracks will be present to make repair

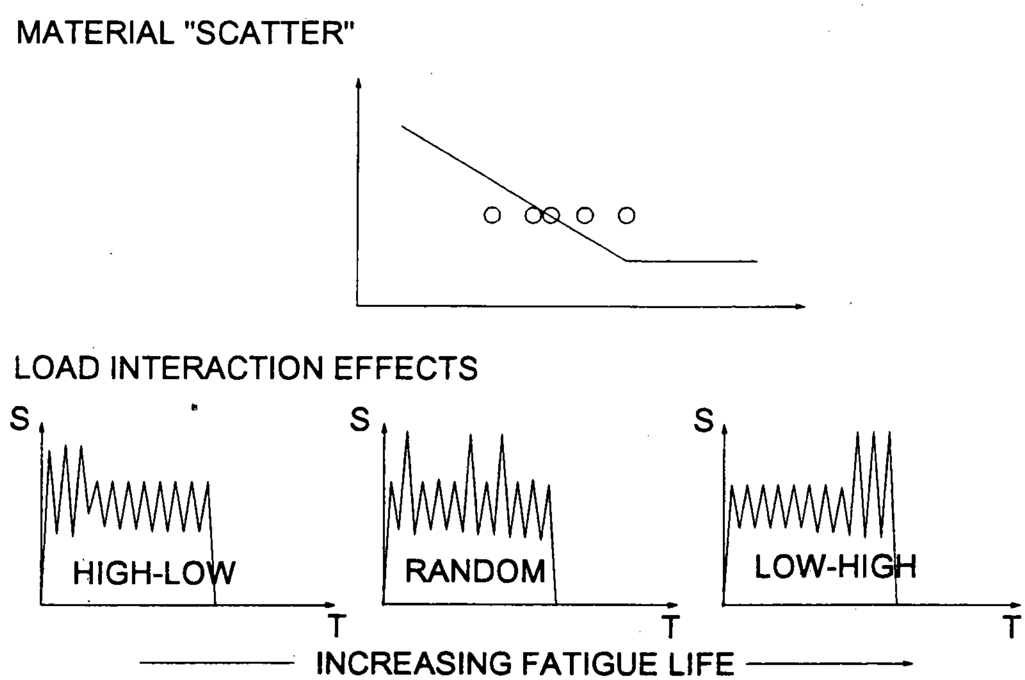

Figure 1-15. Uncertainties addressed by safety factor.

uneconomical. A full-scale fatigue test of a transport airframe prototype is generally conducted to one or two expected service lifetimes for the purpose of verifying that the design meets its useful economic life goal.

Recently, some older airframes have been reexamined to more closely estimate useful economic life. This is done, as a part of the continuing airworthiness program, by ground testing a retired high-time airframe which has reached or exceeded the original economic life goal.

1.3.2 Damage Tolerance Assessment (DTA) Approach

The case histories presented in Section 1.1 show why in modern structural design attention is focused on crack propagation life. Originally, the term damage tolerance meant the ability to endure sudden damage, for example, penetration of a fuselage by a propeller blade without catastrophic failure. It has come to mean setting life limits, i.e., inspection intervals that are based on the time for a crack to lengthen or propagate.

The epitome of a damage tolerance problem is illustrated by the failure of the front lower spar cap of a DC-8-62. A crack in a stiffening element was revealed by a fuel leak observed after 32,000 hours of service. Examination of the failed region gave a clear impression of the process. A count of the striations in the fracture surface indicated the effect of each cycle of loading on the growth of the flaw, from a small crack to a length large enough to allow fuel to escape. Such a pattern is a signature that can be used as forensic evidence to trace size of the crack very nearly on a flight by flight time scale.

This case illustrates the importance of three interconnected notions that are the central elements of FAR 25.571.

> **Crack propagation:** A crack in a structure will increase in size in response to application of cyclic loads. As shown schematically in Figure 1-16, growth is negligible when the crack is very small. Since these effects are nearly impossible to observe, it can be argued that some tiny flaws are always present in a structure. An alternative interpretation is that a small crack is initiated in perhaps 5% of the time range of the diagram due to a manufacturing flaw or material inclusion and then grows during the greater part of the time range to failure. As the crack increases in size, increments of extension get larger until a critical dimension is attained at which the structure fractures in the course of a single cycle of loading.

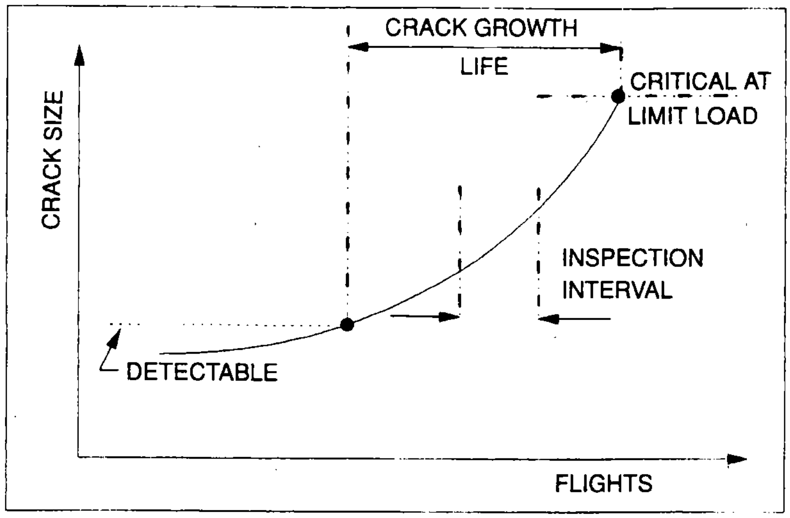

Figure 1-16. Crack growth in response to cyclic loads.

Residual strength: The level of stress that will induce rapid fracture is sensitive to the size of a crack in a structure. Figure 1-17 is a schematic illustration of the inverse relationship of critical stress and crack length. A structure with a history of few cycles of loading and a short crack length has the capacity to resist fracture. This is indicated in the diagram by the vertical distance between a level of service stress (dotted line) and the critical stress-crack length curve. As fatigue loads accumulate, the crack lengthens, reducing the stress level

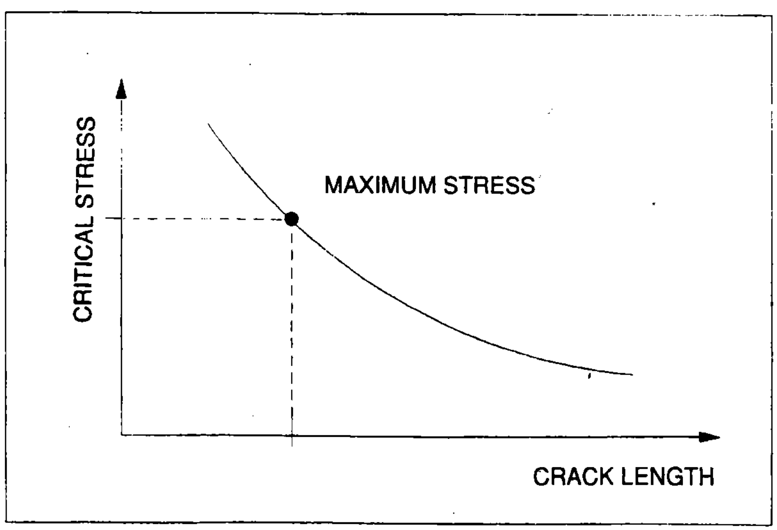

Figure 1-17. Schematic relationship of allowable stress versus crack length.

that will cause unstable crack growth. Figure 1-18 is a typical representation of this margin (residual strength) as a function of time that combines the information contained in the two preceding figures.

Inspection: As Figures 1-16 and 1-18 indicate, crack growth life is the time (measured, for example, in terms of number of flights) it takes a crack to grow from some initial length to a critical size that reduces the strength margin to zero. An initial size at which the crack can be detected marks the start of this time scale. The purpose of damage tolerance analysis is to ensure that crack growth life is greater than any accumulation of service loads that could drive a crack to a dangerous size. This objective can be achieved with an inspection program that detects cracking initiated by fatigue, accident, or corrosion before propagation

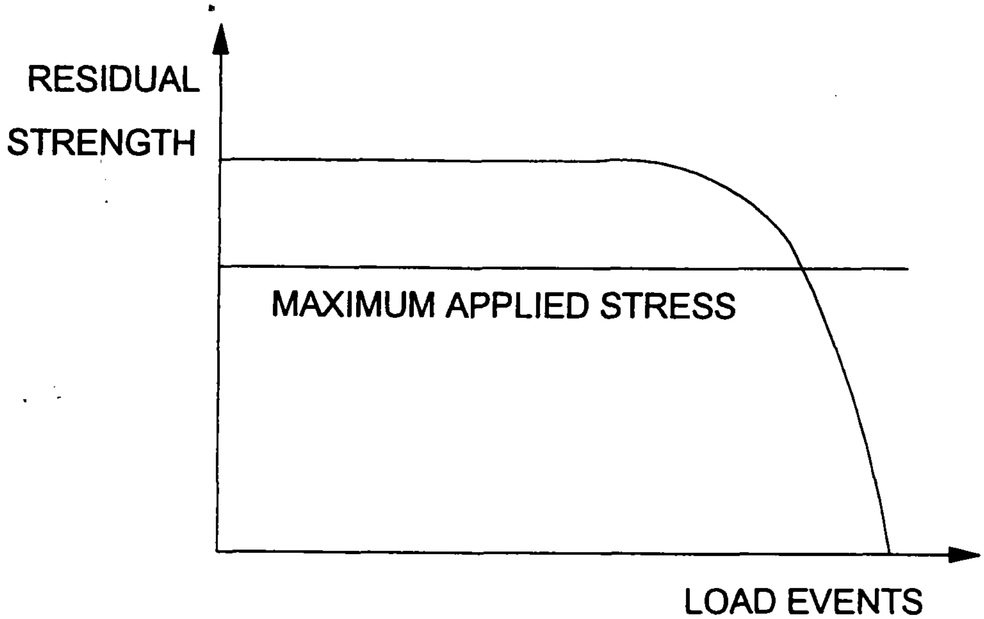

Figure 1-18. Residual strength diagram.

to failure. Inspection frequencies must be at intervals that are fractions of expected growth life to afford the opportunity for corrective action that maintains structural safety if cracks are found. The economic feasibility of an inspection plan must consider the cost trade-off between inspection methods and intervals. As Figure 1-16 suggests, crack growth life for small cracks detected using an expensive nondestructive inspection (NDI) procedure will be longer than the interval corresponding to larger crack sizes that are found with less expensive visual inspection.

A sound knowledge of the principles of fracture mechanics is needed to perform the damage tolerance evaluation required by Part 25 of the FAA regulations. With this objective in mind, this handbook has been planned with a view to providing FAA engineers with appropriate background in order that they may improve their ability to review manufacturers' data.

Fracture mechanics can be looked upon from a metallurgical viewpoint or a stress analysis oriented viewpoint. The former usually takes place after failure with fractographic analysis of the fracture surface, for example. The latter is primarily associated with the calculation of crack growth life and residual strength in order to establish an inspection program to prevent failure. Since the FAA is involved in reviewing damage tolerance evaluations to prevent failures, it is appropriate here to concentrate on the stress analysis oriented fracture mechanics approach.

The concepts of damage tolerance have been organized into three areas. Chapter 2 begins with a description of the fundamentals of crack behavior. The roles played by stress history, crack geometry, and material properties in residual strength assessment are defined and placed in context. The relation of these factors to crack growth is the foundation of DTA.

Chapter 3 is devoted to interpretation of measurements of crack length under cyclic loading. Data for fatigue crack propagation are rigorous and repeatable, not as scattered as S-N curves that are based on a concept as imprecise as crack initiation. However, characterization of crack propagation rates is still largely empirical; laboratory experiments are necessary to determine how cracks actually grow. In addition, data correlation procedures must be applied to account for circumstances of service that are distinct from the experimental conditions. The dependence on such empiricism to develop a crack growth curve for a specific structural element emphasizes the need for continual experimental confirmation of DTA in the design process.

These notions are brought together in Chapter 4 from the point of view of assessing an airframe. Step-by-step procedures and examples are presented to illustrate proper paths for design reviews.

REFERENCES FOR CHAPTER 1

1-1. Damage Tolerance and Fatigue Evaluation of Structure, FAR 25.571.

1-2. Damage Tolerance and Fatigue Evaluation of Structure, Federal Aviation Administration, AC 25.571-1 (1978).

1-3. Airplane Damage Tolerance Requirements, MIL-A-83444 (USAF), 1974. Also, Air Force Guide Specification, AFGS-87221A, June 8, 1990.

1-4. Aircraft Accident Report - Aloha Airlines, Flight 243. Boeing 737-200, N73711, Near Maui, Hawaii, April 28, 1988. NTSB/AAR-89/03.

1-5. Wöhler, A.., Zeitschrift für Bauwesen, 8, 641-652 (1858); 10, 583-616 (1860); 16, 67-84 (1866); 20, 73-106 (1870).

1-6. Timoshenko, S.P., History of Strength of Materials, McGraw-Hill, New York, 1953.

1-7. Osgood, C.C., Fatigue Design, Wiley, New York, 1970.

1-8. Barrois, W.G., Manual on Fatigue of Structures, NATO Advisory Group for Aerospace Research and Development, AFARD-MAN-8-70, June 1970.

1-9. Metallic Materials and Elements for Flight Vehicle Structure, MIL-HDBK-5E (USAF) June 1987.

1-10. Weibull, W., Fatigue Testing and Analysis of Results, Pergamon Press, New York, 1961.

1-11. Palmgren, A., "Die Lebensdauer von Kugellagern," Zeitschrift des Verein Deutscher Ingenieure 68, 339-341 (1924).

1-12. Miner, M.A., "Cumulative Damage in Fatigue," Journal of Applied Mechanics 12, A159-A164 (1945).

1-13. Burris, P.M.and Bender, M.A., Aircraft Load Alleviation and Mode Stabilization (LAMS), The Boeing Company and Honeywell, Inc., AFFDL-TR-68-158, 1969.

1-14. Crandall, S.H.and Mark, W.D., Random Vibration in Mechanical Systems, Academic Press, New York, 1973.

1-15. Schijve, J., The Accumulation of Fatigue Damage in Aircraft Materials and Structures, NATO Advisory Group for Research and Development, AGARD-AG-157, January 1972.

CHAPTER 2:

FRACTURE MECHANICS

2. FRACTURE MECHANICS

Fracture mechanics is an outgrowth of the field of strength of materials. Early work on the strength of materials focused first on basic properties and later, as the theories of elasticity and plasticity were developed, on the strength of structures or components containing known stress raisers [2-1]. Fracture mechanics deals with the strengths of materials and structures which contain flaws in the form of detectable or visible sharp cracks.

2.1 STRESS CONCENTRATION, FRACTURE AND GRIFFITH THEORY

Many structures have discontinuities such as holes and notches. Often these discontinuities produce local elevation of stress in comparison to the applied stress. The resulting stress concentration is defined as the ratio of the local elevated stress to the applied nominal stress.

Stress concentration factors can be derived by applying the theory of elasticity to specific problems. Two problems of great historical and practical importance are the circular hole and the elliptical hole. The circular hole is shown in Figure 2-1 for a uniform stress, S, in the y-direction. A plate without a hole produces a uniform stress, S, throughout the plate, while at the highly stressed points A and B at the hole, the normal stress rises to $3S$. Thus the circular hole in a large plate has a stress concentration factor of 3, which is independent of the hole radius. The elliptical hole in a large plate is shown in Figure 2-2. The analysis by Inglis [2-2] produces a stress concentration factor $k_t = (1 + 2a/b)$, where a and b refer to the semi-major and -minor axes, respectively. Since the radius of curvature at the end of the major axis of an ellipse is $\rho = b^2/a$, the stress concentration factor can be rewritten as

$$k_t = \frac{\sigma_{max}}{\sigma} = 1 + 2\sqrt{a/\rho} \quad , \qquad (2\text{-}1)$$

or

$$k_t = 1 + 2\frac{a}{b}$$

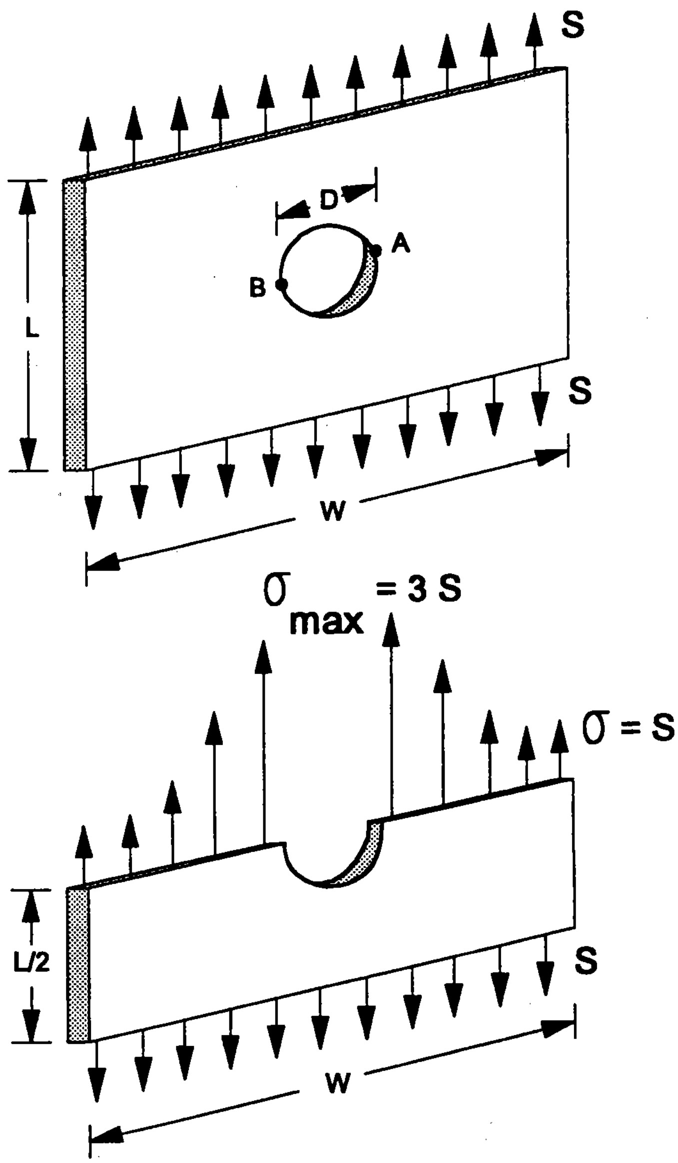

Figure 2-1. Circular hole in a large plate.

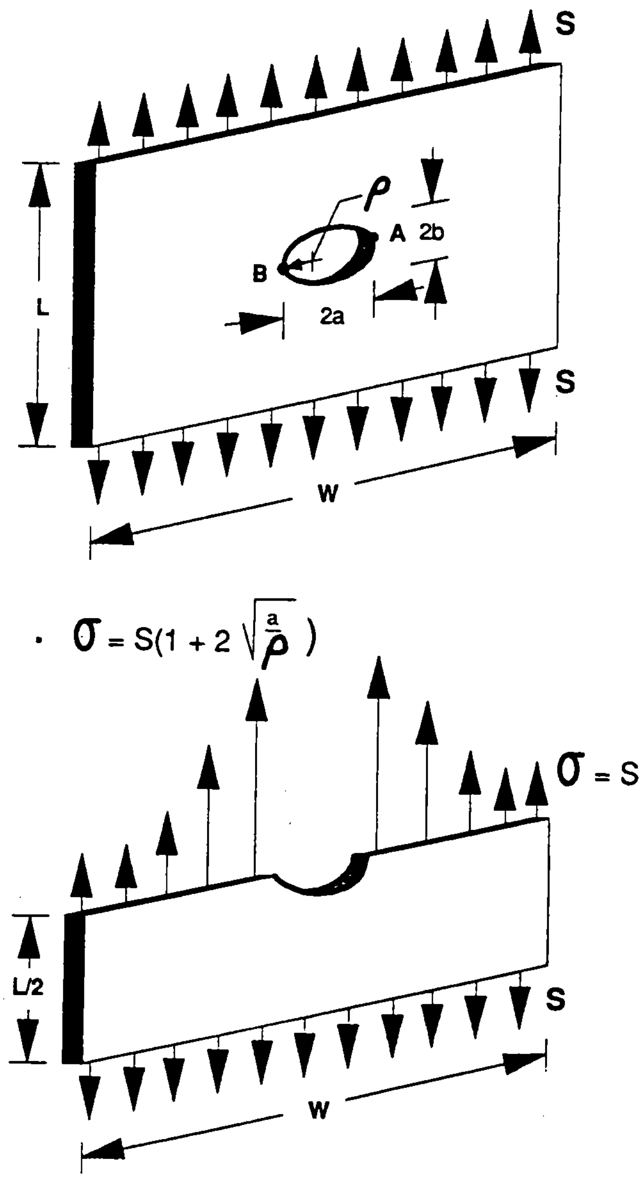

at A, B:

$$\sigma_{max} = S\left(1 + \frac{2a}{b}\right) = \left(1 + 2\sqrt{\frac{a}{\rho}}\right)$$

Figure 2-2. Elliptical hole in a large plate.

which is dependent on the geometry of the ellipse. For the limit of a circular hole, $\rho = a$ and $k_t = 3$. If we model a sharp crack as an ellipse for which $\rho \to 0$ then $k_t \to \infty$ and an infinite stress is predicted, which implies that a structure with a crack of any size will immediately fail! However, we know from experience that practical structural systems such as airplanes, automobiles, and railroad cars and tracks, have a multitude of cracks and defects, yet they very rarely fail in use.

It is reported [2-3] that Inglis was not welcomed at professional engineering society meetings for some years after his paper was published. Contemporary engineers certainly would have had no difficulty in recognizing the fact that most structures continued to stand, in defiance of the new theory, and they should have looked forward to challenging the theoretician. Perhaps they felt uncomfortable with a stress concentration factor, apparently supported by the principles of mathematics, but which increased without limit unless one was willing to fearlessly set an arbitrary minimum on the elusive crack tip radius, ρ. To take such a step in an affair concerning safe design practice, with no supporting data, is something most engineers would be reluctant to do.

It later turned out that the engineers' discomfort was well founded. The stress concentration factor could not be used reliably for crack problems. A different approach was needed. The first step in the new direction was taken in 1920 by Griffith [2-4], who based his approach on an energy balance analysis supported by experimental data.

Griffith introduced the idea of a sharp crack as a strength-limiting flaw from the results of a series of experiments on glass rods. It is of historical interest to note that Griffith worked for the Royal Aircraft Establishment in England, and one of his reasons for examining glass rods was to study failures in glass windshields on airplanes. He measured the breaking strengths of glass rods which were of the same diameter and original length, and he found a wide variation in their strengths. He then continued the experiment on the broken halves of the original rods, on the halves of the halves, and so forth, finding that the average breaking strength increased in each trial. He explained the results by postulating that glass contains surface cracks with randomly distributed sizes, and that the largest crack in a given specimen determines the strength of the specimen.

Thus, each trial breaks the largest cracks still present in the group of rods, and the increase of average strength in succeeding trials simply reflects a decrease in the sizes of the largest remaining cracks. Based on these experiments, he used a theoretical analysis to derive a relation between crack size and breaking strength by considering the energy balance associated with a small extension of a crack in an idealized brittle unbounded two-dimensional elastic medium. Griffith's approach is the basis for modern concepts of fracture mechanics.

Before discussing Griffith's energy theory, it is useful to review some elastic energy concepts. Figure 2-3 shows how we can account for the elastic energy stored in (a) a long slender rod loaded by a weight, and (b) a uniformly stressed thin plate.

First consider the rod, which has a length L, cross-sectional area A, with a material that has Young's modulus E. The force P from the attached weight will stretch the rod by some amount x, i.e., its length when loaded is $L+x$. Since we have assumed that the rod is elastic and obeys Hooke's law, it would stretch only half as much ($x/2$) if it had to support only half the weight. Furthermore, we can achieve the same result whether we add a second rod in parallel and identical to the first one, to support the entire weight, or if we use a single rod with twice the area. Conversely, if the two rods with area A are connected in series and the entire weight is hung at the bottom, each rod is loaded by the same force P and stretched by the same amount x. The total stretch in this case is then $2x$, a result we also could achieve by supporting the weight with a single rod of area A and length $2L$.

The results of these hypothetical experiments can be summarized by saying that the stretch is directly proportional to the applied load and the length of the rod, and inversely proportional to the rod's area. The constant of proportionality happens to be Young's modulus for the material from which the rod is made, so that:

$$x = \left(\frac{L}{EA}\right)P$$

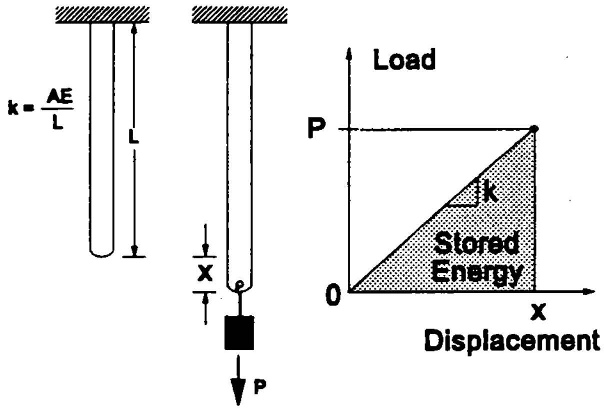

Strain energy $= \frac{1}{2}Px = \frac{1}{2}kx^2$

(a) Slender rod.

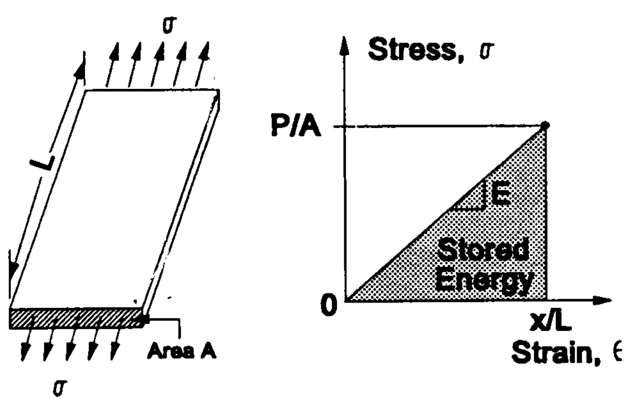

$\sigma = P/A$; Volume $V = AL$

Strain energy $= \frac{1}{2}\sigma\varepsilon V = \frac{1}{2}\sigma^2 V/E$

(b) Uniformly stressed thin plate.

Figure 2-3. Energy principles.

which can be rewritten as

$$P = kx$$

where the quantity $k = EA/L$ is called the stiffness of the rod. The equation $P = kx$ is represented by the straight line with slope k on the graph at the right of Figure 2-3(a).

Another way to interpret this equation is to consider the work done on the rod by the applied load as it simultaneously increases and moves through a distance equal to the stretch. Since the load is proportional to the stretch, the work done is represented by the shaded area under the line, or:

$$\text{Work} = \frac{1}{2}Px = \frac{1}{2}kx^2$$

This work is stored in the rod as internal energy, which can be thought of as a reservoir available to do work elsewhere when it is released.

The thin plate shown in Figure 2-3(b) behaves in the same manner, i.e., it possesses a stiffness, $k = EA/L$ determined by its cross-sectional area, length, and Young's modulus. The expression of Hooke's law for the plate can also be rearranged in the form:

$$\frac{P}{A} = E\frac{x}{L}$$

or

$$\sigma = E\varepsilon$$

This last equation is just the expression of Hooke's law for the material, in terms of the stress $\sigma = P/A$ and strain $\varepsilon = x/L$. It is also informative to rearrange the work/energy expression:

$$\text{Work (energy)} = \frac{1}{2}Px = \frac{1}{2}(A\sigma)(L\varepsilon)$$

or

$$\text{Work (energy)} = \left(\frac{1}{2}\sigma\varepsilon\right)(AL)$$

The quantity AL is just the total volume of the plate, and thus we can think of $\frac{1}{2}\sigma\varepsilon$ as the work or energy stored per unit volume. Substitution of Hooke's law provides the equivalent expressions:

$$\frac{1}{2}\sigma\varepsilon = \frac{\sigma^2}{2E} = \frac{1}{2}E\varepsilon^2$$

for this quantity, which is usually referred to as strain energy or strain energy density.

Griffith analyzed a system similar to the previously mentioned uniformly stressed plate, but considered the plate to have a pre-existing crack of length $2a$ as shown in Figure 2-4(a), with the corresponding load-displacement curve up to load P and displacement x. (The displacement x refers to the displacement of the load application points, as for example at the grips of a tensile testing machine.) He then analyzed the change in energy of the system if the crack were to grow by a small amount $2\Delta a$ with the load application points remaining fixed, i.e., the displacement x not changing. As the crack length increases, the plate becomes less stiff (more flexible) and the slope of the load displacement curve decreases as shown in Figure 2-4(b). The applied load for the case of a crack of length $2(a + \Delta a)$ then decreases from P to P-ΔP. The change in energy storage in the system, the strain energy decrease, is the *difference* in the two shaded energy storage triangles in Figure 2-4.

Griffith postulated that this release of elastic energy is used to overcome the resistance to crack growth. The resistance is a consequence of the surface energy required to break interatomic bonds and form the new crack surface, represented by $2\Delta a$. He reasoned that in order for a crack to elongate, the rate of strain energy release with crack extension must be equal to (or greater than) the rate of energy absorption required to overcome the resistance to crack growth.

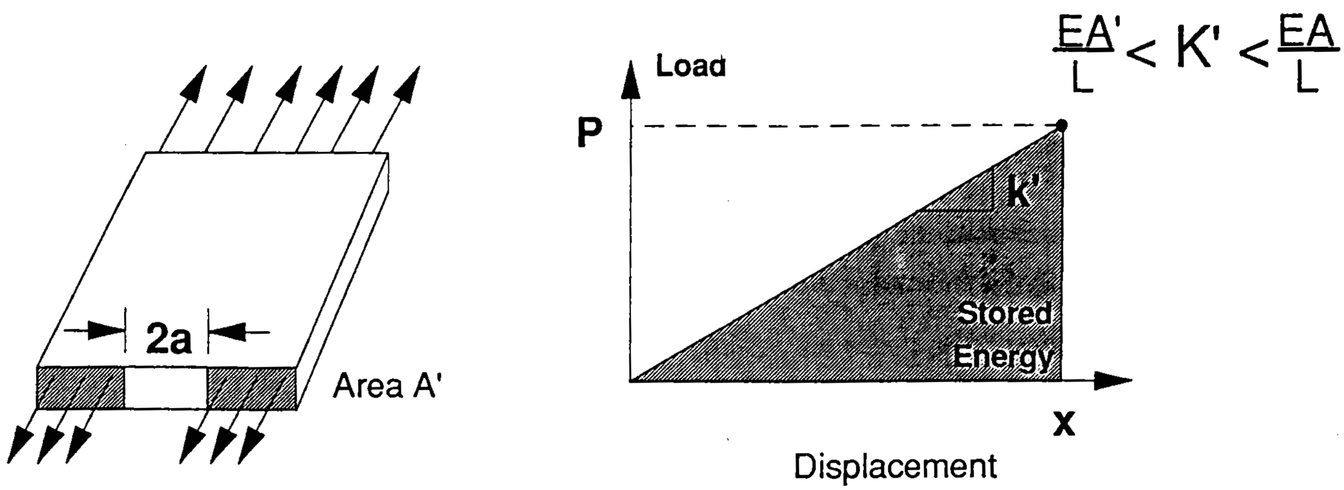

Stored energy $= \frac{1}{2}Px$

(a) Initial crack length 2a

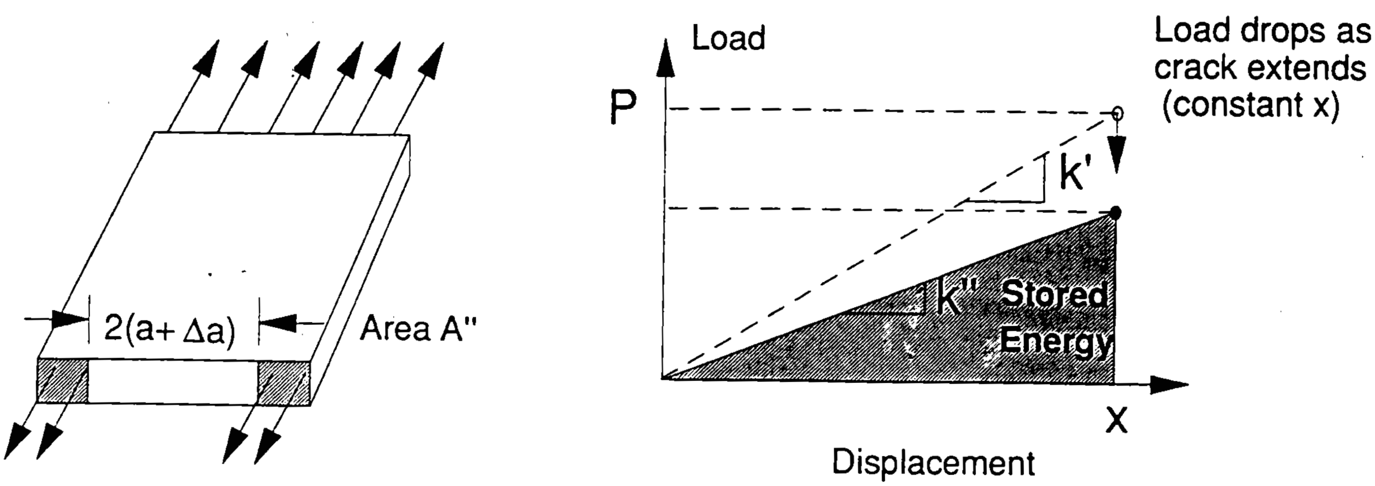

Stored energy $= \frac{1}{2}(P - \Delta P)x$

b) Elongated crack length $2(a + \Delta a)$

Figure 2-4. Energy principles for cracked plate.

Griffith used this energy principle to produce the following simple relation governing the onset of crack propagation from an existing crack:

$$\sigma_c \sqrt{a} = \text{constant} \tag{2-2}$$

where σ_c is the critical stress, a is half the original crack length, and the constant is a material property depending on the material surface energy and elastic modulus. Equation (2-2) indicates that crack extension occurs in an ideally brittle material when $\sigma\sqrt{a}$ reaches a constant critical value for a given material.

It is important to also consider the possibility that the boundaries of the structure can supply additional energy to make the crack propagate. For example, the flexibility of the testing machine could add system energy to the crack extension. Therefore, the testing machine should be much stiffer than the cracked plate being tested. In the fuselage of an aircraft, the pressurized air is also a source of additional energy.

The idea behind the energy balance can be explained in a simple and direct manner. If a crack in a body is imagined to extend, then the sum of energy remaining in the body after extension, work done on the body during the extension, and energy dissipated into irreversible processes occurring during the extension should equal the energy which was stored in the body before the extension. This is nothing more than a restatement of the fundamental physics principle that work and energy are equivalent, and that energy cannot be created or destroyed.

A convenient feature of the energy approach to problems in stress analysis is that we can take great liberties with the assumptions we make to define the problem. Taking such liberties may produce a solution in error by a large numerical factor, but the basic relationships between key variables are preserved. For example, consider the extension of the crack in the plate depicted in Figure 2-4. In order to simplify the analysis, we shall make the following assumption about the stress distribution in the cracked plate (see Figure 2-5).

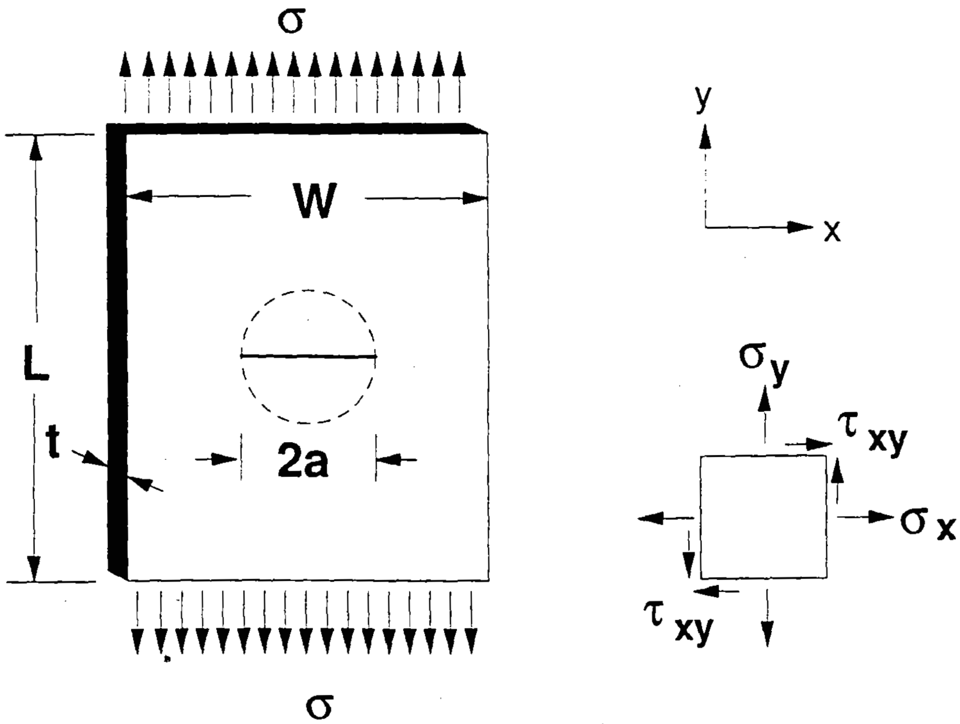

Figure 2-5. Plate with a center crack.

Draw a circle on the plate with the crack as its diameter. Assume that the stress σ_y is equal to the applied stress σ everywhere in the plate outside the circle, that $\sigma_y = 0$ everywhere inside the circle, and that all the other stress components are zero everywhere. Although this is not quite correct, since we expect stresses σ_x, σ_y and τ_{xy} to exist near the crack, the assumption quickly leads to a useful result when it is used in an energy analysis.

Let U_I be the strain energy stored in the plate in its initial state, when the crack length is $2a$. In an earlier example, we saw that the strain energy density in material uniformly stressed by $\sigma_y = \sigma$ could be expressed as $\sigma^2/2E$. The total energy is then the product of this density and the volume of the plate, less the volume in the unstressed circle:

$$U_1 = \frac{\sigma^2}{2E}[WLt - \pi a^2 t]$$

Now consider what happens when the crack is imagined to extend to the length $2(a + \Delta a)$, where the extension $2\Delta a$ is assumed to be extremely small compared to the original crack length $2a$, while the applied stress is assumed to remain constant. This last assumption corresponds to an experiment in which the plate is loaded by a dead weight, rather than by a testing machine with grips kept in a fixed position. In a real experiment, the dead weight would move, stretching the more flexible plate and thus doing work on it. Conversely, another curious and unrealistic property of the assumed stress distribution is that the strain $\varepsilon_y = \sigma/E$ remains constant, the plate does not stretch, and the weight remains stationary and does no work.

However, the energy U_2 stored in the plate after the crack extension is less than the original energy U_1. This follows directly from a consistent application of the stress distribution assumption:

$$U_2 = \frac{\sigma^2}{2E}\left[WLt - \pi(a + \Delta a)^2 t\right]$$

The elastic energy released by the crack extension is then:

$$U_1 - U_2 = \frac{\sigma^2}{2E}[2\pi at\Delta a + \pi t(\Delta a)^2] \cong \frac{\pi\sigma^2 at\Delta a}{E}$$

since the small quantity $\pi(\Delta a)^2$ can be neglected in comparison to $2\pi a\Delta a$.

It is more convenient to express the last result as the rate of energy released per unit of new crack surface area. The new area is $2t\Delta a$. The energy release rate per unit of new crack area (defined by the symbol G) is thus given by:

$$G = \frac{U_1 - U_2}{2t\Delta a} \cong \frac{\pi\sigma^2 a}{2E}$$

How are the new surfaces created? Evidently, the bonds between atoms lying on either side of a line extended from the crack tips must be broken, and energy is required to do this. Since the material is assumed to be homogeneous, we can postulate that the energy dissipated in the bond-breaking process, per unit of new surface area, is a constant property of the material. For historical reasons, physicists have always counted the upper and lower surfaces of a crack as separate areas, and the dissipation rate γ_e was defined accordingly. Thus, the energy account for the crack extension is represented by $G - \gamma_e$. We can now argue, as Griffith did, that the balance of $G - 2\gamma_e$ determines whether the crack will actually extend or not. If G is less that $2\gamma_e$, then more energy is needed to create the new surface than is released from the elastic storehouse, and the crack will not extend. Conversely, if G is greater than $2\gamma_e$, the crack will extend spontaneously, and the difference $G - 2\gamma_e$ will be dissipated in other ways (vibration and heating of the plate, sound, etc.).

The crack will also extend spontaneously if just enough energy is released, i.e., if $G = 2\gamma_e$. Substituting the expression previously derived for G and rearranging then leads to:

$$\sigma\sqrt{a} = \sqrt{\frac{4E\gamma_e}{\pi}}$$

Thus, we have derived from basic physical principles the result that the strength of a cracked body is determined by a relationship of the form $\sigma\sqrt{a}$ = constant.

Griffith's analysis was similar but was based on the accurately derived Inglis solution [2-2] for the stress around an elliptical hole. Consequently, Griffith was able to find the correct numerical results:

$$G = \frac{\pi\sigma^2 a}{E}$$

$$\sigma\sqrt{a} = \sqrt{\frac{2E\gamma_e}{\pi}} \tag{2-3}$$

In 1957, Irwin [2-5] reexamined the problem of the stress distribution around a crack. He used advanced mathematical methods to directly model a medium containing an idealized sharp cut, thus eliminating the crack-tip radius which had made the Inglis ellipse solution so controversial.

In order to understand the character of Irwin's solution, consider again the thin plate with a central crack of length $2a$ and uniform tension $\sigma_y = \sigma$ applied to the ends. We now focus our attention on a small area near one end of the crack, where polar coordinates (r, θ) are centered at the crack tip (Figure 2-6). Very close to the crack tip ($r \ll a$), Irwin's stresses are dominated by the terms:

$$\sigma_x = \frac{K_I}{\sqrt{2\pi r}} \cos\frac{\theta}{2}\left[1 - \sin\frac{\theta}{2}\sin 3\frac{\theta}{2}\right]$$

$$\sigma_y = \frac{K_I}{\sqrt{2\pi r}} \cos\frac{\theta}{2}\left[1 + \sin\frac{\theta}{2}\sin 3\frac{\theta}{2}\right] \tag{2-4}$$

$$\tau_{xy} = \frac{K_I}{\sqrt{2\pi r}} \cos\frac{\theta}{2}\sin\frac{\theta}{2}\cos 3\frac{\theta}{2}$$

$$\sigma_z = 0$$

where K_I is a scaling factor and z indicates out-of-plane direction. The stresses all increase without limit as the crack tip is approached ($r \to 0$), i.e., they behave in the way that Inglis predicted by modeling a crack as the limiting case of an elliptical hole. Thus, neither solution can be used to define a stress concentration factor. However, Irwin's scaling factor K_I does define the rate of stress concentration and thus provides a way to compare different situations. K_I is called a stress intensity factor to reflect its rate-measuring character and distinguish it from the stress concentration factors.

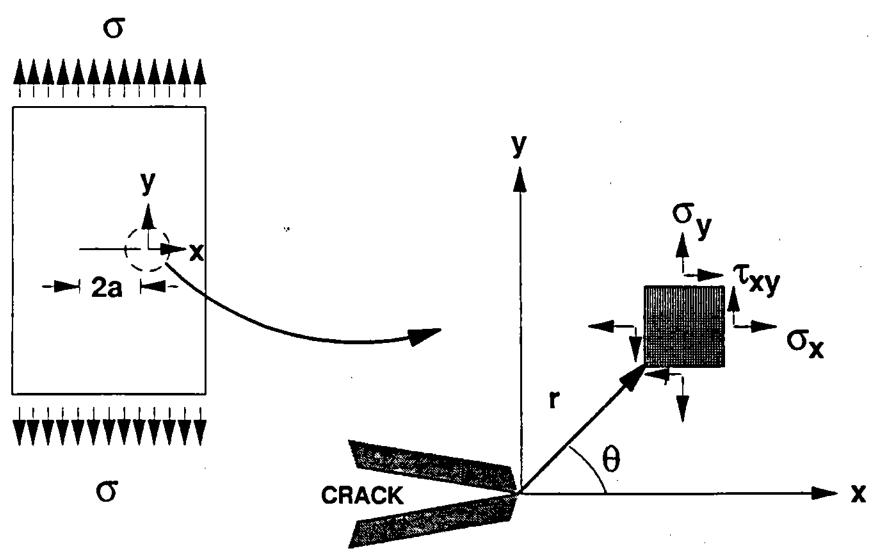

Figure 2-6. Stress components in Irwin's analysis.

For the case of a crack length much smaller than the length and width of the plate, Irwin found that

$$K_I = \sigma\sqrt{\pi a} \tag{2-5}$$

He thus established a connection between the stress intensity factor and Griffith's energy release concept, namely, that the combination $\sigma\sqrt{a}$ is the essential factor which determines the strength of a cracked body. Repeating Griffith's analysis of an imaginary crack extension, he showed that the stress intensity factor was related to the energy release rate by the formula:

$$G = \frac{K_I^2}{E}, \text{ plane stress} \tag{2-6}$$

for thin plates.

Griffith's analysis led to a criterion that the strength of a cracked body is determined by $G = G_c$, where G_c is a material property. It then follows that an equivalent criterion can be based on the stress intensity factor:

$$K_I = K_c \tag{2-7}$$

where K_c is a critical value based on material, loading, and geometry. In other words, a crack will propagate when the stress intensity factor reaches the critical value K_c.

Irwin also considered the case of a body for which the lateral dimensions are very small compared to the thickness. The limiting case for such thick bodies is plane strain condition. The front and back lateral surfaces of the body are assumed to be rigidly restrained against expansion or contraction in the through-thickness (z) direction. As a result, the strain ε_z is zero and the effect of Poisson's ratio induces a through-thickness stress $\sigma_2 = \nu(\sigma_x + \sigma_y)$ when the body is loaded by stresses σ_x and σ_y, even though these stresses are uniformly distributed through the thickness. Irwin's plane strain solution for the cracked plate discussed earlier has the same local stress terms as those given in equations (2-4), but contains the additional through-thickness stress:

$$\sigma_z = \nu(\sigma_x + \sigma_y) = \frac{2K_I}{\sqrt{2\pi r}}\nu\cos\frac{\theta}{2} \tag{2-8}$$

In the case of plane strain, the relation between the stress intensity factor and the energy release rate is changed to:

$$G = \frac{(1 - \nu^2)K_I^2}{E}, \text{ plane strain} \tag{2-9}$$

The elastic stress intensity factor has become one of the most commonly used means of translating material properties into structural behavior. Stress intensity factor solutions for numerous configurations of cracks in standard laboratory test specimens and cracks near typical structural details are now available in several handbooks [2-6 to 2-9]. Results are typically presented in the form

$$K_I = \beta\sigma\sqrt{\pi a} \tag{2-10}$$

where β is a function of crack length and key structural dimensions such as plate width. Formulae for stress intensity factor are determined from analytic procedures (stress analysis) or experimental techniques (photoelasticity). Some typical examples of center- and edge-cracked plates are shown in Figure 2-7. Additional examples are contained in Appendix A. The material between the crack tip and the edge of the plate is commonly called a ligament. For the edge-cracked plate shown in Figure 2-7(b), the ligament width is $(W - a)$.

The following simple example based on Figure 2-7 illustrates how the stress intensity factor concept is applied to find critical crack length. Suppose that a 10-inch wide plate is found to contain an edge crack 2 inches long. The plate is 1/4 inch thick and has a yield strength $Y = 39$ ksi. Its design limit load is 65,000 pounds, based on 2/3 of the material yield strength. Would the cracked plate be able to support its design limit load?

A laboratory test is conducted on a smaller specimen of the same material and thickness. The test specimen is 2 inches wide and contains a central crack 1 inch long. The test specimen fractures at a load of 10,000 pounds.

The formula from Figure 2-7(a) is first applied to find the material fracture toughness. From the laboratory test

$$\sigma_c = \frac{10,000}{Wt} = \frac{10,000}{2x0.25} = 20,000\,psi = 20\,ksi$$

$$a = 0.5 \text{ inch}$$

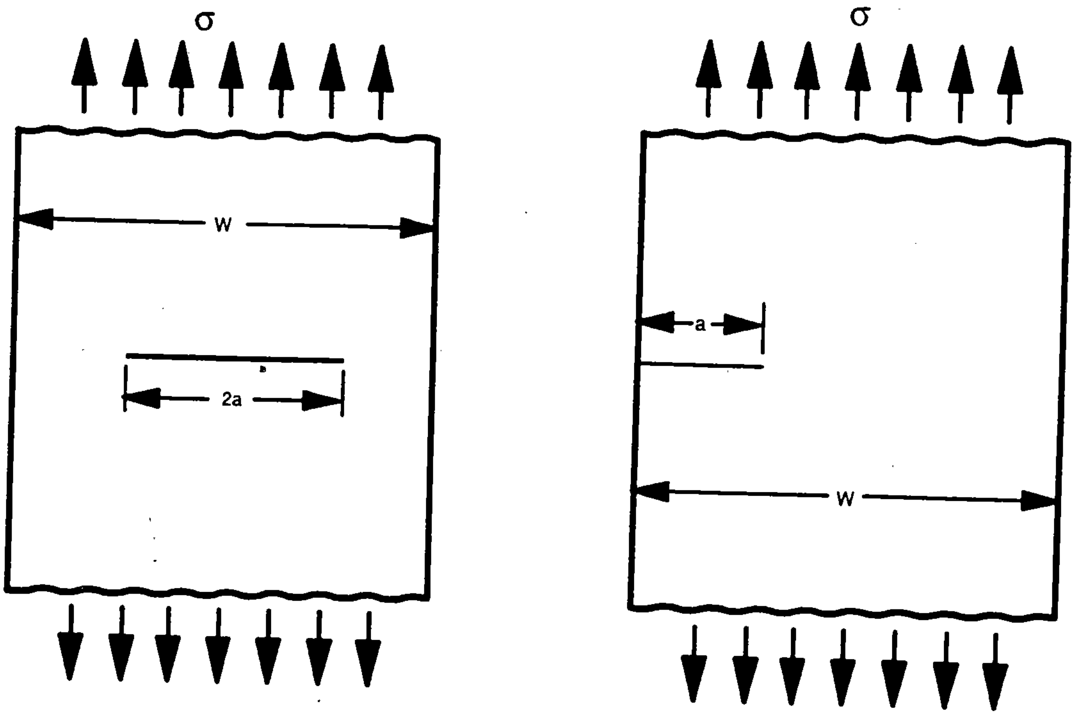

$$K_I = \beta\sigma\sqrt{\pi a}$$

$$\beta\left(\frac{a}{W}\right) = \left[\sec\frac{\pi a}{W}\right]^{\frac{1}{2}}$$

$$K_I \sim \sigma\sqrt{\pi a} \text{ for large } W$$

(a) Plate with center crack under tension.

$$K_I = \beta\sigma\sqrt{\pi a}$$

$$\beta\left(\frac{a}{W}\right) = 1.12 - 0.231\left(\frac{a}{W}\right) + 10.55\left(\frac{a}{W}\right)^2 - 21.72\left(\frac{a}{W}\right)^3 + 30.39\left(\frac{a}{W}\right)^4$$

(b) Plate with edge crack under tension.

Figure 2-7. Stress intensity factor formulae for some common geometries.

Thus, at the point of fracture:

$$K_I = \sigma_c \sqrt{\pi a} \left[\sec\left(\frac{\pi a}{W}\right) \right]^{\frac{1}{2}} = 20\sqrt{\pi \times 0.5} \left[\sec\left(\frac{\pi \times 0.5}{2}\right) \right]^{\frac{1}{2}}$$

$$K_I \cong 29.8 \; ksi\sqrt{in} = K_c$$

This value of fracture toughness is a material property and can be used to estimate the critical crack length for the edge cracked plate, based on the edge crack formula in Figure 2-7(b). At design limit load, $\sigma_{DLL} = \frac{2}{3}Y = 26 \; ksi$ and therefore:

$$\sigma_{DLL} \sqrt{\pi a}\, \beta\left(\frac{a}{W}\right) = K_c$$

$$26\sqrt{\pi a}\, \beta\left(\frac{a}{W}\right) = 29.8$$

Calculation with a few trial crack lengths is sufficient to find the critical length:

<u>a = 0.3 inch</u>

$a/W = 0.03$

$\beta = 1.12$

$K_I = 26 \sqrt{\pi \times 0.3} \times 1.12 = 28.27 < K_c$

<u>a = 0.4 inch</u>

$a/W = 0.04$

$\beta = 1.13$

$K_I = 26\sqrt{\pi \times 0.4} \times 1.13 = 32.93 > K_c$

From linear interpolation:

$\underline{a_c = 0.33\ inch}$

$a/W = 0.033$
$\beta = 1.12$
$K_I = 26\sqrt{\pi \times 0.33} \times 1.12 = 29.75 \cong K_c$

Based on the results of the small specimen test, the critical crack length for the 10-inch wide panel at design limit load is about 1/3 inch. Thus, not only would the panel with the 2-inch edge crack be unable to support the limit load, but also one would want to inspect other such panels quite carefully because of the short critical crack length.

2.1.1 Fracture Modes

The subscript "I" in the stress intensity factor K_I denotes the fact that K_I is associated with loads that apply tension across the crack and thus tend to open it. This type of loading is referred to as Mode I or the opening mode. Irwin also recognized the possibility that a crack might not be oriented directly across a tensile load, and he defined two other modes corresponding to shear loading. In one, the crack surfaces slide over each other perpendicular to the crack front (Mode II). In the other, the sliding is parallel to the crack front (Mode III). Mode III is usually called "tearing." The crack-tip stress intensity factors associated with the three modes are denoted by K_I, K_{II}, and K_{III}. Figure 2-8 illustrates the actions of the three basic loading modes.

Tension at any angle to the crack surface can always be resolved into equivalent components of tension across the surface, shear across the crack front, and shear parallel to the crack front.

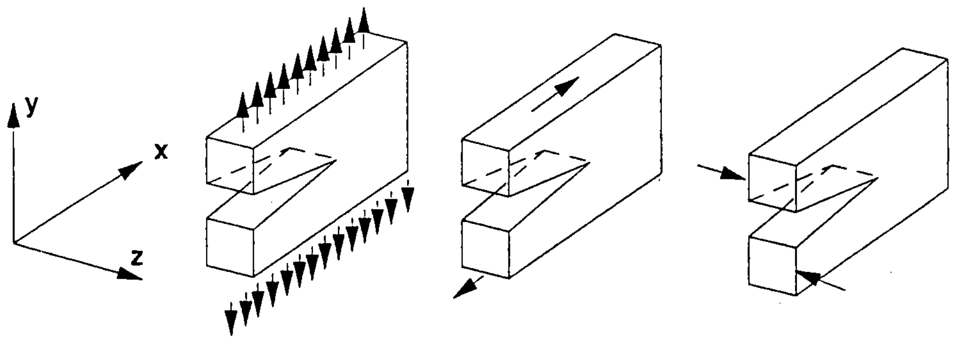

Mode I Opening

Mode II Shear

Mode III Tearing

Figure 2-8. Fracture modes

Thus, any case of interest can be completely described by three stress intensity factors, one for each basic mode. The near tip stress field for Mode I was given in equation (2-4). For Mode II, the dominant terms near the crack tip are:

$$\sigma_x = -\frac{K_{II}}{\sqrt{2\pi r}}\sin\frac{\theta}{2}\left[2 + \cos\frac{\theta}{2}\cos 3\frac{\theta}{2}\right]$$

$$\sigma_y = \frac{K_{II}}{\sqrt{2\pi r}}\sin\frac{\theta}{2}\cos\frac{\theta}{2}\cos 3\frac{\theta}{2}$$

$$\tau_{xy} = \frac{K_{II}}{\sqrt{2\pi r}}\cos\frac{\theta}{2}\left[1 - \sin\frac{\theta}{2}\sin 3\frac{\theta}{2}\right]$$

Mode III loading has an entirely different character. It induces only shear stresses through the thickness:

$$\tau_{xz} = -\frac{K_{III}}{\sqrt{2\pi r}}\sin\frac{\theta}{2}$$

$$\tau_{yz} = \frac{K_{III}}{\sqrt{2\pi r}}\cos\frac{\theta}{2}$$

2.2 EXTENSION OF LINEAR ELASTIC FRACTURE MECHANICS TO METALS

Griffith's energy theory and Irwin's stress intensity factor could easily be applied to explain fracture phenomena for brittle materials (glass, ceramics, etc.). The measured strengths of cracked bodies made of such materials appeared to be in agreement with the surface energy absorption rates G_c that could be estimated from the available physical test data. The conceptual problem posed by unbounded stresses could be explained away by simply arguing that the theory should not be expected to give an accurate picture of interatomic forces but nevertheless could get the "big" picture right at scales larger than a few hundred or a few thousand atoms, where the treatment of bodies as homogeneous continua made sense.

When the ideas of fracture strength were first extended to metals, the critical crack lengths measured in experiments were found to be much greater than the values predicted from physical estimates of the fracture surface energy absorption rate γ_e. The discrepancy was explained by Irwin [2-10] and Orowan [2-11], who recognized that the concentration of stresses near the crack tip would cause a metal to yield and undergo local plastic deformation. Orowan suggested adding a plastic energy absorption term γ_p to the surface energy term in the Griffith theory, i.e.:

$$\sigma\sqrt{a} = \sqrt{\frac{2E(\gamma_e + \gamma_p)}{\pi}} \qquad (2\text{-}11)$$

He also showed that $\gamma_p \cong 1000\,\gamma_e$ for typical metals, so that the original surface energy term γ_e could be neglected entirely.

Since it was based on fundamental physical principles, the concept of including plastic work in the energy balance had a natural appeal. However, it was not easy to translate the concept into engineering practice. It was difficult to measure the fracture energy absorption rate because experiments required extremely stiff, well-controlled surroundings to avoid excess elastic energy availability. Also, the elastic energy release rate in a loaded specimen was difficult to calculate with the computational tools available in the early 1960s, even assuming that dynamic effects could be entirely neglected during crack extension. These difficulties were compounded by the tendency of contemporary airframe stress engineers to be somewhat uncomfortable with energy as a basis for ranking structural design details.

On the other hand, the stress intensity factor concept began to be seen as the basis of a practical approach. It had the appeal of being something like the stress concentration factor, a concept long familiar to airframe engineers. It also eliminated the major difficulty associated with the Inglis approach by removing the need to assume anything about a crack-tip radius. There remained a conceptual problem, however, in applying an elastic solution to a problem which was acknowledged to involve plasticity.

This problem was resolved by arguing that the volume in which plastic deformation occurs is only a small part of the volume of the whole structure or test specimen. Thus, most of the strain energy released by crack extension is still released by elastic unloading, i.e., G or a stress intensity factor based on an elastic analysis still provides a good estimate for the energy available to drive a fracture, even though most of that energy is absorbed by plastic deformation.

The elastic solution can also be used to make an estimate of the plastic zone size. Figure 2-9 depicts a simplified model of the plastic zone, which is assumed to be bounded by a circle with one diameter lying on the x-axis ahead of the crack. The diameter of the circle defines the size of the plastic zone, and an approximate estimate for its value can be obtained from the local stress terms in the Irwin solution. The simplest estimate for Mode I loading is obtained by neglecting all stresses except σ_y in equation (2-4) and calculating the polar distance from the crack tip at which σ_y reaches the yield strength Y for $\theta = 0$. This leads directly to:

$$r_p \cong \frac{1}{2\pi}\left(\frac{K_I}{Y}\right)^2 \qquad (2\text{-}12)$$

Better estimates of the plastic zone shape can be obtained from numerical stress analyses in which the effect of yielding is taken into account. Figure 2-10 illustrates the general character of the plastic zone shape obtained using von Mises criterion in conjunction with an elastic analysis.

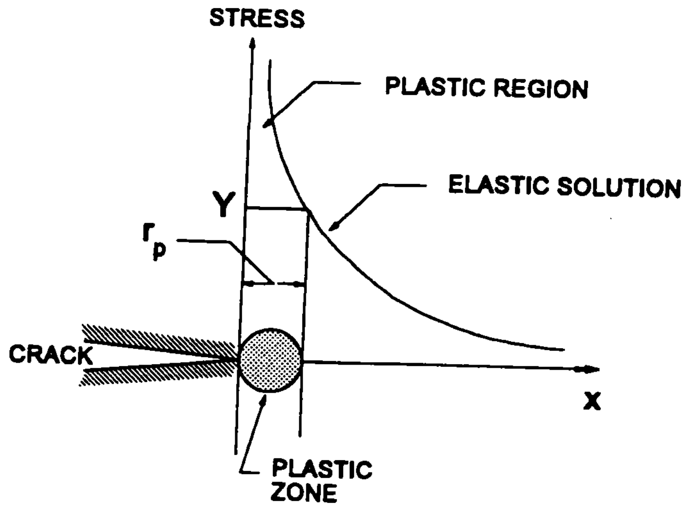

Figure 2-9. Plastic zone formation ahead of crack tip.

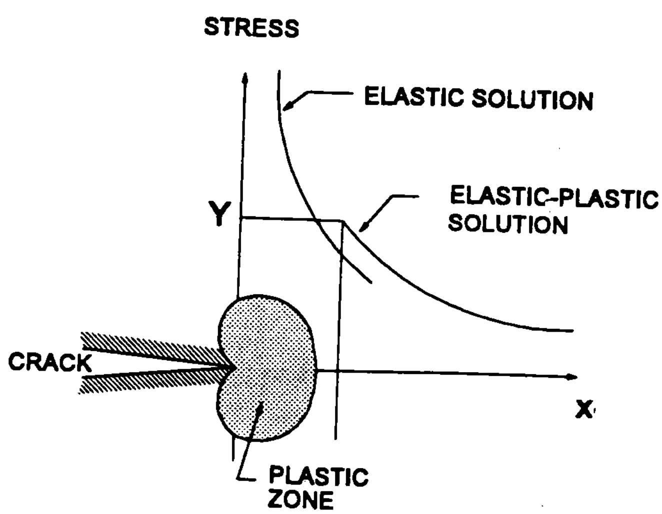

Figure 2-10. Refined estimate of plastic zone formation ahead of crack tip.

Also shown is the effect that yielding would have on the stress redistribution if an elastic-plastic analysis was performed.

2.2.1 Plastic Zone Size and the Mises-Hencky Yield Criterion

The size of the plastic zone can be estimated using an elastic solution. All of the stress components must be taken into account to determine whether the material yield strength has been exceeded. For ductile materials, the Mises-Hencky criterion is generally accepted as a predictor of the onset of yield. It is based on the premise that the portion of strain energy that causes change in shape is a measure of the yield strength of a material, Y. This notion can be applied by ensuring that Y is not exceeded by the value of an equivalent stress:

$$\overline{\sigma} = \sqrt{\tfrac{1}{2}\left[(\sigma_x - \sigma_y)^2 + (\sigma_y - \sigma_z)^2 + (\sigma_z - \sigma_x)^2\right] + 3\left[\tau_{xy}^2 + \tau_{yz}^2 + \tau_{xz}^2\right]} \qquad (2\text{-}13)$$

Material which has just reached the yield point (e.g., the plastic zone boundary) is defined by $\overline{\sigma} = Y$, or:

$$\tfrac{1}{2}\left[(\sigma_x - \sigma_y)^2 + (\sigma_y - \sigma_z)^2 + (\sigma_z - \sigma_x)^2\right] + 3\left[\tau_{xy}^2 + \tau_{yz}^2 + \tau_{xz}^2\right] = Y^2$$

Plastic zone size estimates can be obtained by substituting the local terms from the Irwin stress solution in the above equation and solving for the radius r at specific angular positions θ. For example, from the Mode I plane stress solution given in equations (2-4), the non-zero stress along $\theta = 0$ are:

$$\sigma_x = \sigma_y = \frac{K_I}{\sqrt{2\pi r}}$$

Substitution of these stresses into the previous relation then leads to:

$$\frac{1}{2}\left[\left(\frac{K_I}{\sqrt{2\pi r}} - \frac{K_I}{\sqrt{2\pi r}}\right)^2 + \left(\frac{K_I}{\sqrt{2\pi r}} - 0\right)^2 + \left(0 - \frac{K_I}{\sqrt{2\pi r}}\right)^2\right] = Y^2$$

$$r_p = \frac{1}{2\pi}\left(\frac{K_I}{Y}\right)^2 \qquad \text{(plane stress)} \qquad (2\text{-}14)$$

This result happens to be identical to the estimate obtained from σ_y alone, equation (2-12). However, a quite different result which includes the effect of Poisson's ratio is obtained for the case of plane strain:

$$\sigma_x = \sigma_y = \frac{K_I}{\sqrt{2\pi r}}, \quad \sigma_z = \nu(\sigma_x + \sigma_y) = \frac{2\nu K_I}{\sqrt{2\pi r}}$$

$$r_p = \frac{(1 - 2\nu)^2}{2\pi}\left(\frac{K_I}{Y}\right)^2 \qquad (2\text{-}15)$$

For aluminum alloys, $\nu \cong 1/3$, and the plastic zone size estimate becomes:

$$r_p \cong \frac{1}{18\pi}\left(\frac{K_I}{Y}\right)^2$$

As Figure 2-10 suggests, the distance from the crack tip to the edge of the zone can depend on the angle (theta). Figure 2-11 shows the plastic zone size approximations for plane stress and plane strain based on von Mises criterion.

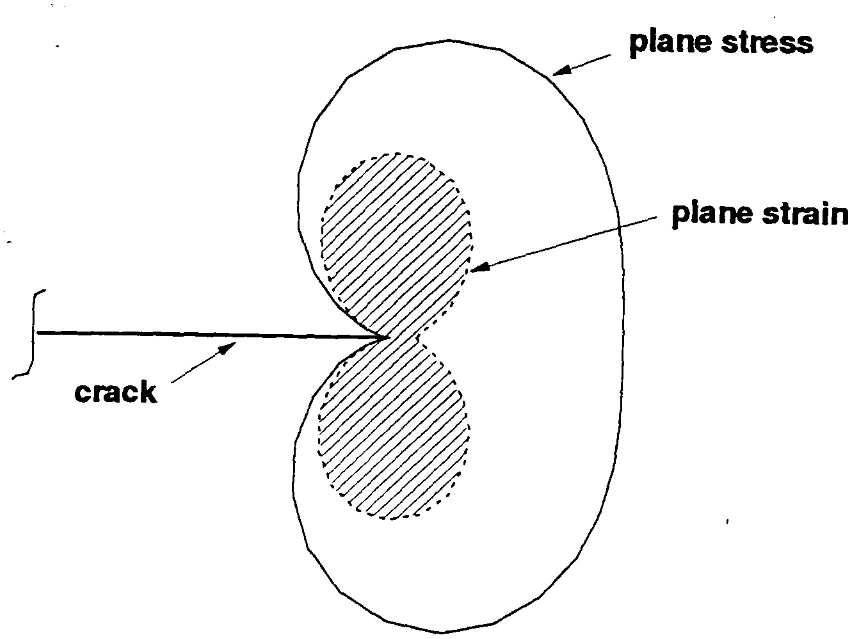

Figure 2-11. Plastic zone approximations based on von Mises criterion

Estimation of the size of the plastic zone is the basis for determining whether the requirement for small-scale yielding (SSY), the volume of plastic deformation is small in comparison to the volume of the entire test specimen, is satisfied.

As an indication of the radius of this plastic zone, consider the 10-inch plate with an edge crack (analyzed on pages 2-18 to 2-19) with $K_c = 29.8\ ksi\sqrt{in}$ and yield strength $Y = 39$ ksi. Using equation (2-12) with $K_I = K_c$ to represent the onset of fracture, produces $r_p = 0.09$ inches.

This radius is quite small in comparison with the lateral plate dimensions. While r_p is also less than the 1/4-inch thickness of the plate, satisfaction of SSY is marginal in this situation. Application of the R-curve techniques or plane strain described in Section 2.4.1 may be needed.

2.3 FRACTURE TOUGHNESS TESTING

A material is characterized in a laboratory setting by measuring the load at which a standard cracked specimen fails. One of the most widely used procedures is the ASTM E-399 plane strain fracture toughness test [2-12] with the so-called Compact Tension Specimen (CTS). Figure 2-12 illustrates a CTS, together with the definition of its dimensions and its stress intensity factor formula.

The stress intensity factor for the CTS does not contain the usual $\sigma\sqrt{\pi a}$ combination because it is given directly in terms of the total applied load P. The effect of crack length appears in $f(a/W)$. The values of $f(a/W)$ are plotted in Figure 2-13 for $0.45 \leq a/W \leq 0.55$, the range of crack lengths allowed in order for the test to be valid.

The CTS has become popular because it is one of the easiest specimens to machine from structural sections and forgings with different crack orientations relative to the structure.

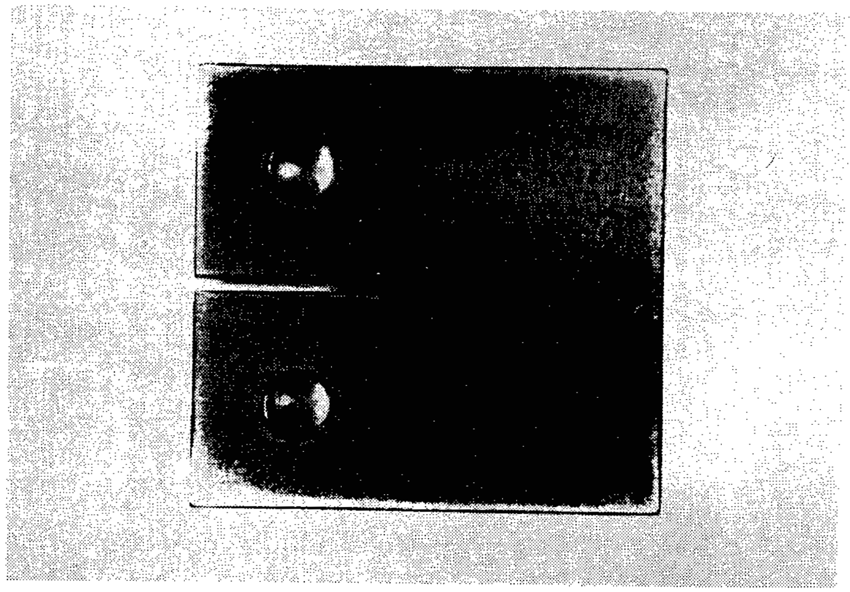

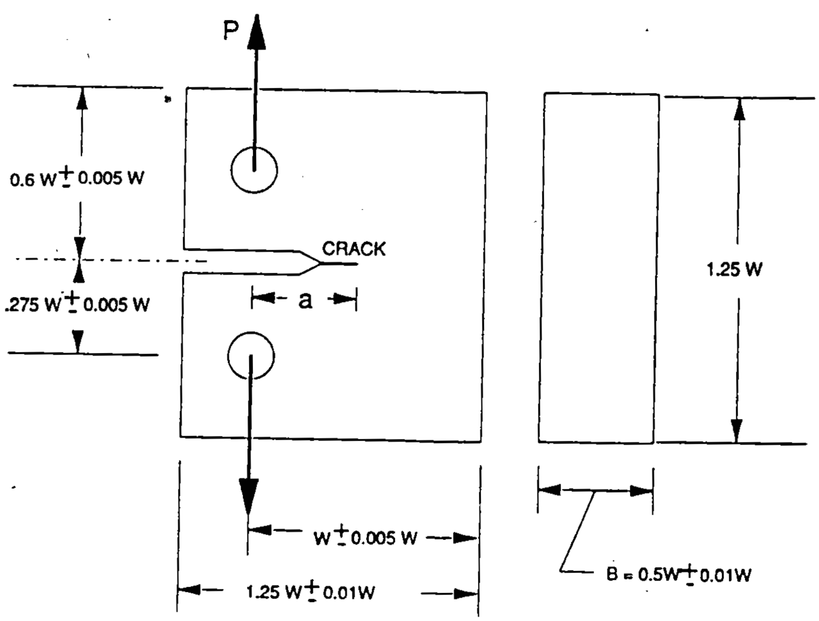

$$K_I = \frac{P}{B\sqrt{W}} f(\alpha), \ \alpha = a/W$$

$$f(\alpha) = \frac{(2 + \alpha)[0.886 + 4.64\alpha - 13.32\alpha^2 + 14.72\alpha^3 - 5.6\alpha^4]}{(1 - \alpha)^{3/2}}$$

Figure 2-12. The compact tension specimen.
[Photograph by permission from Professor R. Pelloux, MIT]

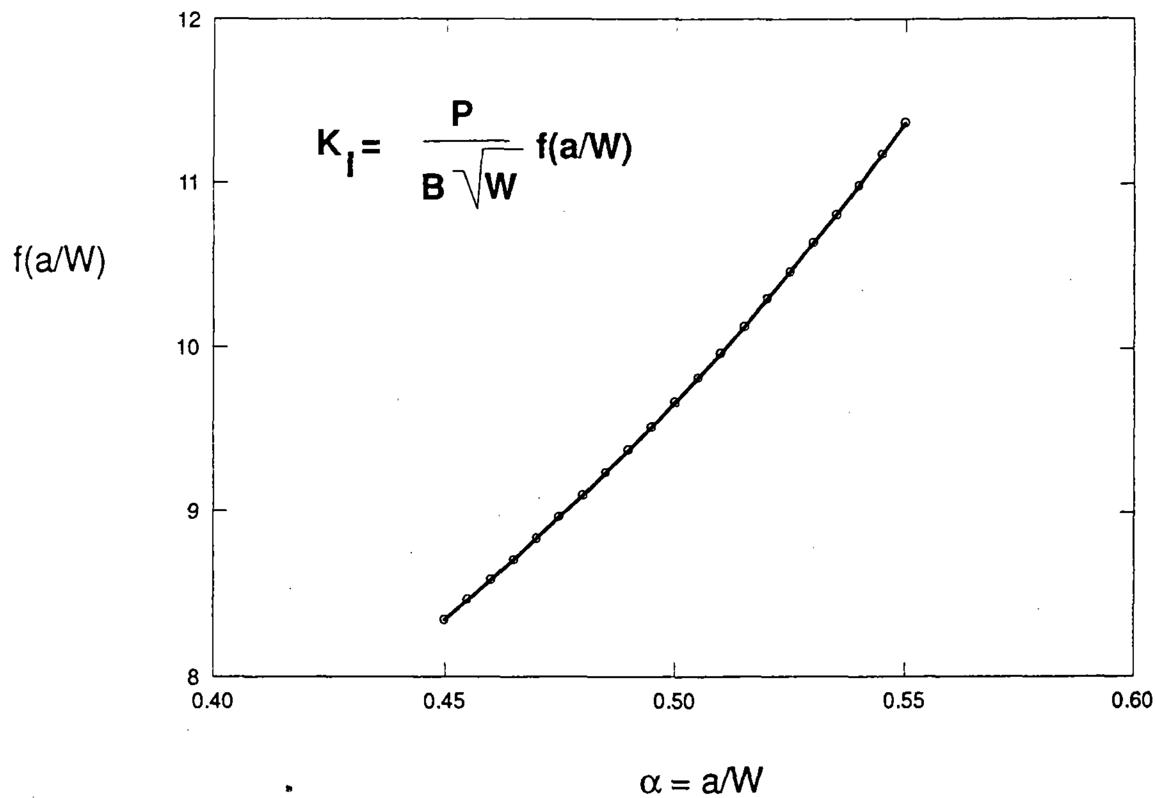

Figure 2-13. CTS stress intensity factor versus crack length.

For example, up to six orientations may be required to fully characterize the material in a thick-section plate or forging. Figure 2-14 illustrates these orientations and summarizes their nomenclature. Two letters describe each orientation: the first indicates the direction of loading and the second the direction of the crack. The test specimen orientation must be specified because the fracture toughness of the material can be affected by its microstructure. The most influential orientation factor in the microstructure is the grain shape. Metal starts as a casting in which the average grain dimensions are isotropic. In rolled or extruded stock, the grains are plastically stretched by a large amount in the rolling or swaging direction and by a lesser amount in the transverse direction for rolled sheet stock. LT and TL are the orientations most commonly tested to characterize plate stock, since they represent through cracks. The LS and TS orientations would best represent surface cracks.

The CTS is machined with a notch designed to act as a crack starter. The specimen is cycled at a low load level to initiate the crack and extend it to a length within the acceptable range

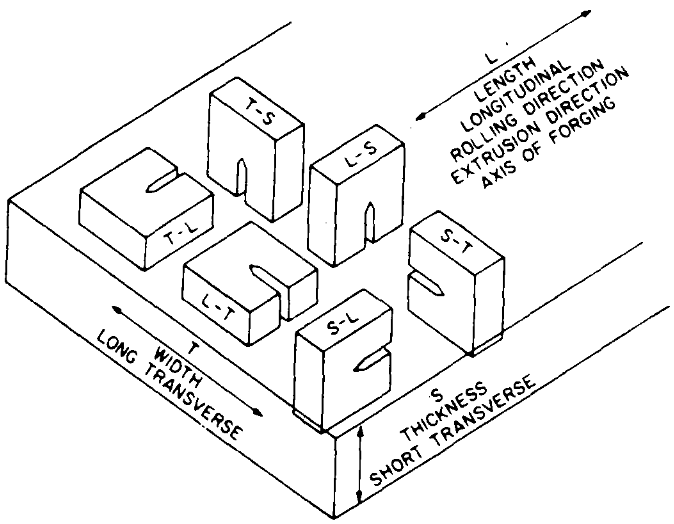

Figure 2-14. CTS orientation.

[Reprinted from Damage Tolerant Design Handbook, 1975, Fig. 2.0-1a, by permission of Battelle, Columbus, Ohio.]

$0.45 \leq a/W \leq 0.55$. (The crack is monitored by means of travelling microscopes, which are focused on the area ahead of the notch on the front and back faces.) The test is then performed by slowly increasing the applied load until the specimen fractures.

After testing, the crack length at which the fracture initiated is measured at three locations. The crack length "a" is defined as the average of the three measurements, and the test is not accepted if the difference between any two measurements is more than 10 percent of the average. The criterion is designed to avoid errors due to specimen misalignment in the testing machine and/or excessive influence of near-surface (plane stress) conditions. (Additional criteria which depend on the notch machining details are given in ASTM Specification E-399.)

Close attention is also paid to the plot of applied load versus displacement of the testing machine grips. A candidate load P_Q for use in the stress intensity factor formula is defined based on the type of load-displacement plot obtained (see Figure 2-15). In each case, the initial slope of the plot $(P/v)_o$ must first be measured, and a straight secant line is then constructed from the origin with a slope of $0.95\ (P/v)_o$. The intersection of the secant line with the plot defines a load called P_5. The candidate load P_Q is then taken to be equal to P_5 or the maximum load P_{max}, depending on the type of load-displacement plot obtained. A candidate fracture toughness value is then calculated from the test conditions and results:

$$K_Q = \frac{P_Q}{B\sqrt{W}} f\left(\frac{a}{W}\right) \tag{2-16}$$

The candidate fracture toughness value is not accepted as valid unless the crack front criteria mentioned above are met and, in addition:

$$P_{max}/P_Q \leq 1.1$$

$$2.5\left(\frac{K_Q}{Y}\right)^2 < a$$

$$2.5\left(\frac{K_Q}{Y}\right)^2 < B \tag{2-17}$$

The additional criteria ensure that the test has actually produced a fast fracture, and that the smallest significant dimensions in the test (the crack length and specimen thickness) are at least on the order of 50 times the plane strain plastic zone size.

If all the above criteria are met, then the candidate K_Q value is accepted as a valid measurement of the material's plane strain fracture toughness. This property is denoted by the special symbol K_{IC}.

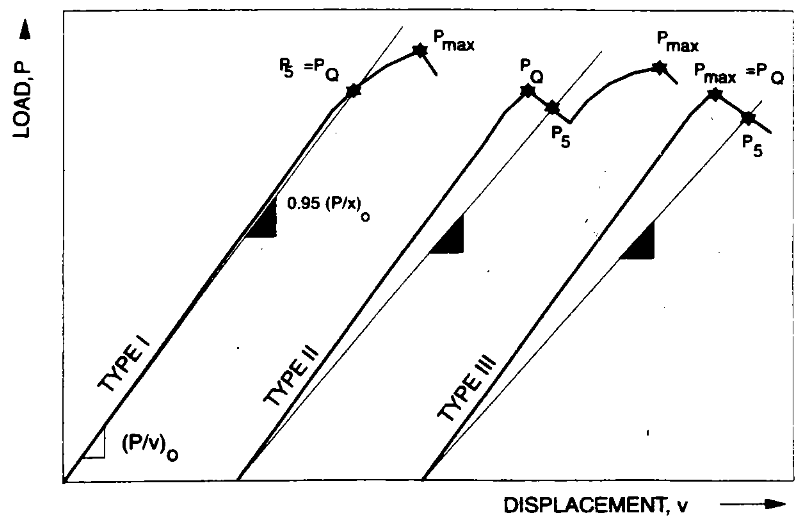

Figure 2-15. Load-displacement plot

[Adapted from John M. Barson/Stanley T. Rolfe, Fracture and Fatigue Control in Structures: Applications of Fracture Mechanics, 2e © 1987, p 73. Reprinted by permission of Prentice Hall, Englewood Clifts, New Jersey.]

Table 2-1 Properties of some common structural materials.

[from R. Pelloux, MIT, by permission] (see Figure 2-13 for orientations)

<u>Aluminum Alloys</u>				
2024 T3:	F_{tu}	LT*	66 (455) ksi (MPa)	
		L	67 (461) ksi (MPa)	
	F_{ty}	LT	45 (310) ksi (MPa)	
		L	50 (345) ksi (MPa)	
	ε%	LT	18	
2024 T851		LT	TL	SL
Typical	$K_{IC}[ksi(MPa\sqrt{m})]$	22(24.2)	20(22)	17(18.7)
2124 T851		LT	TL	SL
Typical	$K_{IC}[ksi(MPa\sqrt{m})]$	29(31.9)	24(26.4)	24(26.4)
2124 T851	F_{tu}	LT	66(455) ksi (MPa)	
	F_{ty}	LT	57(395) ksi (MPa)	
	ε%	LT	8	
<u>Low Alloy High Strength Steel (Q&T)</u>				
AISI 4340	UTS	200 ksi	250 ksi	300 ksi
	Yield	180 ksi	240 ksi	290 ksi
	K_{IC}	$80\ ksi\sqrt{in}$	$60\ ksi\sqrt{in}$	$50\ ksi\sqrt{in}$
	UTS: Ultimate tensile strength			
<u>Maraging Steel</u>				
	UTS	250 ksi		
	Yield	240 ksi		
	K_{IC}	$100\ ksi\sqrt{in}$		

Table 2.1 Properties of some common structural materials. (continued)

Titanium				
Ti 6Al-4V Equiaxed			K_{IC}	
	Yield	130 ksi (910 MPa)	$40-60\ ksi\sqrt{in}$	$44-66\ MPa\sqrt{m}$
Ti 6Al-6V-2 Sn			K_{IC}	
	Yield	155 ksi (1085 MPa)	$30-50\ ksi\sqrt{in}$	$33-55\ MPa\sqrt{m}$
Stainless Steel				
			K_{IC}	
17-7 PH	Yield	171 ksi (1180 MPa)	$32\ ksi\sqrt{in}$	$35\ MPa\sqrt{m}$
	*		K_{IC}	
A286	Yield	112 ksi (769 MPa)	$152\ ksi\sqrt{in}$	$167\ MPa\sqrt{m}$
Low Alloy Medium Strength Steel				
	Yield	$170\ ksi\ (1175\ MPa)$		
	0.35% C	0.65% Mn 0.3% Mo	0.35% Si 0.1% V	3% Ni 0.8% Cr
	at			
	0° C	$K_{IC} = 110\ ksi\sqrt{in}$		
	-100° C	$K_{IC} = 60\ ksi\sqrt{in}$		

(ref.): Application of Fracture Mechanics for Selection of Metallic Structural Materials, Eds. J. E. Campbell, W.W. Gerberich, and J.H. Underwood, ASM 1982.

*Long Transverse

Since within certain limits, K_{IC} is known for a given material, the engineer can use this value to predict critical combinations of stress and crack length for many different configurations, once stress intensity formulas such as those shown in Figure 2-7 are established.

It is worth repeating here that K_I represents the stress intensity applied to a sharp crack in any material, whereas K_{IC} represents the ability of a specific material to resist fracture. In other words, the applied loads and the stress analysis determine K_I, while the material property establishes that fracture will occur when K_I reaches K_{IC}.

2.3.1 Thickness Effects

Why is so much attention paid to plane strain fracture toughness when so many structural components are made of thin sheet stock? The plane strain condition separates the basic material behavior from thickness effects. A change of thickness does not appreciably affect conventional material properties. If the yield strength of a material has been determined by testing a specimen one inch thick, then we expect stock from 1/10 to 10 inches thick to have more or less the same strength.

Conversely, the strength of a cracked thin sheet is a strong function of thickness. Measurements of candidate fracture toughness K_Q typically follow a curve similar to the schematic example in Figure 2-16. The results tend to approach the valid plane strain fracture toughness K_{IC} in specimens thicker than 1/2 inch. For thinner stock, however, K_Q at first increases as the thickness decreases and then declines after reaching a peak (generally at a thickness somewhat less than 1/8

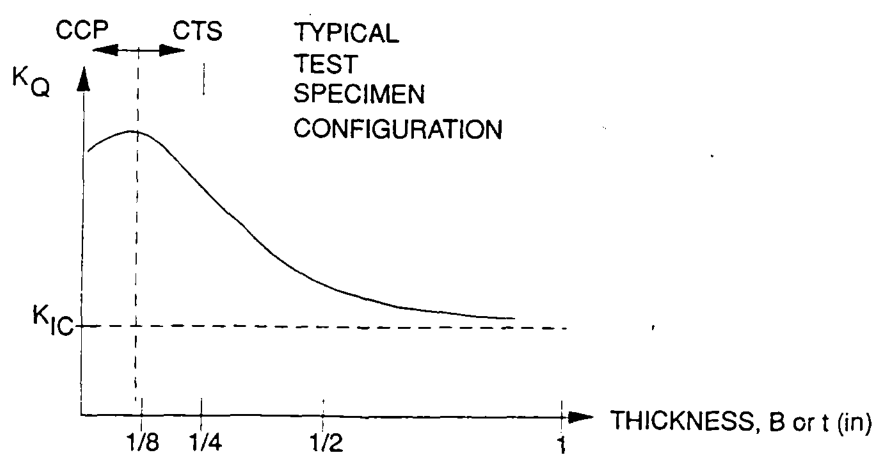

Figure 2-16. Thickness effect on fracture strength.

inch).[1] The peak K_Q value can exceed five times K_{IC} for some materials. Hence, the appropriate K_Q should be used in damage tolerance analysis. Note that K_C is used to denote a K_Q value corresponding to plane stress conditions.

The thickness effect can be explained in terms of Griffith's energy balance idea, taking into account the influence of plastic zone size. Figure 2-17(a) shows how the plastic zone varies through the thickness of a plate, along the crack front. Since σ_z must be zero at the stress-free faces, the surface condition is plane stress, and the plastic zone is large. Well inside the specimen, the surrounding elastic material restrains deformation in the *z*-direction. If the specimen is thick enough, the interior deformation is almost totally restrained ($\varepsilon_z \approx 0$), the condition is plane strain, and the plastic zone is small. Going inward from the surface, the plastic zone undergoes a transition from larger to smaller size. The rate at which this transition progresses is approximately independent of the total thickness.

Figure 2-17(b) illustrates end views of the plastic zones in plates of decreasing thickness. It is evident that, as the thickness decreases, the ratio of total plastic volume to total thickness increases. It then follows that the energy absorption rate per unit thickness must increase. Conversely, the elastic stresses which provide the strain energy storehouse are uniform through the thickness in most of the plate volume. Thus, the strain energy release rate is approximately independent of thickness. When these factors are accounted for in the energy balance, it follows that the thinner the plate, the more applied stress is needed to extend a crack. In other words, the fracture toughness increases.

The plane stress effect leaves behind physical evidence of its presence on the fracture surface. Under plane stress conditions the fracture plane tends to be tilted at a 45° angle to the *z*-axis, unlike the plane strain condition which produces a fracture plane parallel to the *z*-axis. The tilted regions are referred to as shear lips (Figure 2-18). The fracture surface of a valid K_{IC} test will

[1] Stock less than 1/4 inch thick is generally tested in the form of a center cracked panel (Figure 2-7(a)) rather than a CTS.

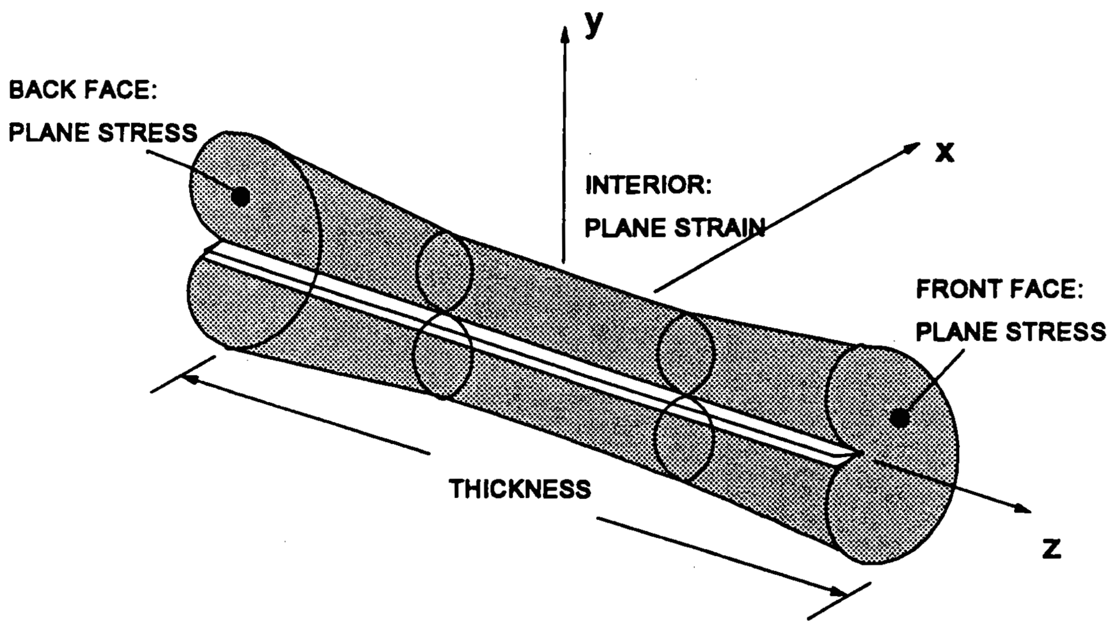

(a) Three-dimensional plastic zone shape.

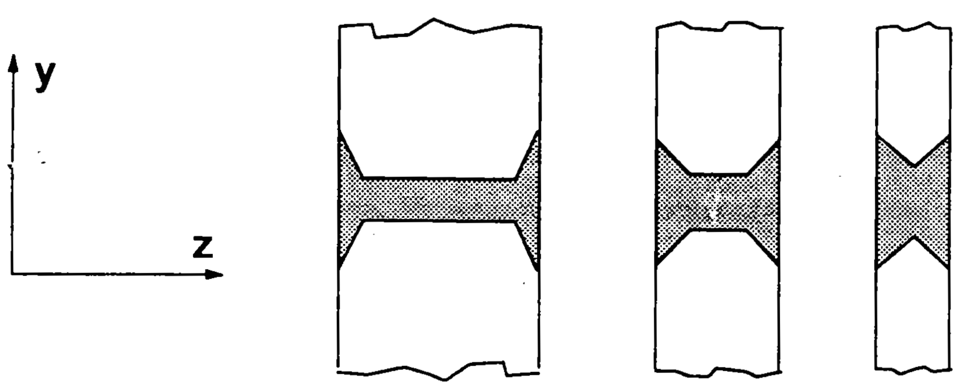

(b) Plastic volume versus thickness.

Figure 2-17. Plane stress-plane strain transition.

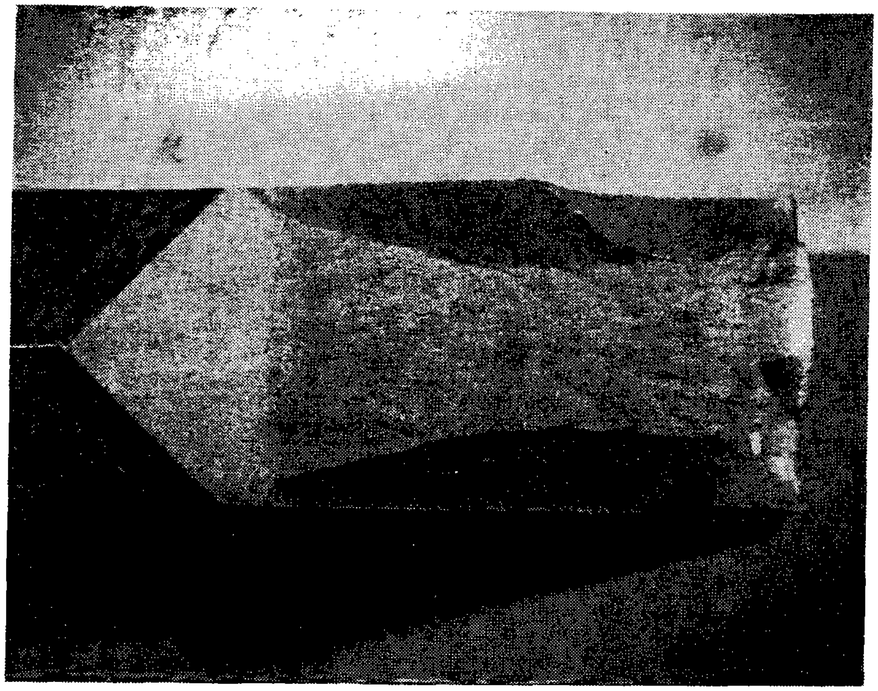

Figure 2-18. Typical fracture surfaces.

have little or no evidence of shear lips. Conversely, a fracture surface with a high percentage of shear lip indicates that plane stress conditions dominated the fracture.

The foregoing analysis does not explain why K_Q eventually declines as the thickness is decreased still further. This phenomenon is a result of an increase in the strain energy release rate which overpowers the energy absorption rate increase associated with plane stress conditions. A complete stress analysis of the region around the crack (not just the crack tip locality) shows that the stress σ_x is compressive in the areas above and below the crack (Figure 2-19).

A well-known property of thin plates loaded in compression is that they will buckle at some critical stress proportional to the square of the ratio of thickness to unsupported span. (The constant of proportionality depends on the manner in which the edges of the plate are supported.)

Evidently, the areas above and below the crack should behave in the same way, with a buckling stress proportional to $(t/a)^2$. For a given crack length, it then follows that there will be some thickness t_{cr} for which the compressive stress σ_x induced by the crack is just enough to cause local buckling when the applied stress is high enough to extend the crack. For $t < t_{cr}$, buckling occurs and releases additional strain energy to drive the crack. The thinner the plate or the longer the initial crack, the more strain energy is released, and this is why K_Q declines.

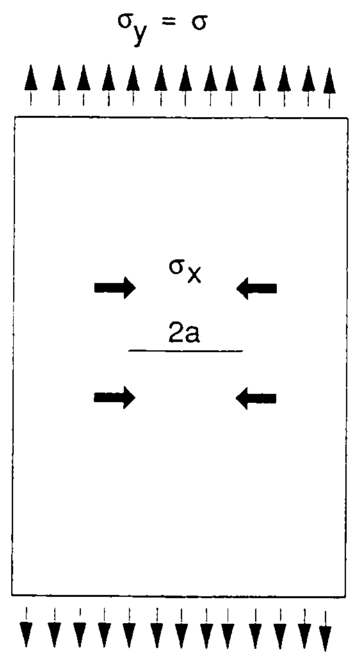

Figure 2-19. Lateral compression above and below the crack.

Lateral buckling deflects the areas above and below the crack out of the xy plane, as shown in Figure 2-20. This has the additional effect of applying a small amount of Mode III loading to the crack tips, and fractures of this type are usually described as tearing. The lateral buckling phenomenon can be easily observed if load is applied slowly in one of the aluminum foil experiments with a long initial crack.

2.3.2 Temperature Effects

The fracture toughness of a metal also depends on its temperature when tested. As its temperature decreases, a metal becomes less able to accommodate the intense crack-tip stresses by yielding, and the energy absorption rate γ_p decreases. As a result, K_{IC} is found to decrease

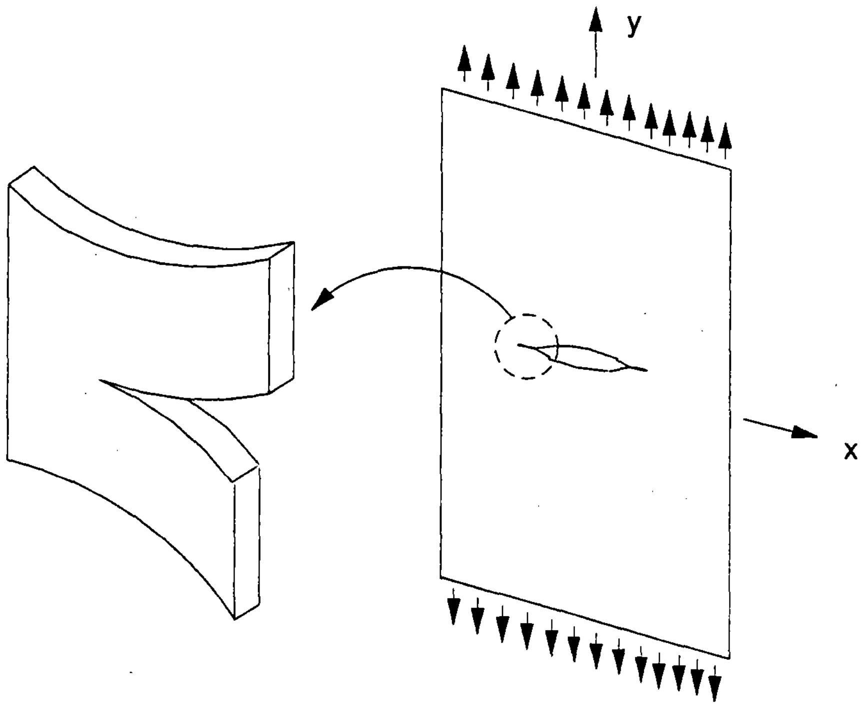

Figure 2-20. Lateral buckling and tearing.

with temperature, generally following an S-shaped curve like the schematics in Figure 2-21. This phenomenon is sometimes referred to as a ductile/brittle transition.

Aluminum alloys are relatively insensitive to temperature over the range corresponding to aircraft service conditions, but must be tested at low temperatures to obtain the correct K_{IC} value for applications such as pressure tanks designed to hold cryogenic liquids (LOX, LH, etc.). Conversely, many steel alloys exhibit a sharp transition in the service temperature range, and the complete transition curve is required to assess the structural strength at the lowest anticipated service temperature.

2.4 FAILURE IN THE PRESENCE OF LARGE-SCALE YIELDING

Other means of strength assessment are required for structures which do not meet the small-scale yielding condition. A variety of different methods and strength parameters have been developed

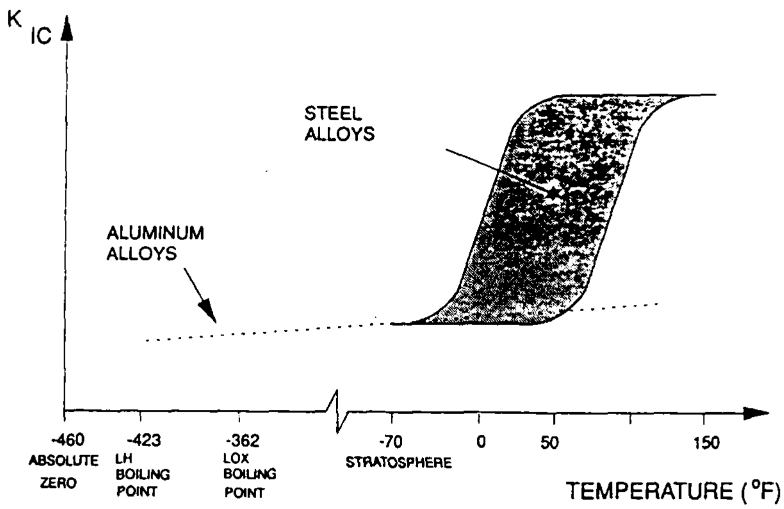

Figure 2-21. Fracture toughness versus temperature.

to deal with such situations. The R-curve method (Section 2.4.1) and the net section failure criterion (Section 2.4.2) are widely used in the aeronautical industry. Both approaches have prominent roles in airframe damage tolerance evaluation. Four other approaches, subjects of theoretical and experimental research for many years, have not yet attracted industry attention but might be used in the future. The crack opening displacement and "J-integral" approaches (Sections 2.4.3 and 2.4.4) are concepts for alternative strength properties used in place of fracture toughness. The strain energy density criterion (Section 2.4.6) and the plastic collapse model (Section 2.4.7) are methods for dealing with mixed-mode loading and three-dimensional cracks.

2.4.1 Resistance Curves

The resistance curve or "R-curve" method was developed to provide reliable estimates for the damage tolerance of plain or stiffened thin-skinned panels [2-13 to 2-17]. Early attempts to use the apparent fracture toughness K_C (Section 2.3.1) as a fracture stability limit analogous to K_{IC} gave inconsistent results.

The key to understanding thin-sheet fracture was discovered when researchers began to pay close attention to the behavior of long initial cracks in large sheets as the applied stress was increased toward the critical value. Based on the fundamental energy balance concept (Section 2.1), one would not expect the crack to extend at all until the stress reached the critical value. Thick-section specimens tended to behave as expected, although a small amount of crack extension just before fracture was sometimes reported for intermediate thicknesses.[2] Conversely, measurements made on thin sheets showed that a considerable amount of stable crack extension would occur at stresses well below the critical value. Figure 2-22 compares the different types of behavior in terms of applied stress intensity factor.

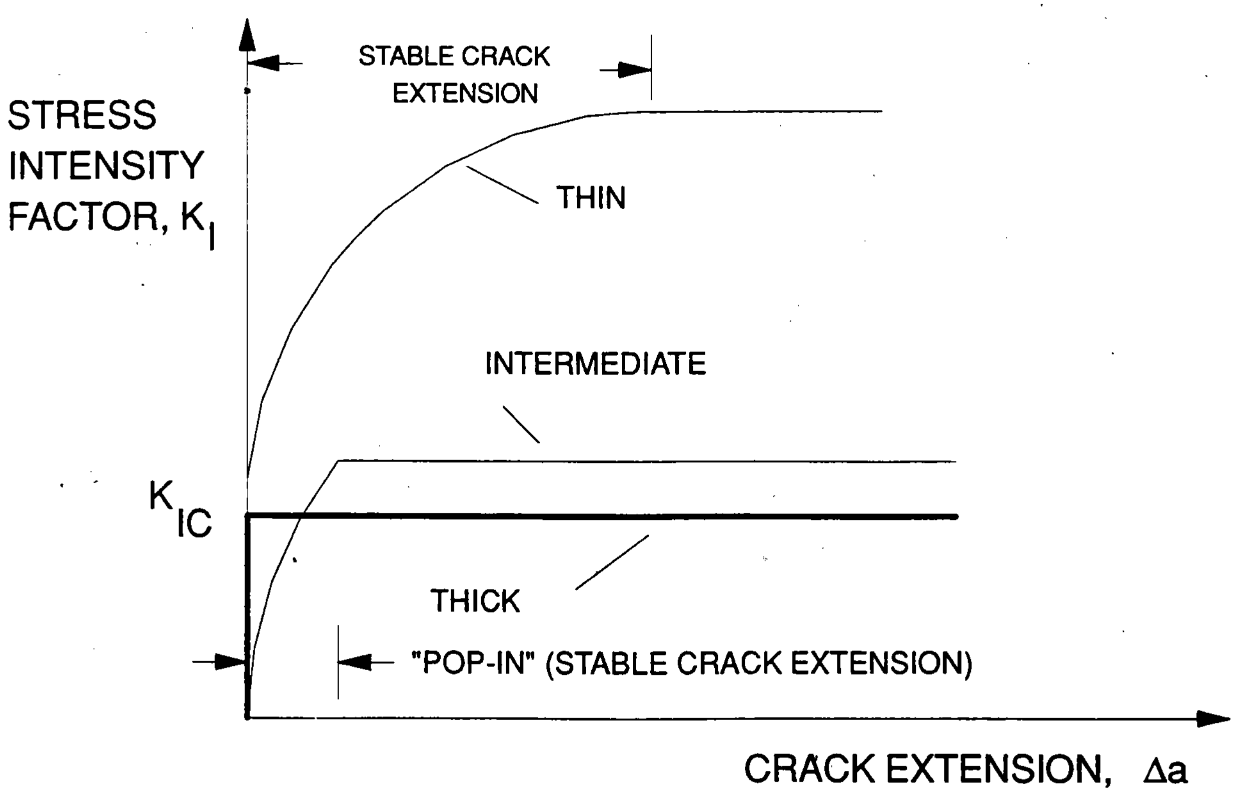

Figure 2-22. Load versus crack extension for different thicknesses.

[2] This phenomenon is called "pop-in."

The concept of the R-curve method is that stable crack extension is a material property which can be described as a relation between a stress intensity factor K_R (obtained from a test) and crack extension Δa, independent of the initial crack length a_o. The actual test is performed by placing a cracked specimen in a testing machine, increasing the applied load incrementally and allowing sufficient time between steps for the crack to stabilize before measuring the new load and crack length. R-curve tests are usually performed on large center-cracked panel specimens.

Consider the case shown in Figure 2-23 for a thin sheet of width W containing an initial crack of length $2a$. As the applied stress is increased in steps to σ_1, σ_2, σ_3, etc., crack lengths $2a_1$, $2a_2$, $2a_3$, etc. are measured. The crack extension at each step Δa is defined as the current value of $a - a_o$, and K_R is based on the formula for stress intensity factor for the center-cracked panel at the current value of stress and crack length. K_C is taken as the value of K_R at the onset of unstable fracture.

This definition sometimes leads to the reporting of the R-curve asymptote as a "critical K" or K_c value. However, K_c as defined above is not strictly a material property, but also depends on the initial crack length. This is simply a consequence of the fact that the strain energy release rate depends upon total crack length, rather than crack extension.

A convenient way to visualize this fact is to overlay the R-curve on a plot of K_I versus half crack length for a fixed value of stress. Since the abscissa of the plot is half crack length, rather than crack extension, the base of the R-curve must be aligned with the initial half crack length a_o. Figure 2-24 illustrates K_I plots for two stress levels: σ_1 and $\sigma_2 > \sigma_1$. The same R-curve has been overlaid at two positions: a_{01} and $a_{02} < a_{01}$, such that each curve is just tangent to the corresponding K_I plot. Both cases represent fracture onset, i.e., the energy release rate always equals or exceeds the energy absorption rate represented by the R-curve. However, note that the K_c values for the two cases are different. As indicated by the shaded areas, the elastic energy is at first released at a slow pace controlled by the rate at which the applied stress is increased. At the point of tangency, however, the structure becomes able to release energy faster than the extending crack can absorb it, and fracture occurs.

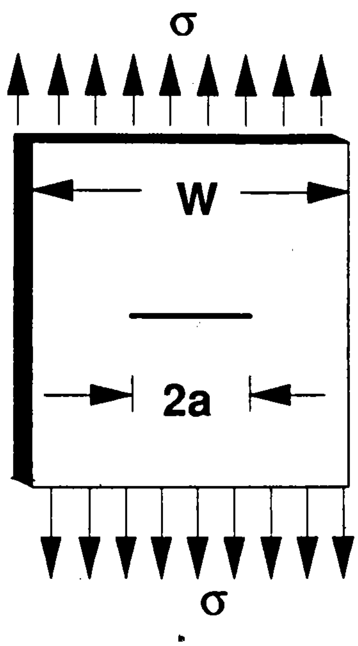

CENTER-CRACKED PLATE

Initial crack length = $2a_o$

$$K_I(\sigma, a) = \sigma\sqrt{\pi a}\left[\sec\frac{\pi a}{W}\right]^{\frac{1}{2}}$$

Obtain test data points (σ_n, a_n) *for* increasing stress levels $\sigma_1, \sigma_2, \sigma_3, \ldots$

$$(\Delta a)_n = a_n - a_o$$

$$K_R[(\Delta a)_n] = K_I(\sigma_n, a_n)$$

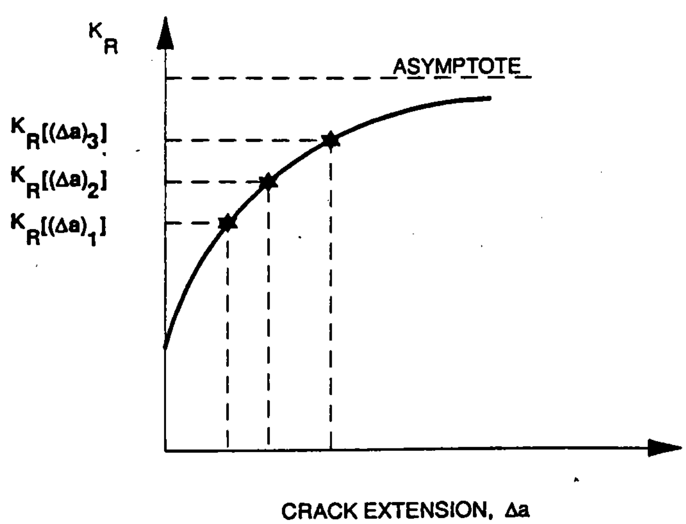

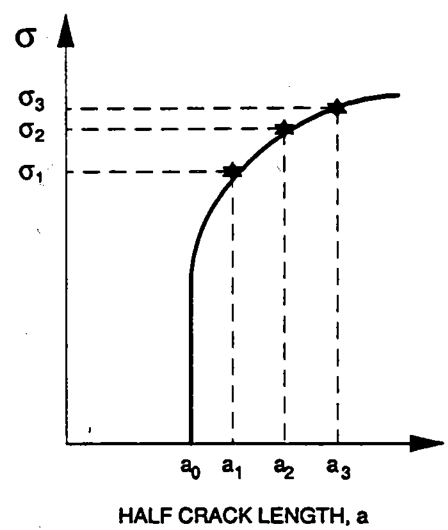

Figure 2-23. Experimental determination of R-curve.

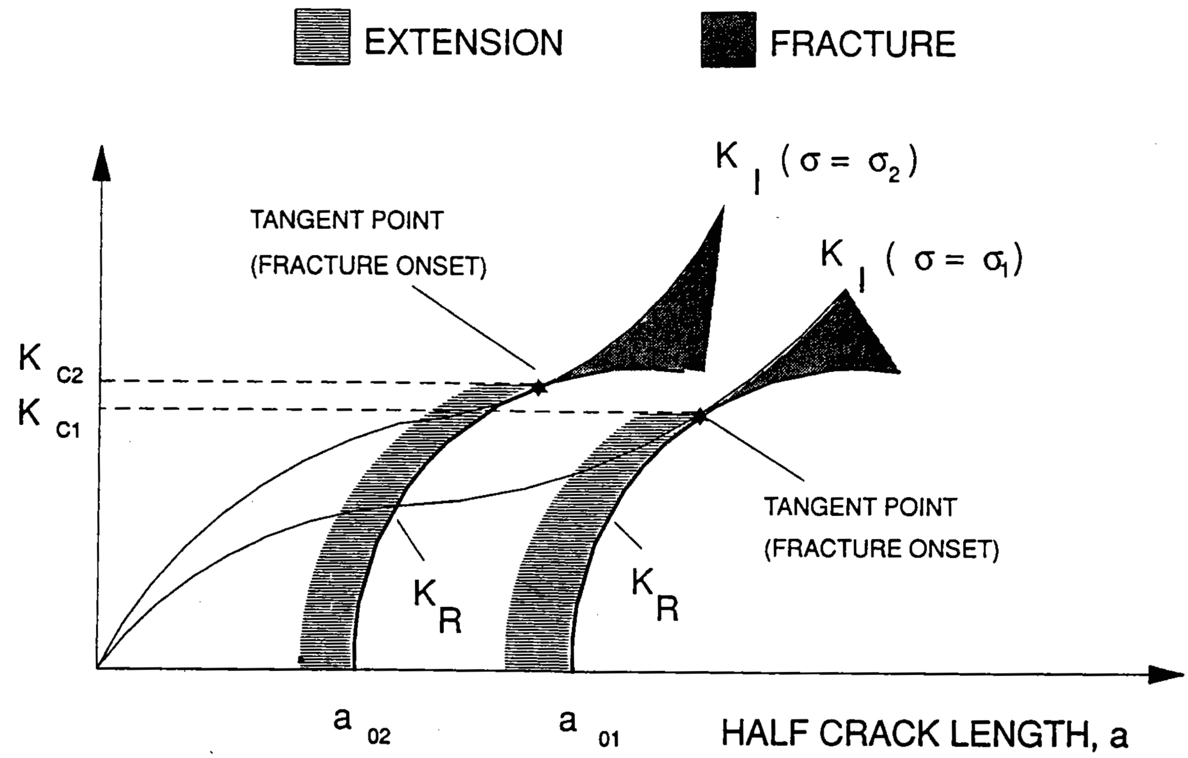

Figure 2-24. Dependence of K_c on crack length.

2.4.1.1 Graphical Construction of Thin-Section Strength Plots

The following example shows how R-curves can be used to predict the strength of a thin sheet or its critical crack length for a given applied stress. A center-cracked panel 20 inches wide and subject to uniform tension is to be analyzed. The Mode I stress intensity factor for the panel,

$$K_I = \sigma\sqrt{\pi a}\left[\sec\frac{\pi a}{W}\right]$$

is plotted in Figure 2-25(a) as a function of half crack length, for an applied stress $\sigma = 10$ ksi. In Figure 2-25(b) an estimated R-curve is plotted for 1/4-inch thick aluminum. (This curve was estimated from a curve for 1/16-inch thick aluminum and reported K_c values for 1/4-inch thick aluminum.)

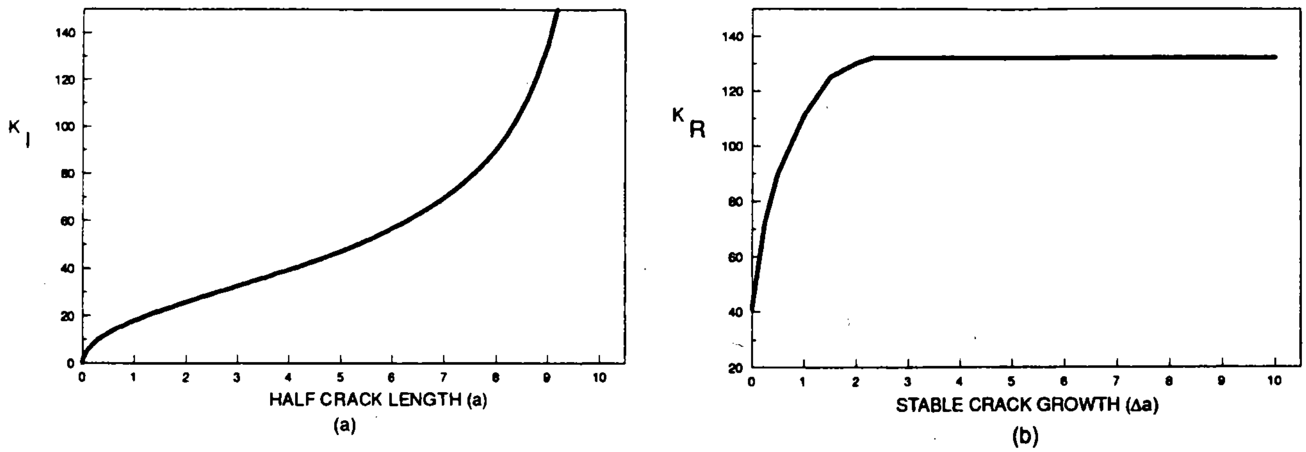

Figure 2-25. K_I and K_R curves

What would the critical crack length be for a 10 ksi stress applied to a 20-inch wide 2024-T3 aluminum panel of this thickness? The above graphs cannot be directly used to answer this question because the scales are different and the K_I plot goes off scale below the point of tangency. While rescaling, it is more convenient to replot both curves using a logarithmic scale on the ordinate as shown in Figure 2-26.

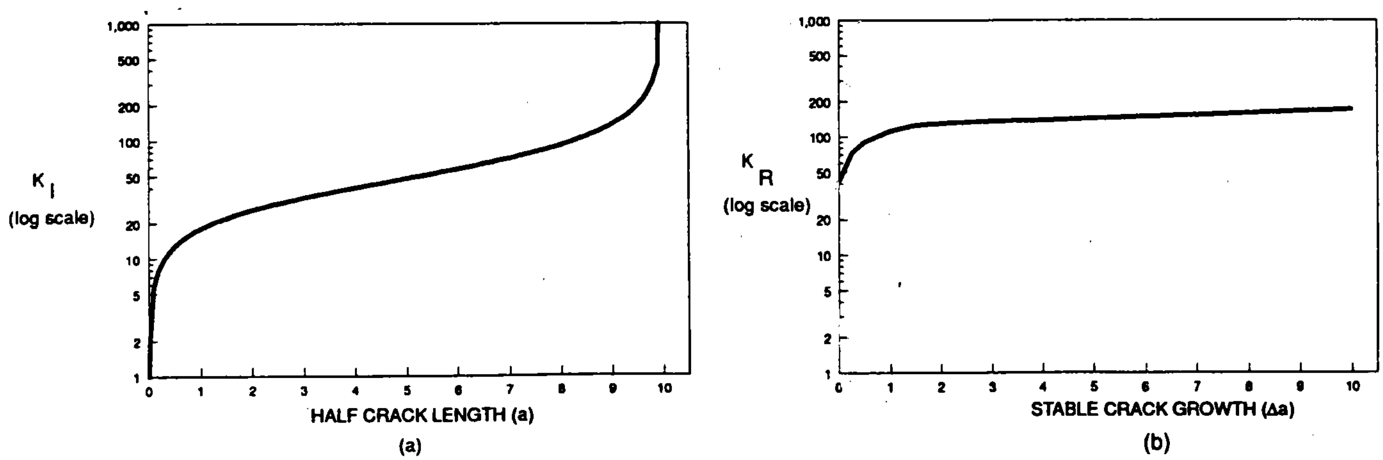

Figure 2-26. K_I and K_R curves (logarithmic scale)

The R-curve can now be overlaid and aligned properly on the K_I plot over the entire range of half crack length. In figure 2-27, the R-curve has been overlaid to find the tangent point, which corresponds to $K_c = 105$ $ksi\ \sqrt{in}$. The base of the R-curve is located at $a = 7.6$ inches. Thus, the critical crack length ($2a$) is 15.2 inches.

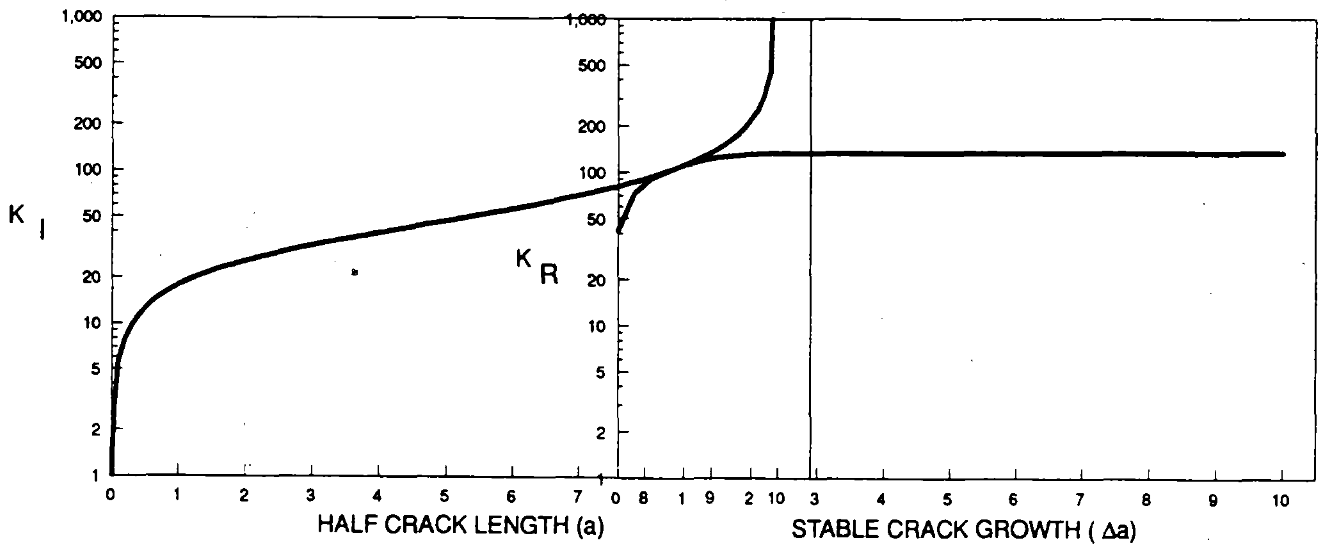

Figure 2-27. Overlay of K_I and K_R curves to determine critical crack length

Figures 2-28 and 2-29 contain enlarged copies of the logarithmic plots. The reader will find it useful to make a transparency of the enlarged R-curve and repeat the above overlay procedure. The enlarged K_I plot and R-curve overlay should also be used to follow through the rest of the example.

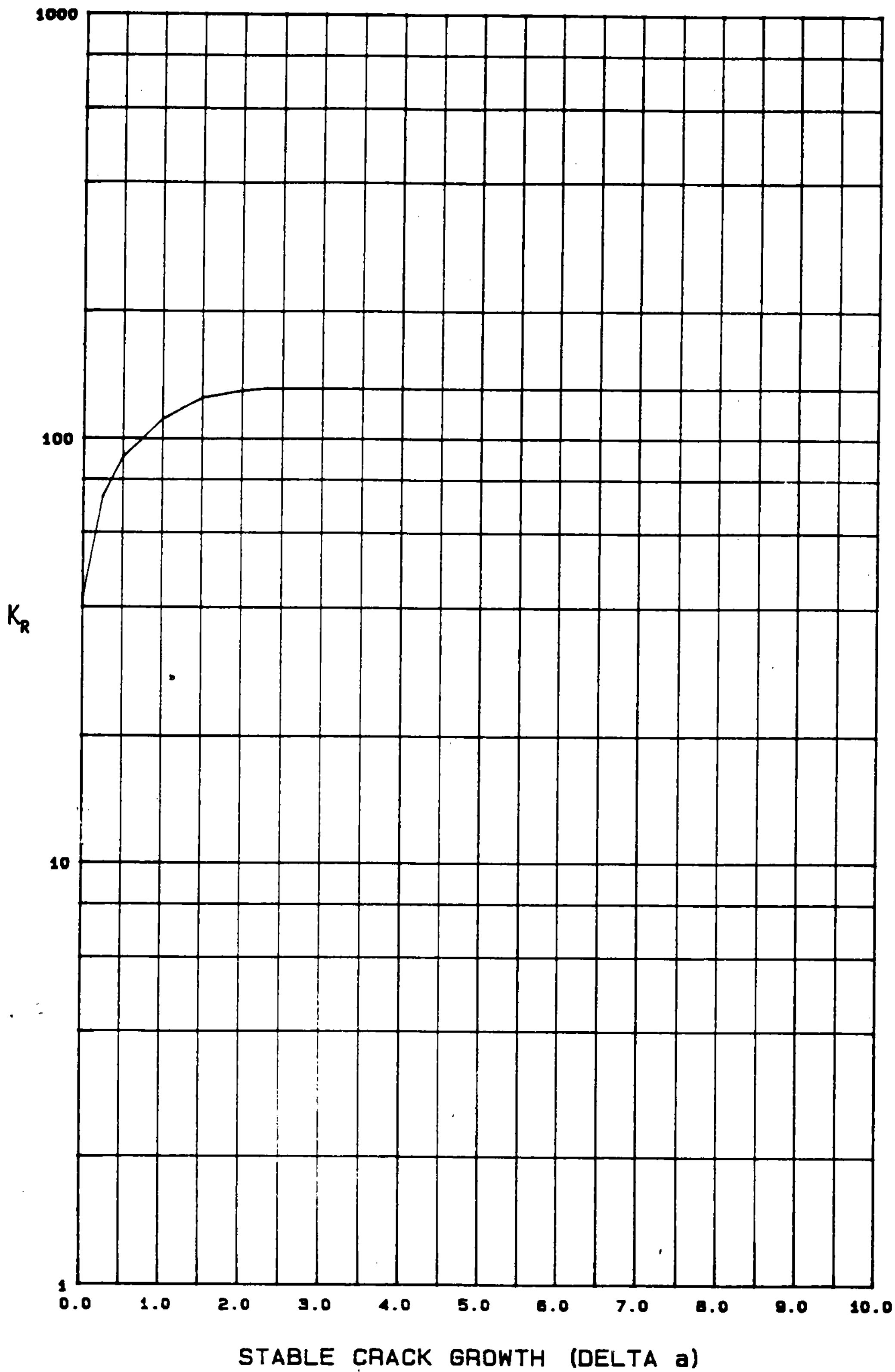

Figure 2-28. R-Curve for 2024-T3

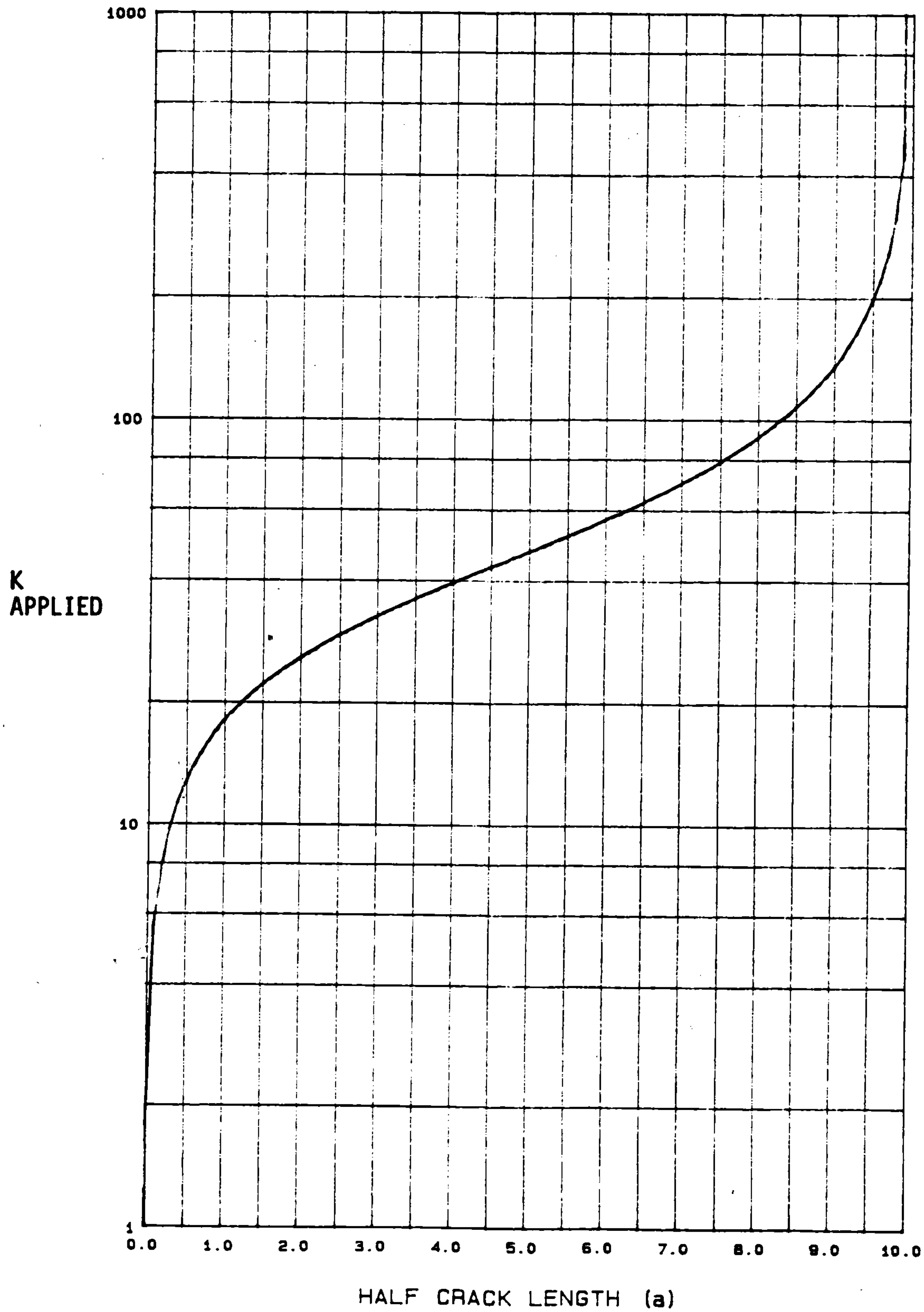

Figure 2-29. *K* applied versus crack length

One obvious question to ask is what one would estimate for the critical crack length if only the "critical K" value (132 $ksi\ \sqrt{in}$) had been reported and were treated as if it were like a K_{IC} value. If the overlay is flipped over (left to right reversal), the left side can be used as a "no-extension R-curve": vertical step at the left edge to $K = 132\ ksi\ \sqrt{in}$ with a sharp corner. Overlaying this "R-curve" to find the tangent point puts the base at $a = 9$ inches. Thus, the improper use of a reported K_c in this case would lead to an unconservative prediction of 18 inches for the critical crack length (Figure 2-30).

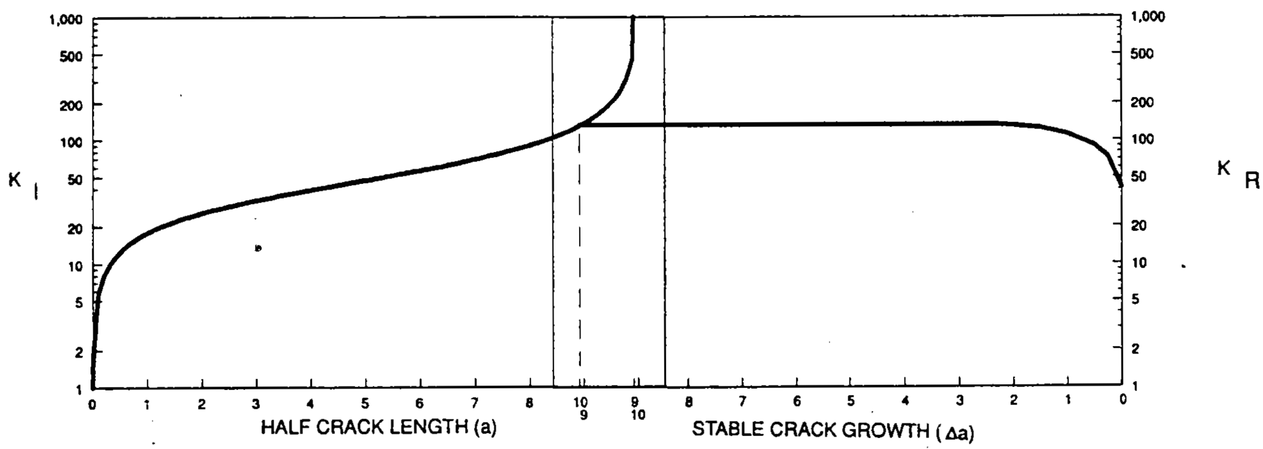

Figure 2-30. Use of critical K to determine critical crack length

The same two logarithmic plots can also be used to estimate the critical stress and crack length for other values of applied stress. The R-curve is simply aligned to find the tangent point for a specified half crack length. K_c is then read directly from the R-curve overlay scale. The critical stress σ_c can also be found by starting at 10 (the reference stress) on the scale K_I and reading across to the R-curve scale.

For example, what is the critical stress for a crack length $2a = 8$ inches? Figure 2-31 shows the correct overlay position and the answers.

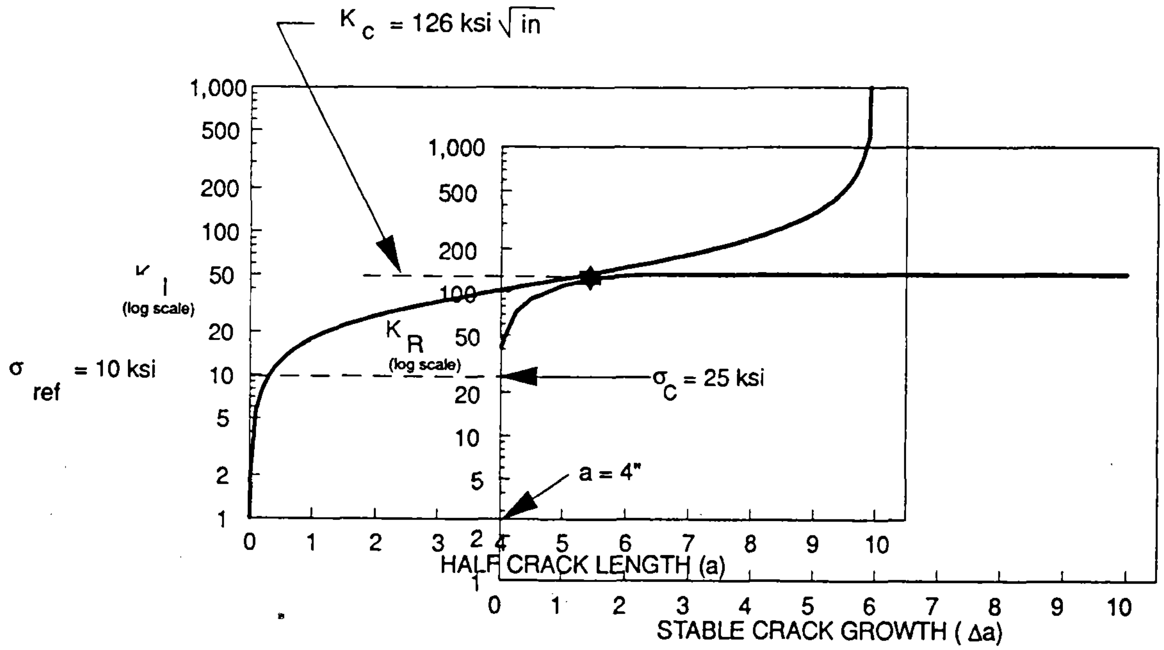

Figure 2-31. Critical stress determinations with K_I and K_R curves.

The above procedure, originally invented by Creager [2-18], allows one to rapidly construct plots of K_c and σ_c versus crack length. These plots are shown in Figure 2-32 for the 20-inch wide aluminum panel example.

The R-curve approach is useful and practical for correlating the fracture resistance of typical aircraft panel-and-stringer construction, but limitations still exist. The most useful application is to damage tolerance assessment of situations involving an isolated long crack, since R-curves are typically derived from tests of single long cracks in wide panels. However, K_R depends on section thickness as well as alloy material, and only a few curves for a few skin thicknesses have been published in the open literature. Several examples from references [2-16] and [2-19] have been reproduced in Appendix B.

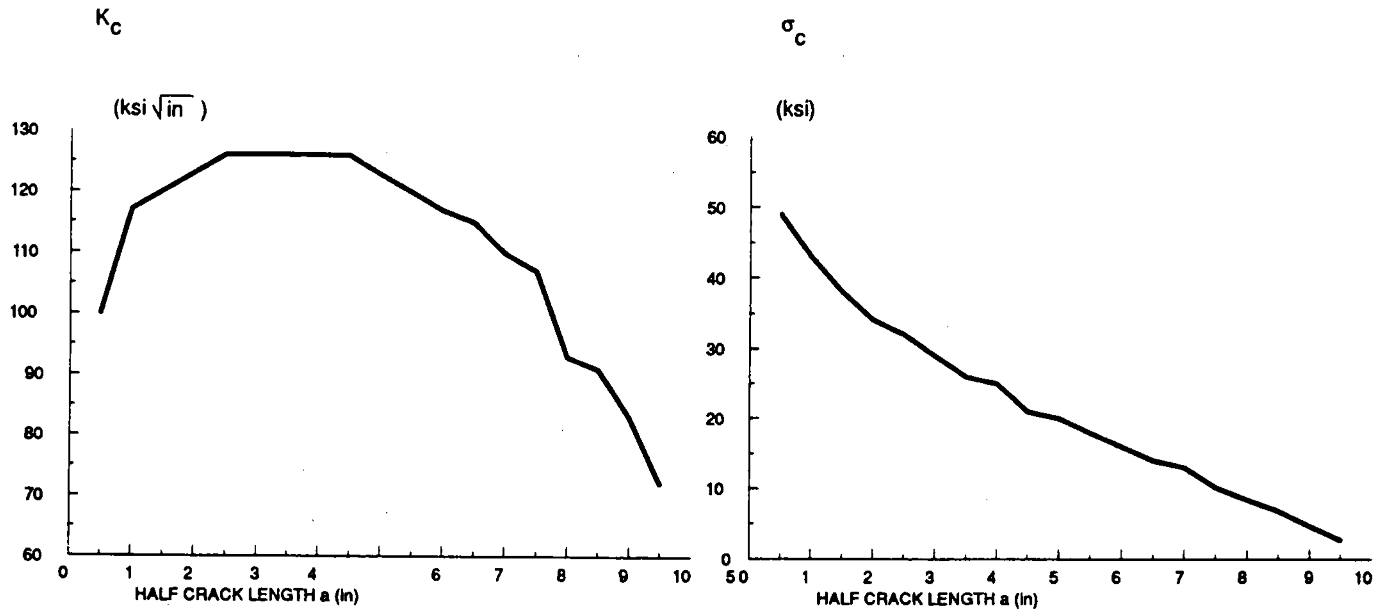

Figure 2-32. K_c and σ_C vs. a for a 20-inch aluminum panel.

Another important limitation is that the R-curve does not strictly depend on crack extension alone. What really counts is the volume of new material that undergoes plastic deformation when the crack extends. Figure 2-33 illustrates three different examples of what can happen. In example (a), a crack has extended from an initial length $2a_o$, much larger than the plastic zone size to a length $2a$, much smaller than the panel width. The contoured areas depict the new plastic volumes, which are independent of each other and the panel edges.

Example (b) shows what happens when the initial crack length is of the same order as the plastic zone size. Example (c) shows what happens when the initial crack is long enough to place the crack tips near the panel edges. In example (b), the two crack-tip stress concentrations reinforce each other, while in example (c) the nearby free edge reduces the panel's ability to constrain the deformation. In both cases, the result is a larger plastic volume for the same crack extension as in example (a), i.e., an R-curve derived from a test of a medium-length crack should not be expected to characterize the strength of similar bodies with very long or very short cracks.

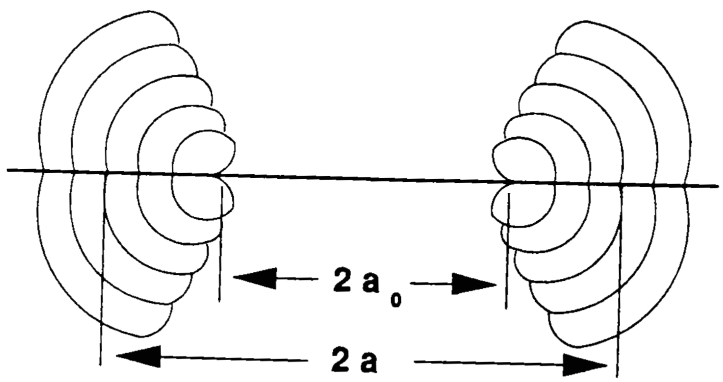

(a) Isolated medium or long crack.

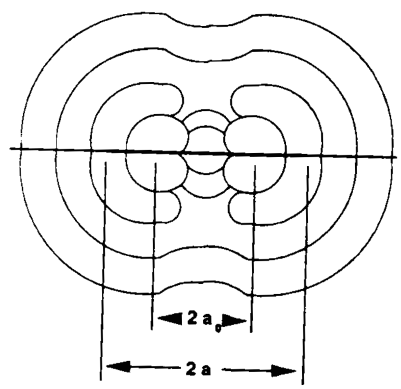

(b) Short crack.

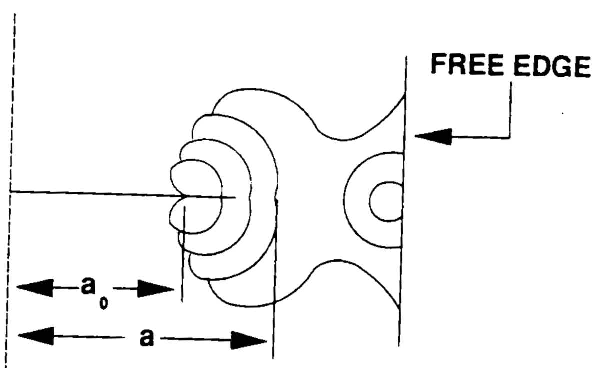

(c) One crack tip near edge of a panel.

Figure 2-33. Effect of surroundings on energy absorption rate.

2.4.2 The Net Section Failure Criterion

The net section failure criterion has its roots in the traditional static strength design practices used by the aeronautical industry almost ever since airframes have been made from metal. Joints made with bolts or rivets have always played a prominent role in metal airframes. The skins or webs in these joints were subject to stress concentration around each fastener hole, but early designers of metal airframes had neither the modern numerical stress analysis methods nor the computers which the methods require. Therefore, approximate methods of analysis which could be carried out by hand calculation were highly valued.

The net section failure criterion was one such method. The criterion was based on observations that ductile metals subjected to concentrated stress tend to reduce the stress when they yield. There was ample field experience to support these observations. For example, if one fastener in a joint happened to have an excessive bearing load because parts had been misaligned when the holes were drilled, the parts would yield under load and deform until the fastener bearing forces were equalized.

From the foregoing observations, it was a short step to the hypothesis that the elastic stress concentrations around all of the fastener holes in a joint would be progressively smoothed out, as the applied load increased, until the tension across the minimum ("net") section between the holes was distributed uniformly just as the stress level reached the material's ultimate strength. Thus, the critical load capacity of the joint could be estimated as the product of the net section area and the ultimate strength.

Figure 2-34 shows how the net section failure criterion is applied to a tensile coupon of width W containing an open hole of diameter D. At low stress, the coupon remains elastic, and a stress concentration factor of 3 is realized. As the applied stress is increased, yielding progresses from the edge of the hole until the net section $(W - D)\,t$ is stressed to the ultimate tensile strength σ_{ult}. The critical load is then estimated as $P = \sigma_{ult}\,(W - D)\,t$.

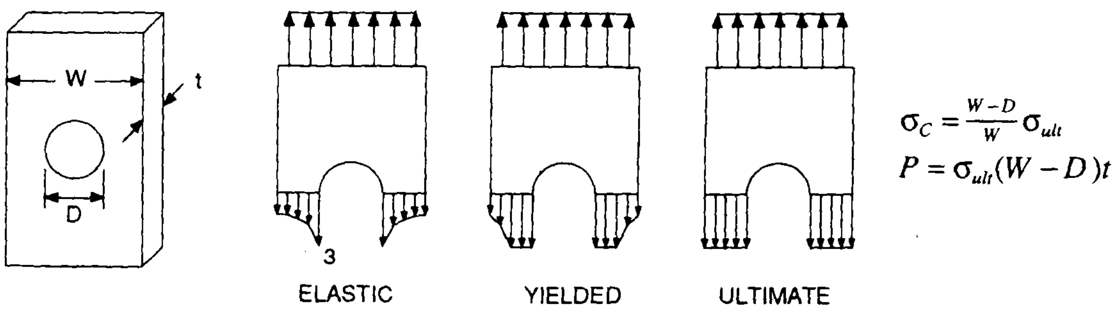

Figure 2-34. Net section failure criterion.

In its simplest form, the net section failure criterion tends to overestimate the critical load because there are other components of stress besides the principal tension in the yielded region. Consequently, the criterion is modified for practical application by substituting a so-called "flow stress" σ_f for the ultimate strength, based on correlation with strength tests of coupons like the one shown in Figure 2-34. Extensive tests on aluminum coupons suggest that the flow stress for alloys used in airframes ranges from five percent above the yield strength to five percent below the ultimate strength.

It is a natural step to apply the net section failure criterion to thin sheets containing cracks, even though the criterion does not account for stable crack extension. In this case, the critical crack length plays the role which was played by the fastener hole diameter. Thus, for example, the net section in a thin sheet of width W containing a center crack of length $2a$ is $(W - 2a)t$, and the critical applied stress (load divided by nominal area) is:

$$\sigma_c = \frac{W - 2a}{W}\sigma_f \tag{2-18}$$

2.4.2.1 Failure Mode Determination and the Feddersen Diagram

When should the net section failure criterion be used in place of the R-curve method to estimate the strength of a cracked thin sheet? The answer is obtained by comparing the strength plots for a specific situation.

In the example R-curve analysis presented in Section 2.4.1, an R-curve strength plot was constructed for a 1/4-inch thick 2024-T3 sheet 20 inches wide. A reasonable choice for the flow stress of 2024-T3 aluminum might be $\sigma_f = 48$ ksi. A net section strength plot based on this flow stress is shown in Figure 2-35 together with the R-curve strength plot from the preceding section. It is evident from the comparison that the R-curve strength estimate is unconservative for crack lengths shorter than 2a = 4 inches and longer than 15 inches in this case.

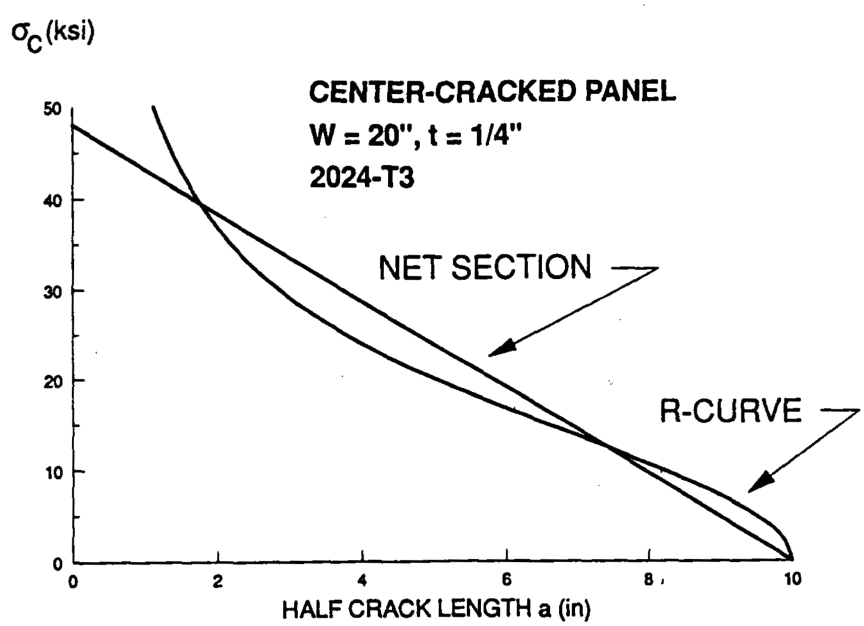

Figure 2-35. Net section and R-curve strength curves.

Failure mode determination should also be an essential step in the qualification of test results used to derive R-curve data. An important aspect of thin-sheet behavior is that highly ductile sheets of moderate width can be net-section critical for almost the entire range of crack length. Figure 2-36 illustrates an example based on the same 2024-T3 material and a panel width of 10 inches. Such comparisons show that the more ductile the material and the thinner the sheet, the wider the panel must be in order to have the opportunity to perform a valid R-curve test.

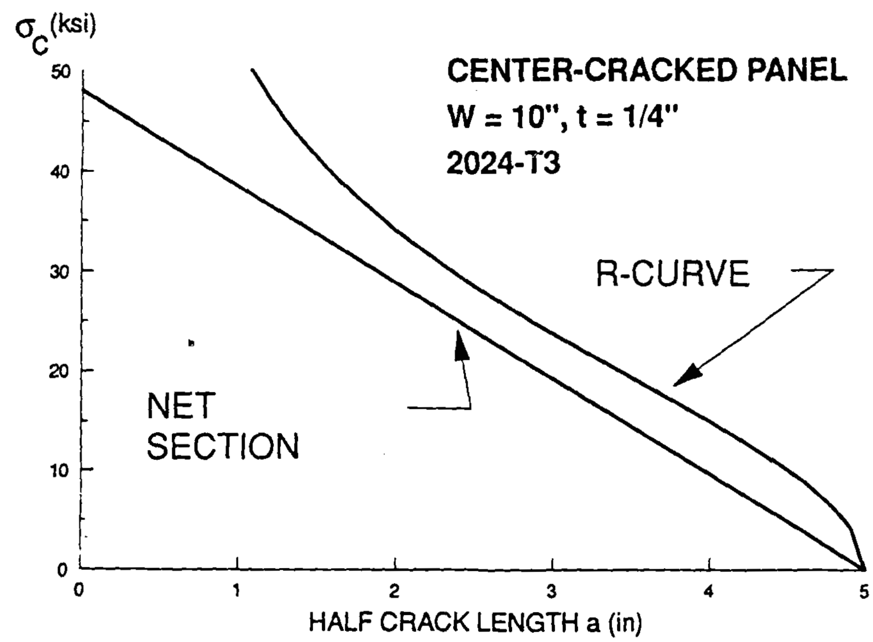

Figure 2-36. Illustration of the width effect on thin sheet strength.

In reality, the transition between the ductile fracture and plastic yield failure modes is gradual. Feddersen [2-20] has proposed an empirical construction, based on the R-curve and net-section strength plots, to account for the transition effect. The construction procedure, using the idealized R-curve, is as follows: (1) from the point on the R-curve corresponding to $\sigma_c = 2\sigma_f/3$ draw the tangent which intercepts the ordinate at σ_f; (2) from the point on the R-curve corresponding to $a = W/3$, draw the tangent which intercepts the abscissa at $W/2$. Figure 2-37 repeats the strength plots from the previous example ($W = 20$ inches) to illustrate the construction.

The strength envelope consisting of the two tangent lines and the included segment of the R-curve is called a Feddersen diagram. Before an R-curve derived from a panel test is accepted, it should be verified that the initial crack length lies in the included R-curve segment on the Feddersen diagram.

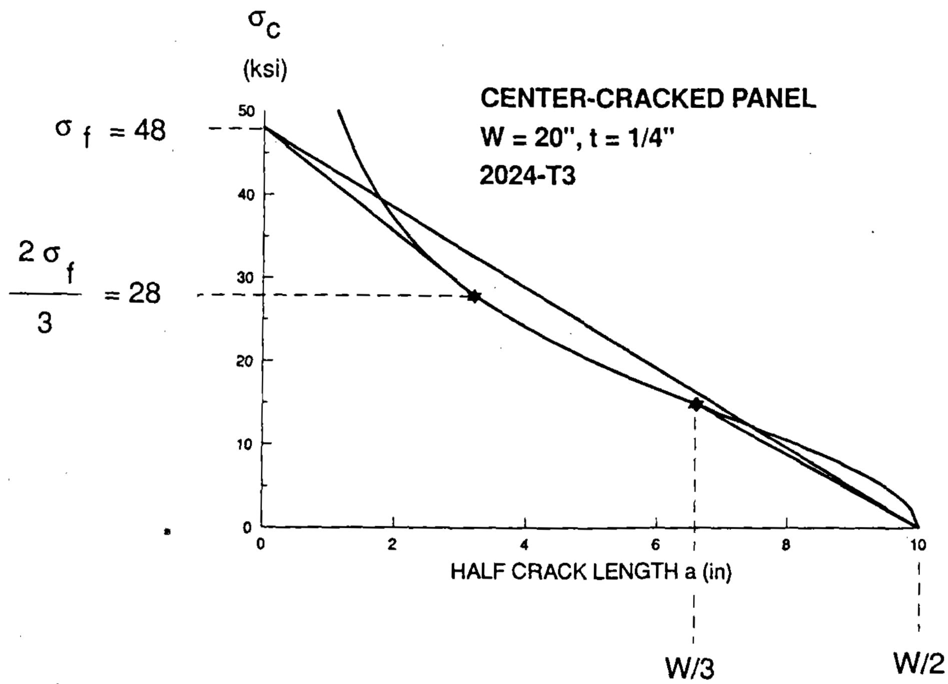

Figure 2-37. Construction of Feddersen diagram.

2.4.3 Crack Opening Displacement

Determination of the onset of unstable crack propagation by means of measurement of crack opening displacement is another approach to the problem of fracture with large-scale yielding. Crack opening displacement (COD)[3] can be used as a fracture toughness parameter in a similar manner to K_{IC}, i.e., at a critical value of COD a crack will propagate unstably. The advantage of the COD approach is that COD values can be measured throughout the entire plane strain, elastic-plastic, and fully plastic behavior regions.

[3] The common definition of COD is the displacement at the crack mouth, as measured by means of a clip gauge, and sometimes called CMOD. However, some models are based on the so-called crack tip opening displacement (CTOD), which is actually an extrapolation.

The COD approach has been developed mainly in England, specifically at the Welding Institute. The chief purpose was to find a characterizing parameter for welds and welded components of structural steels. A procedure for measuring COD [2-21] involves a slow-bend test on a three-point bend test specimen.

A displacement clip gauge containing electrical resistance strain gauges is used to obtain a continuous load-displacement record throughout the test. Since direct measurement of crack opening at the crack tip cannot be done, the clip gauge is used to measure the crack opening at the surface of the cracked specimen. As the specimen is loaded, the pretensioned clip gauge tends to expand with the crack opening displacement. The crack tip opening displacement is then determined from this measured quantity by using the principles of mechanics. The fracture toughness predicted from COD tests is a material property that is a function of temperature, loading rate, specimen thickness, and specimen geometry. Caution should be exercised in any attempt to extrapolate COD values to geometries that are not roughly identical to those used in tests. Since the conditions at the crack tip must be inferred from the remote measurements using analytical methods based on linear elastic fracture mechanics (LEFM), the validity of the results must be correspondingly limited. To date, the COD procedure has not been as widely accepted by engineers to characterize fracture with large-scale yielding as the R-curve and plastic collapse methods.

2.4.4 J-Integral

The so-called J-integral method is a similar approach, with a somewhat more convenient relation to physical behavior. The J-integral is an expression of plastic work (J) done when a body is loaded. From basic principles of mechanics, it has been shown that J can be calculated by integrating a specified function of the body's displacement distribution along any contour in the body which completely encloses the plastic zone [2-22]. Thus J, like COD, can be calculated from elastic-plastic models which do not precisely describe the local stress field at a crack tip. As with COD, the J-integral method still has the problem of representing physical behavior with an approximate elastic-plastic computational model. However, the theorem on which the J-integral is based extends to the boundaries of the body, and it has been shown that simple measurements of plastic work (e.g., the product of applied load and testing machine crosshead travel) are equivalent to J. The J-integral method is occasionally applied in the course of ad hoc assessments of the integrity of ductile structures but has not been reduced to routine engineering practice.

2.4.5 Practical Developments

As the concept of fracture mechanics began to be widely applied to airframe damage tolerance evaluation in the early 1970s, the evaluators had to extrapolate the stress intensity factor formulas in ways not envisioned by the founders of the theory. The problem was that cracks in real structures often displayed a three-dimensional character, whereas Griffith's energy analysis, Irwin's stress solution, and most of the related developments have a fundamentally two-dimensional nature.

The two-dimensional character is built into the theories by the basic assumptions that the cracked structure has a two-dimensional geometry and that the crack extends along its own line. Thus, one must deal with through-cracks having flat surfaces in areas of structure where (at least near the crack) the thickness is constant and any details such as fastener holes are through-drilled with no taper or countersink.[4] Even the simplest of these situations has at least one three-dimensional aspect: the transition from plane strain to plane stress conditions at the lateral faces of the structure. Fortunately, the theories were found to work well enough in practice despite this inconsistency when empirical modifications were made to account for thickness effects (e.g., the R-curve method).

Conversely, some of the cracking encountered in real structures introduced other three-dimensional factors that fundamentally contradicted the theoretical assumptions.

---

[4] One other valid case is a circular ("penny-shaped") internal crack in a body large enough so that free-surface effects can be neglected. The geometry is still two-dimensional in this case because of axial symmetry (see Section 2.5).

Figure 2-38 illustrates some typical examples, and the following paragraphs indicate the ad hoc nature of the procedures that damage tolerance evaluators had to adopt.

Example (a) is a common type of fatigue crack which remains flat-surfaced but changes the shape of its crack front as it extends. This is not normally a problem for strength analysis because such cracks have generally become through-cracks well before reaching critical size. However, the change of shape does affect the stress intensity factor which must be used to estimate the slow crack growth life of the flaw under fatigue loads (Chapter 3). The common approach is to patch two simplified models together: a quarter-circular corner stress intensity factor (Section 2.5) until the crack radius equals the skin thickness, and a through-crack stress intensity factor thereafter. (The ligament area between the two "stages" is implicitly assumed to have a negligible life.)

Example (b) shows an internal surface flaw in the wall of a high-pressure gas cylinder. The problem in this case involves more than the estimation of critical crack size. A much more serious question is how long the flaw can be in relation to its depth without risk of bursting the cylinder. Whatever basic method of strength determination is used (K_{IC}, R-curve, etc.), the analyst must still make a judgment based on a comparison of critical stresses for the assumed flaw and an equivalent through-crack of the same length.

Example (c) illustrates a typical through-crack which may be found at the corners of fuselage frame cutouts. The crack may not be aligned across the frame when it reaches critical size, and so may change direction when it fractures. In such cases, analysts often resort to straight crack models which reproduce some key characteristic of the actual crack. Two possible choices are shown: (1) fracture assumed along the original crack line; or (2) a crack across the tension and of a length such that the frame is cut to the same height as the actual crack.

While the ad hoc procedures have proved to be useful for making estimates of damage tolerance, they are not well-founded and require frequent calibration by comparing estimates with test results. This limitation is one reason why researchers continue to develop theories of fracture strength such as those summarized in the next two sections.

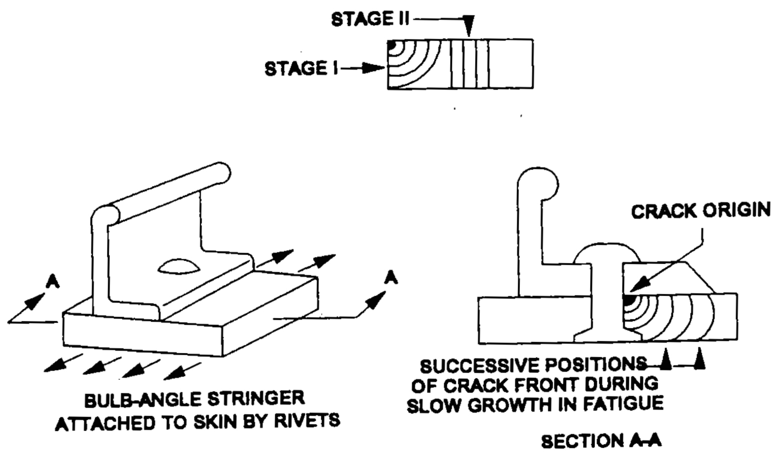

(a) Corner crack at a fastener hole.

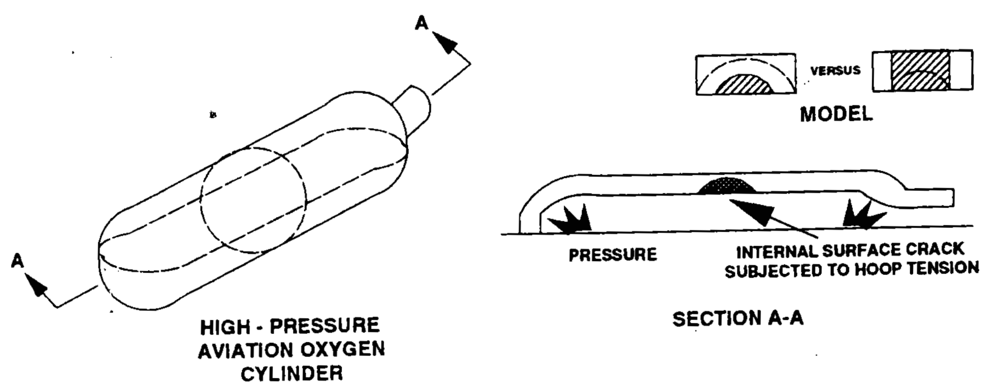

(b) Axial crack in an oxygen cylinder.

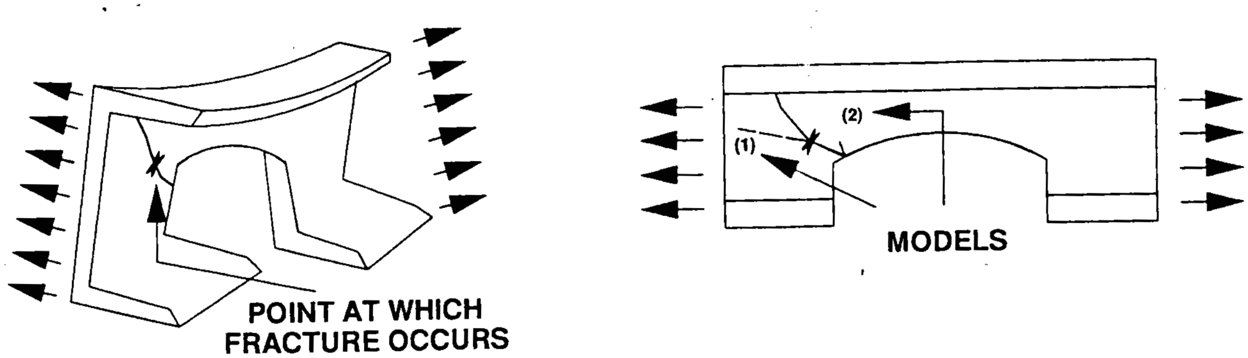

(c) Through-crack at a fuselage frame corner detail.

Figure 2-38. Typical examples of three-dimensional aspects of cracks.

2.4.6 Strain Energy Density Criterion

The strain energy density criterion was developed by Sih in the 1970s [2-23, 2-24] and was originally applied to problems in linear elastic fracture mechanics. Later, the criterion was found to be applicable to ductile fracture as well [2-25, 2-26, 2-27].

We saw earlier that strain energy density is proportional to the square of stress, and that the stresses near a crack tip in an elastic body are proportional to $1/\sqrt{r}$, where r is the radial distance from the crack tip. Therefore, the strain energy density at any point near the crack tip can be expressed as:

$$U = \frac{S}{r} \tag{2-19}$$

where S is called the strain energy density factor and, like the stress intensity factor, depends only on the externally applied loads, the crack length, and the geometry of the structure. Since the material has been assumed to be elastic, the strain energy density factor can be expressed in terms of the stress intensity factors for the different modes of fracture:

$$S = a_{11}K_I^2 + 2a_{12}K_IK_{II} + a_{22}K_{II}^2 + a_{33}K_{III}^2 \tag{2-20}$$

where:

$$a_{11} = \frac{1}{16\mu\pi}(3\text{-}4\nu - \cos\theta)(1 + \cos\theta)$$

$$a_{12} = \frac{1}{8\mu\pi}\sin\theta\,(\cos\theta - 1 + 2\nu)$$

$$a_{22} = \frac{1}{16\mu\pi}[4(1 - \nu)(1 - \cos\theta) + (3\cos\theta - 1)(1 + \cos\theta)]$$

$$a_{33} = \frac{1}{4\mu\pi} \tag{2-21}$$

where ν is the Poisson's ratio and

$$\mu = \frac{E}{2(1 + \nu)}$$

is the shear modulus.

From these expressions, it is evident that the criterion can be applied to problems that include mixed modes.

We have also seen that the local stresses lose their $1/\sqrt{r}$ character in the plastic zone. Conversely, as long as the strain energy density is properly calculated as the area under the stress-strain curve, it can be shown that U retains its $1/r$ character even when plastic deformation occurs. Thus, it is possible to calculate the strain energy density factor S at any point in a body, as long as numerical results are available from an elastic-plastic stress analysis.

Sih's criterion is based on a fundamental property of the strain energy density function under conditions of plane strain. Sih found that, when the stresses at any point in a body are expressed in terms of principal stresses σ_1, σ_2, and $\sigma_3 = \nu(\sigma_1 + \sigma_2)$, the strain energy density U could be expressed as a sum of two terms:

$$U = U' + U'' \tag{2-22}$$

$$U' = \frac{1+\nu}{3E}[\sigma_1 + \sigma_2 + \nu(\sigma_1 + \sigma_2)]^2 - \frac{1+\nu}{E}[\sigma_1\sigma_2 + \nu(\sigma_1 + \sigma_2)^2] \tag{2-23}$$

$$U'' = \frac{1-2\nu}{6E}[\sigma_1 + \sigma_2 + \nu(\sigma_1 + \sigma_2)]^2 \tag{2-24}$$

where U' contains all the energy associated with shear and U'' contains all the energy associated with volume expansion. Sih suggested that the likelihood of crack extension should increase when the ratio of expansion to shear energy increases. When he used equations (2-23) and (2-24) to calculate U''/U', he found that the ratio increases steadily as the values of σ_1 and σ_2 approach each other.

Applying this idea to the local stresses near a crack tip, Sih also showed that when the total strain energy density U is a minimum, U'' is much greater than U' [2-28]. Thus, when the strain energy density factor S is expressed in terms of the Irwin solution (see Section 2.2), the minimum defines the angle θ at which the crack should extend (Figure 2-39). The hypothesis is consistent with the known behavior of cracks subjected to Mode I loading ($\theta = 0$), but it also gives other crack extension angles for mixed-mode loading.

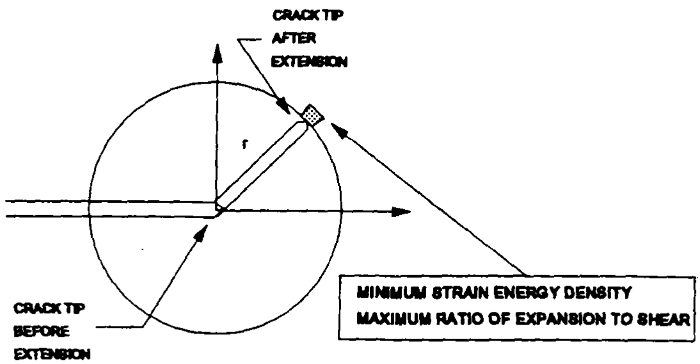

Figure 2-39. Strain energy density criterion.

The amount and character of the crack extension is governed by two parameters which can be derived from conventional material properties. The critical strain energy density U_c is equated to the area under the elastic-plastic stress-strain curve obtained from a tension test (Figure 2-40). This definition is based on the assumption that the tensile stress-strain curve is also the equivalent plastic stress versus equivalent plastic strain curve (a hypothesis commonly adopted in elastic-plastic stress analysis). One physical interpretation of U_c is that crack extension must somehow be associated with exhaustion of the ductility of the material around the crack tip.

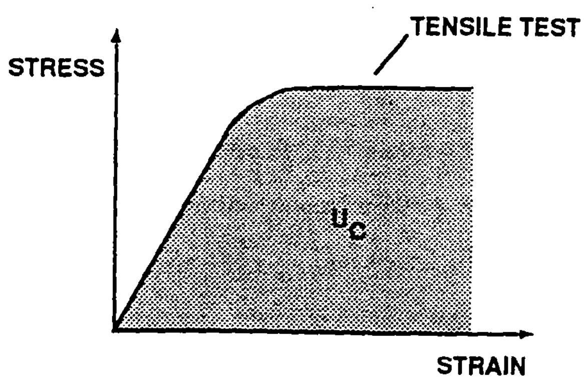

Figure 2-40. Definition of critical strain energy density.

The critical strain energy density factor S_c is related to the plane strain fracture toughness via the Irwin solution. Since K_{IC} is obtained from a test with pure Mode I loading, it follows from equation (2-20) that:

$$S_c = a_{11}K_{IC}^2 \tag{2-25}$$

A third parameter r_c is derived from the first two parameters:

$$r_c = \frac{S_c}{U_c} \tag{2-26}$$

Application of the strain energy density criterion to practical problems requires a numerical elastic-plastic stress analysis from which the strain energy density factor can be calculated. In any *xy* plane like the one shown in Figure 2-40 the criterion is applied by calculating the crack extension $r = S/U_c$. The extension is considered to be stable as long as $r < r_c$, and fracture is assumed to occur when r first reaches the critical value.

The strain energy density criterion is applied to three-dimensional cracks by repeating the above analysis in several *xy* planes spaced through the thickness. Since the results of the three-dimensional stress analysis may vary through the thickness, different crack extension values (r, θ) will generally be calculated for each plane, i.e., the criterion can be used to deal with cracks of arbitrary shape.

2.4.7 Plastic Collapse Model

The plastic collapse model was originally developed by Erdogan [2-29] to estimate the strength of high-pressure gas transmission pipelines with surface or internal wall cracks. Gas transmission pipelines are made of highly ductile steels which can be either fracture critical or net section critical depending on the crack dimensions, wall thickness, and pressure stress levels. The situation is further complicated by the fact that under typical operating pressures the wall area around the crack tends to bulge outward and distort the local distribution of stress.

Erdogan's model is based on the fact that pipeline steels are ductile enough to be treated as if the stress-strain curve exhibits no plastic hardening. The material is assumed to behave as if its strength is limited by a flow stress σ_f, usually defined to be five percent above the yield strength.

In Erdogan's model, the Mises-Hencky yield condition[5] is used in the form:

$$\frac{1}{2}\left[(\sigma_x - \sigma_y)^2 + (\sigma_y - \sigma_z)^2 + (\sigma_z - \sigma_x)^2\right] + 3\left[\tau_{xz}^2 + \tau_{yz}^2 + \tau_{xz}^2\right] = \sigma_f^2 \qquad (2\text{-}27)$$

Yielding is assumed to be confined to the plane in which the crack lies, and a numerical stress analysis is performed to find both the local stress distribution and the location of the plastic zone boundary (Figure 2-41). A COD value for the point of deepest penetration is also calculated.

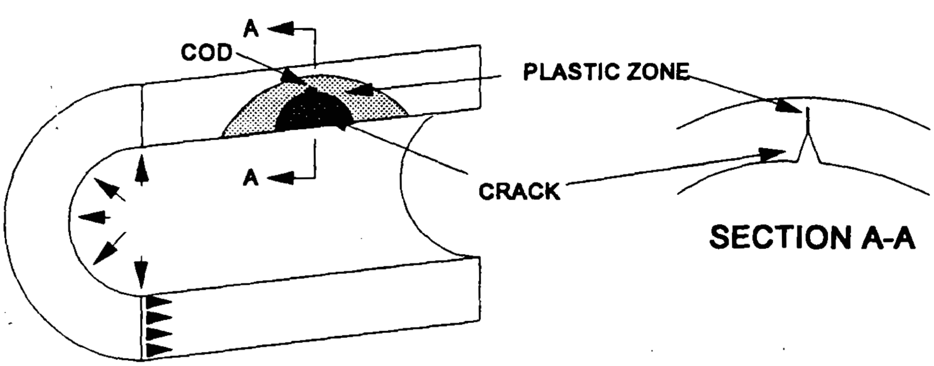

Figure 2-41. Erdogan's plastic zone model.

The plastic collapse model requires calibration with the COD measurements on laboratory specimens and coupon tests to establish the flow stress. (Both types of test have been performed extensively on pipeline steels.) The model stresses and COD are then calculated as the applied

[5] See Section 2.2

load is increased in a series of small steps. No provision is made to account for stable crack extension, but the critical load and failure mode are determined when one of the following two conditions is first met: (1) the calculated COD reaches the critical value determined from specimen tests; or (2) the plastic zone grows so rapidly that it would spread through the entire section containing the crack plane if the load were increased again. These two conditions are analogous to ductile fracture (with no R-curve effect) and net section failure, respectively.

2.5 INTERNAL, SURFACE, AND CORNER CRACKS

The foregoing discussion has implicitly assumed a two-dimensional configuration of the cracked body, e.g., a skin panel with a through-thickness crack. The stress fields associated with such cracks are also two-dimensional for practical purposes (i.e., the stresses are uniform through the thickness), except for panels subjected to out-of-plane bending loads. In the latter case, a two-dimensional treatment by means of conventional plate and shell theories is also appropriate.[6]

However, many practical cracking situations have a three-dimensional character. Fatigue and/or corrosion damage generally appears in the form of small surface or corner cracks. Although these cracks are not likely to produce immediate fracture under service loads, it is important to characterize their stress intensity factors for the purpose of estimating crack growth life (see Chapter 3).

The basic solution for such situations is the Sneddon formula [2-30] for the stress intensity factor of a circular ("penny") crack in an unbounded solid elastic medium:

$$K_I = 2\sigma \sqrt{\frac{a}{\pi}} \tag{2-28}$$

where σ is a uniform tensile stress applied to the body and directed perpendicular to the plane of the crack, and a is the crack radius. Shah and Kobayashi have extended Sneddon's formula to

[6] The bending stresses are assumed to be zero at the panel midplane (neutral plane for panel-stringer combinations) and to vary linearly through the thickness.

deal with elliptical cracks subjected to uniform tension and/or bending, either in unbounded bodies or located near a free surface [2-31, 2-32]. Approximate solutions have also been derived from these results for the stress intensity factors associated with half-ellipse cracks extending inward from a free surface and corner cracks extending inward from two free surfaces intersecting at right angles, with either circular or elliptical arcs defining the crack front [2-33].

The approximate stress intensity factors for surface and corner cracks are routinely used in damage tolerance assessments. These factors are expressed in the form:

$$K_I = M_{K1} M_{K2} \sigma \sqrt{\frac{\pi a}{Q}}$$

for the stress intensity at the deepest point of penetration[7] through the thickness, where M_{K1}, M_{K2} and Q are factors depending on the crack shape (Figures 2-42, 2-43 and 2-44).

For stress intensity factor solutions of various other crack configurations, see Appendix A and ref. [2-34].

2.6 ENVIRONMENTAL EFFECTS

Fracture toughness is not directly affected by corrosive environments. However, some high-strength materials may experience rapid crack propagation when subjected to static load while immersed in a corrosive medium. This phenomenon, known as stress corrosion cracking, is an extreme example of crack growth driven by chemical attack at the crack front. (The static load serves to hold the crack open, allowing circulation and diffusion to continually replenish the corrosive medium at the crack front.) For a given load, the crack grows at a constant rate with respect to time. Material susceptibility is determined by means of a series of static tests at decreasing loads, until a threshold for stress corrosion cracking is established. The corresponding stress intensity factor K_{ISCC} is reported as the threshold property.[8] For susceptible high-strength materials, K_{ISCC} is much smaller than K_{IC}.

[7] This is also the maximum stress intensity.

[8] The terminology was recently changed to "environmentally assisted cracking" with corresponding nomenclature K_{IEAC} .

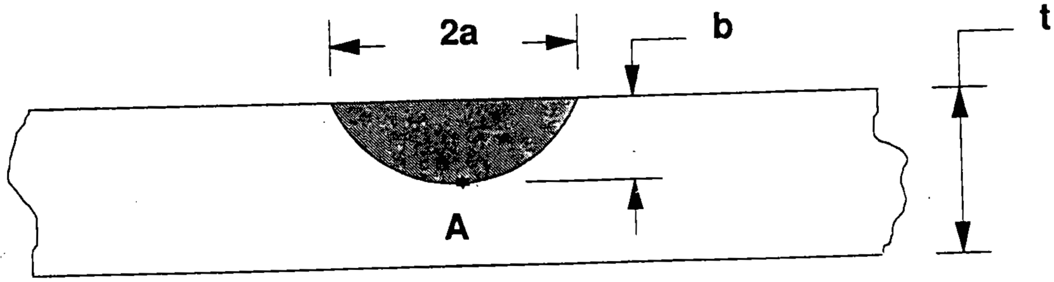

At point A: $K_I = 1.12\, M_{k2}\, \sigma \sqrt{\frac{\pi a}{Q}}$

for $b/2a < 0.5$, $(M_{kl} = 1.12)$

(a) Flaw shape parameter for surface flaws.

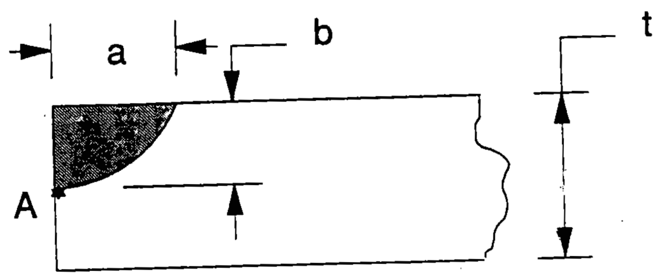

At point A: $K_I = 1.25\, M_{k2}\, \sigma \sqrt{\frac{\pi a}{Q}}$

for $b/2a < 0.5$, $(M_{kl} = 1.12 \times 1.12 \cong 1.25)$

(b) Flaw shape parameter for internal flaws.

Figure 2-42. Geometries of surface and corner cracks.

σ = gross stress

σ_{ys} = yield strength

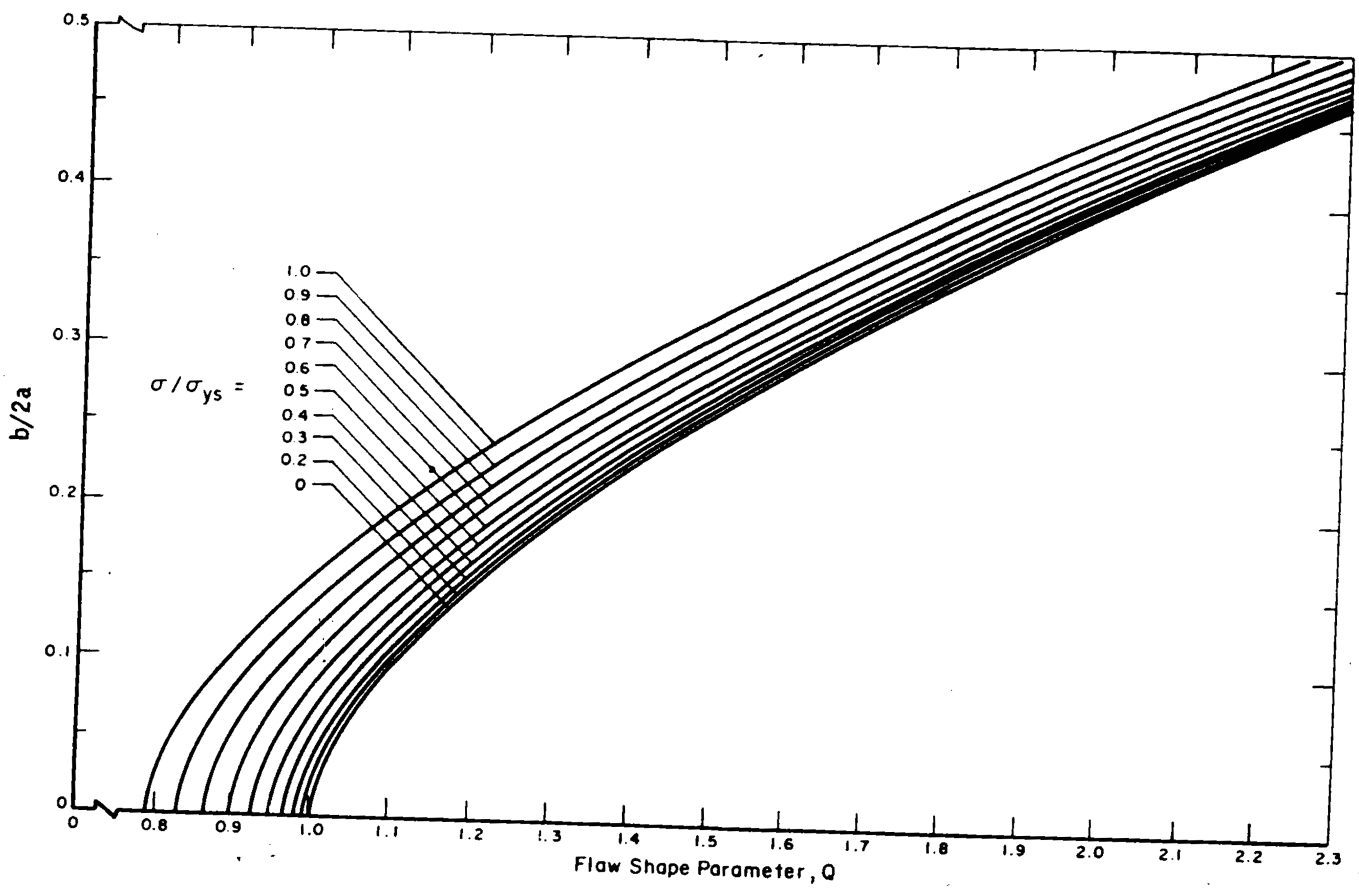

Figure 2-43. Stress intensity factors for surface and corner cracks.

[Reprinted from Damage Tolerant Design Handbook, 1975, Fig. 11.1.1-1, by permission of Battelle, Columbus, Ohio.]

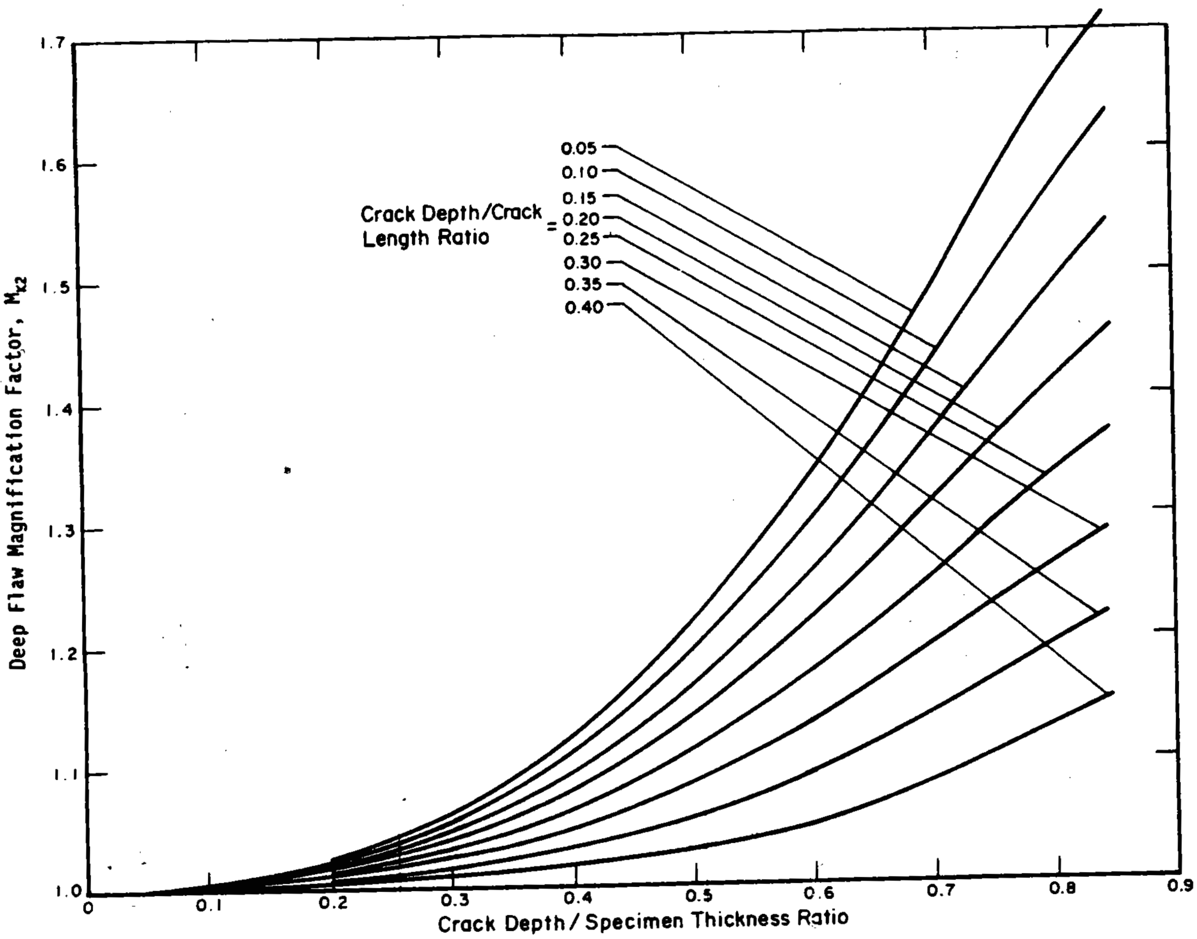

Figure 2-44. Deep flaw magnification factor curves.

[Reprinted from Damage Tolerant Design Handbook , 1975, Fig. 11.1.1-2, by permission of Battelle, Columbus, Ohio.]

REFERENCES FOR CHAPTER 2

2-1. Timoshenko, S.P. History of Strength of Materials, McGraw-Hill, 1953.

2-2. Inglis, C.E., "Stresses in a Plate Due to the Presence of Cracks and Sharp Corners," Transactions of the Institute of Naval Architects, Vol 55, 219-231, 1913.

2-3. Gordon, J.E., Structures or Why Things Don't Fall Down, Plenum Press, 1978.

2-4. Griffith, A.A., "The Phenomenon of Rupture and Flow in Solids," Philosophical Transactions of the Royal Society of London, A221, 163-197, 1920.

2-5. Irwin, G.R., "Analysis of Stresses and Strains Near the End of a Crack Traversing a Plate," Trans. ASME, J. Appl. Mech., Vol. E24, 1957, 361.

2-6. Tada, H., Paris P.C., and Irwin G.R., The Stress Analysis of Cracks Handbook, Del Research Corporation, Hellertown, PA, 1973.

2-7. Rooke, D.P., and Cartwright, D.J., Compendium of Stress Intensity Factors, H.M., Stationery Office, London, 1975.

2-8. Sih, G.C., Handbook of Stress Intensity Factors, Lehigh University, Bethlehem, PA, 1973.

2-9. Murakami, Y. (ed.), Stress Intensity Factors Handbook, Pergamon Press, New York, 1987.

2-10. Irwin, G.R., "Fracture Dynamics," Fracturing of Metals, American Society for Metals, 147-166, 1948.

2-11. Orowan, E., "Fracture and Strength of Solids," Reports on Progress in Physics, XII, 185, 1948.

2-12. Standard Method of Test for Plane-Strain Fracture Toughness of Metallic Materials, ASTM E-399-83, American Society for Testing Materials, 1985.

2-13. Barsom, J.M., and Rolfe, S. T., Fracture and Fatigue Control in Structures, 2nd Edition, Prentice-Hall 1987.

2-14. Kanninen, M.F., and Popelar, C. H., Advanced Fracture Mechanics, Oxford University Press, New York 1985.

2-15. Broek, D., The Practical Use of Fracture Mechanics, Kluwer Academic Publishers, Dordrecht, Netherlands, 1988.

2-16. McCabe, D.E. (ed.), Fracture Toughness Evaluation by R-Curve Methods, ASTM STP 527, American Society for Testing and Materials, Philadelphia, PA, 1973.

2-17. Standard Practice for R-Curve Determination, ASTM Standard E-561-81, Vol 03.01, Metal-Mechanical Testing.

2-18. Creager, M., "A Note on the Use of a Simplified Technique for Failure Prediction Using Resistance Curves," Fracture Toughness Evaluation by R-Curve Methods, ASTM STP 527, American Society for Testing and Materials, Philadelphia, PA, 1973.

2-19. Ratwani, M.M. and Wilhem, D.P. Development and Evaluation of Methods of Plane Strain Fracture Analysis, Northrop Corporation, Aircraft Division, Los Angeles, CA, AFFDL-TR-73-42, April 1975.

2-20. Feddersen, C.E., Evaluation and Prediction of the Residual Strength of Center-Cracked Panels. ASTM STP 486, American Society for Testing and Materials, Philadelphia, PA, 1970.

2-21. British Standard Institution BS5762, Methods for Crack Opening Displacement Testing, BSI (1979), London.

2-22. Rice, J.R., "A Path Independent Integral and the Approximate Analysis of Strain Concentration by Notches and Cracks, " Journal of Applied Mechanics, 35, 379-386, 1968.

2-23. Sih, G.C., "Strain-Energy-Density Factor Applied to Mixed Mode Crack Problems," International Journal of Fracture 10, 305-321, 1973.

2-24. Sih, G.C., "Some Basic Problems in Fracture Mechanics and New Concepts," Engineering Fracture Mechanics 5, 365-377, 1974.

2-25. Sih, G.C., and Madenci, E., "Fracture Initiation Under Gross Yielding, Strain Energy Density Criterion" Engineering Fracture Mechanics 18, 667-677,1983.

2-26. Sih, G.C. and Chen, C., "Non-self-similar Crack Growth in Elastic-Plastic Finite Thickness Plate," Theoretical and Applied Fracture Mechanics 3, 125-139, 1985.

2-27. Sih, G.C., "Fracture Mechanics of Engineering Structural Components," in Fracture Mechanics Methodology: Damage Evaluation of Structural Components Integrity (Sih, G.C. and de O. Faria, L. ed.), Martinus Nijhoff, Netherlands, 1984.

2-28. Sih, G.C. and MacDonald, B., "Fracture Mechanics Applied to Engineering Problems-Strain Energy Density Fracture Criterion," Engineering Fracture Mechanics 6, 361-386, 1974.

2-29. Erdogan, F., Theoretical and Experimental Study of Fracture in Pipelines Containing Circumferential Flaws, Lehigh University, Bethlehem, PA, DOT-RSPA-DMA-50/83/3 (1982).

2-30. Sneddon, I.N., "The Distribution of Stress in the Neighbourhood of a Crack in an Elastic Solid," Proceedings of the Royal Society A, 187-229 (1946).

2-31. Shah, R.C. and Kobayashi, A.S., "Stress Intensity Factor for an Elliptical Crack Under Arbitrary Normal Loading," Engineering Fracture Mechanics 3, 71-96 (1971).

2-32. Shah, R.C. and Kobayashi, A.S., "Stress Intensity Factor for an Elliptical Crack Approaching the Surface of a Semi-Infinite Solid," International Journal of Fracture 9, 133-146 (1973).

2-33. Campbell, J.E., Damage Tolerant Design Handbook, Metals and Ceramics Information Center, Battelle Columbus Laboratories, 505 King Avenue, Columbus, OH 43201, MCIC-HB-01, 1975.

2-34. Gallagher, J.P., Giessler, F.J., and Berens, A.P., USAF Damage Tolerant Design Handbook: Guidelines for the Analysis and Design of Damage Tolerant Aircraft Structures, Flight Dynamics Laboratory, Air Force Wright Aeronautical Laboratories, Wright-Patterson Air Force Base, OH 45433, AFWAL-TR-82-3073, May 1984.

CHAPTER 3:

FATIGUE CRACK PROPAGATION

3. FATIGUE CRACK PROPAGATION

Fatigue crack propagation was not treated as a subject separate from fatigue failure until the mid-1960s. Before then engineers were accustomed to dealing with metal fatigue based on time-to-failure data (see Chapter 1). They understood that a crack had to form and propagate to fail a test specimen, but they recognized that crack formation consumed most of the time, and they saw no need to consider the relatively short propagation phase as a significant phenomenon in its own right.[1] After all, structures were not intentionally built with cracks in them, and fatigue life (time to crack occurrence) was therefore the main concern for the designer. Not until 1970 did engineers begin to realize the importance of crack propagation as a distinct aspect of structural damage tolerance.[2] Laboratory and theoretical studies of crack propagation paved the way for that advance.

3.1 ENERGY-BASED THEORY OF CRACK PROPAGATION

In the mid-1960s, research scientists working in the field of fracture mechanics began to consider the effects of repeated subcritical loads on cracks from an energy viewpoint.

Griffith's energy balance concept of fracture did not include stable crack extension, but the contradiction could be addressed by arguments based on the "pop-in" phenomenon. Recall that a small but measurable stable crack extension ("pop-in") is observed in some fracture toughness tests as the critical load is approached. One could then postulate that crack extension would be proportional to the stress intensity factor range at lower loads but too small to measure (Figure 3-1).[3]

---

[1] Crack formation typically consumes 95 percent of the measured life of a rotating bending fatigue test specimen. The percentages for other common types of fatigue test specimens are comparable.

[2] The effect of crack propagation was dramatically demonstrated by the crash of an F-111 at Nellis Air Force Base, Nevada in 1969. The crash was caused by the catastrophic failure of the wing carry-through box lower skin during a training mission. An extremely large forging flaw in the skin propagated to critical size in 105 flight hours. Based on the older fatigue analysis approach, the F-111 airframe was estimated to have a safe-life of 8,000 flight hours.

[3] Since Mode I loading is used in most laboratory fatigue crack growth tests and is assumed in most damage tolerance analyses, the simpler notation K is used to represent K_I in this chapter.

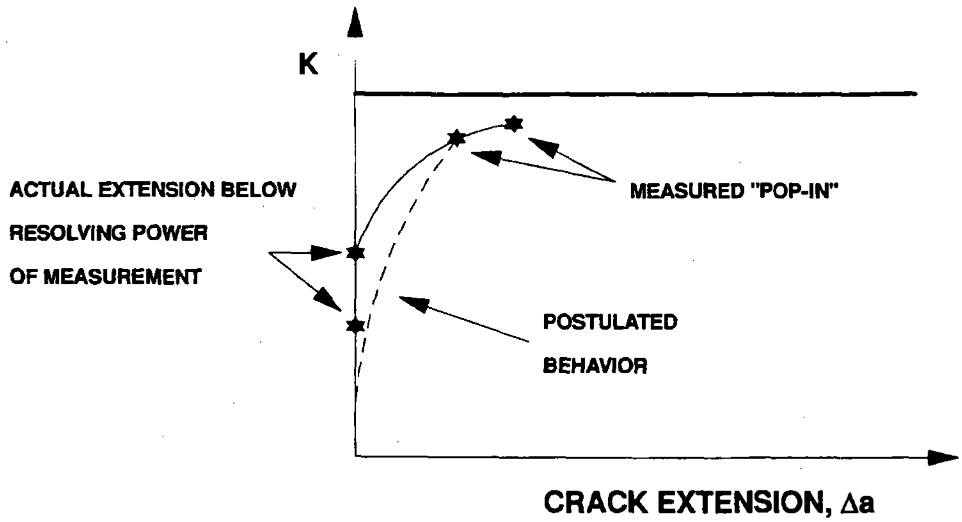

Figure 3-1. Argument for relating fatigue crack growth rate to applied stress intensity factor.

Fatigue crack propagation was explained by further assuming that repeated cycles from zero load to the same stress intensity factor K would cause the same amount of crack extension per cycle. The extension Δa per cycle was given the special notation da/dN to reflect its interpretation as a crack growth rate. The notation ΔK was also adopted in place of K to symbolize the range (minimum to maximum) of the fatigue loading cycle. Thus, based on the energy concept, fatigue crack growth rates were expressed in the general form [3-1]:

$$\frac{da}{dN} = C(\Delta K)^2 \tag{3-1}$$

where C is a constant which depends on the material.

If the range of the fatigue stress ΔS or load ΔP is kept constant, the crack growth rate should gradually increase as the lengthening crack increases the stress intensity factor range ΔK. This effect was observed in fatigue crack growth experiments [3-2]. An example is shown in Figure 3-2.

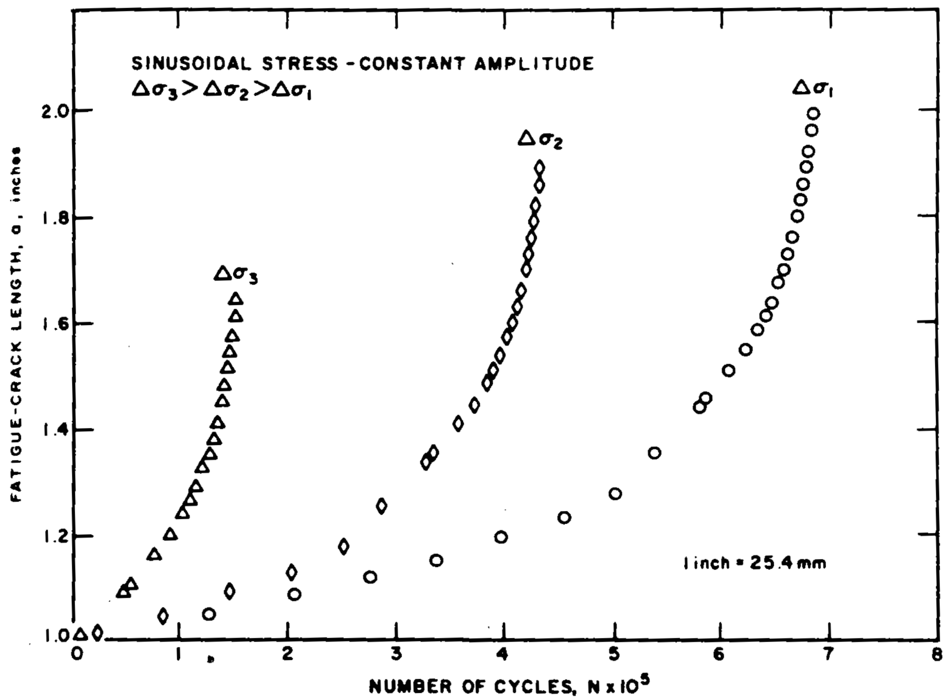

Figure 3-2. Effect of cyclic load range on crack growth in Ni-Mo-V alloy steel for released tension loading.

[Reprinted from John M. Barsom and Stanley T. Rolfe, Fracture and Fatigue Control in Structures: Applications of Fracture Mechanics, 2e, © 1987, Fig. 8.2, by permission of Prentice Hall, Englewood Cliffs, NJ.] [3–11]

3.2 EMPIRICAL CRACK GROWTH RATE EQUATIONS

When analysts calculated crack growth rates from the test results, they found that most materials did not follow equation (3-1). However, the results could usually be correlated with the more general expression:

$$\frac{da}{dN} = C(\Delta K)^m \tag{3-2}$$

where the rate exponent was also treated as a material property.[4] Equation (3-2) is often called a Paris equation after the author of the original concept [3-1 and 3-3].

Additional phenomena were discovered as further experiments extended to higher and lower ΔK values. At low values, a rapid decline in the crack growth rate was observed, and the observations led to the idea of a threshold stress intensity factor, K_{TH}, defining the limit of fatigue crack propagation.[5] At high values, a rapid increase in crack growth rate was observed.

Additional static tensile stress superimposed on the fatigue stress cycle was also found to affect the crack growth rate and threshold stress intensity factor in some materials, as it affects fatigue life. The stress cycles in such crack growth rate tests are characterized by the stress range ΔS and the stress ratio R:

$$\Delta S = S_{max} - S_{min} \tag{3-3}$$

$$R = \frac{S_{\min}}{S_{\max}} = \frac{K_{\min}}{K_{\max}} \tag{3-4}$$

instead of the older amplitude and mean stress terminology.[6] Figure 3-3 illustrates the definitions and relations between the two systems.

---

[4] Generally one finds values in the range $2 \leq m \leq 5$ for a wide variety of aluminum, steel, and titanium alloys.

[5] In practice the threshold is set by how long the experimenter is willing to continue a test. The typical limit is about 10^{-9} inch per cycle.

[6] Note that under the new system, stress ranges from zero to tension correspond to $R = 0$. If the minimum stress is also tensile, then R is a positive number between 0 and 1. These are the conditions used in most crack growth rate tests. Conversely, the older rotating bending fatigue test (alternating tension and compression with zero mean stress) corresponds to $R = -1$.

OLD SYSTEM

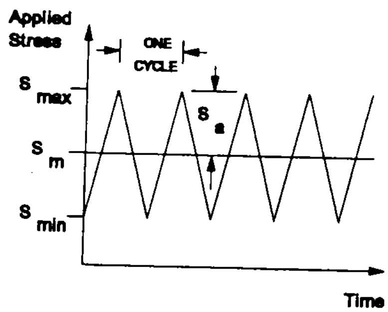

NEW SYSTEM

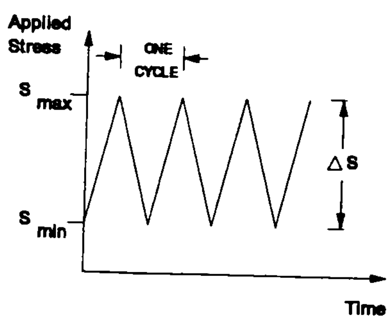

RELATIONS BETWEEN OLD AND NEW DESCRIPTORS:

$$2S_a$$

$$= \Delta S = S_{max} - S_{min}$$

$$\frac{S_m - S_a}{S_m + S_a} = R = S_{\min}/S_{\max}$$

Figure 3-3. Alternate definitions of stress cycle.

The next two figures illustrate these phenomena. Figure 3-4 shows the most common graphical format for presenting the results of a crack growth rate test. The test data are plotted on logarithmic scales, log (*da/dN*) versus *log* ΔK, so that a relation like the Paris equation, equation (3-2), plots as a straight line with slope *m*, i.e.,

$$\log\left(\frac{da}{dN}\right) = \log C + \mathrm{m}\log(\Delta K)$$

In this case, a line with slope $m = 2.3$ appears to fit the upper edge of the data band reasonably well in the slow crack growth rate region. Most of the data in this region falls within a factor of two scatter band.[7] (This is typical of fatigue crack growth rate data and is much less than the scatter usually observed in the older fatigue tests for time to crack occurrence.)

The intercept at $\Delta K = 10$ ksi $\sqrt{in}$ is a convenient point to use for calculating the growth rate constant C. In this case, the result $C \cong 5 \times 10^{-8}$ is obtained from $10^{-5} = C\,(10)^{2.3}$ as shown by the summary at the right hand edge of the plot. Thus, this particular set of test data is represented by:

$$\frac{da}{dN} \cong 5x10^{-8}(\Delta K)^{2.3} \tag{3-5}$$

The small positive stress ratio ($R = 0.05$) is typically used to investigate behavior near $R = 0$, in order to avoid specimen misalignment that would occur under slack grip conditions at $R = 0$.

Note that the data points near $\Delta K = 10$ ksi $\sqrt{in}$ begin to fall below the scatter band. This suggests that a threshold stress intensity factor, KTH might have been determined, had the tests included some results at ΔK values a bit less than 10 ksi $\sqrt{in}$.

Conversely, the data at ΔK values exceeding 45 ksi $\sqrt{in}$ follows a trend above the scatter band. This region of accelerated crack growth rates reflects the transition from slow crack growth to the stable extension regime in the R-curve (see Section 2.4.1). For this material and thickness, one

7 The more common practice in damage tolerance analysis is to fit the results with a slightly lower line passing through the average of the slow crack growth rate region.

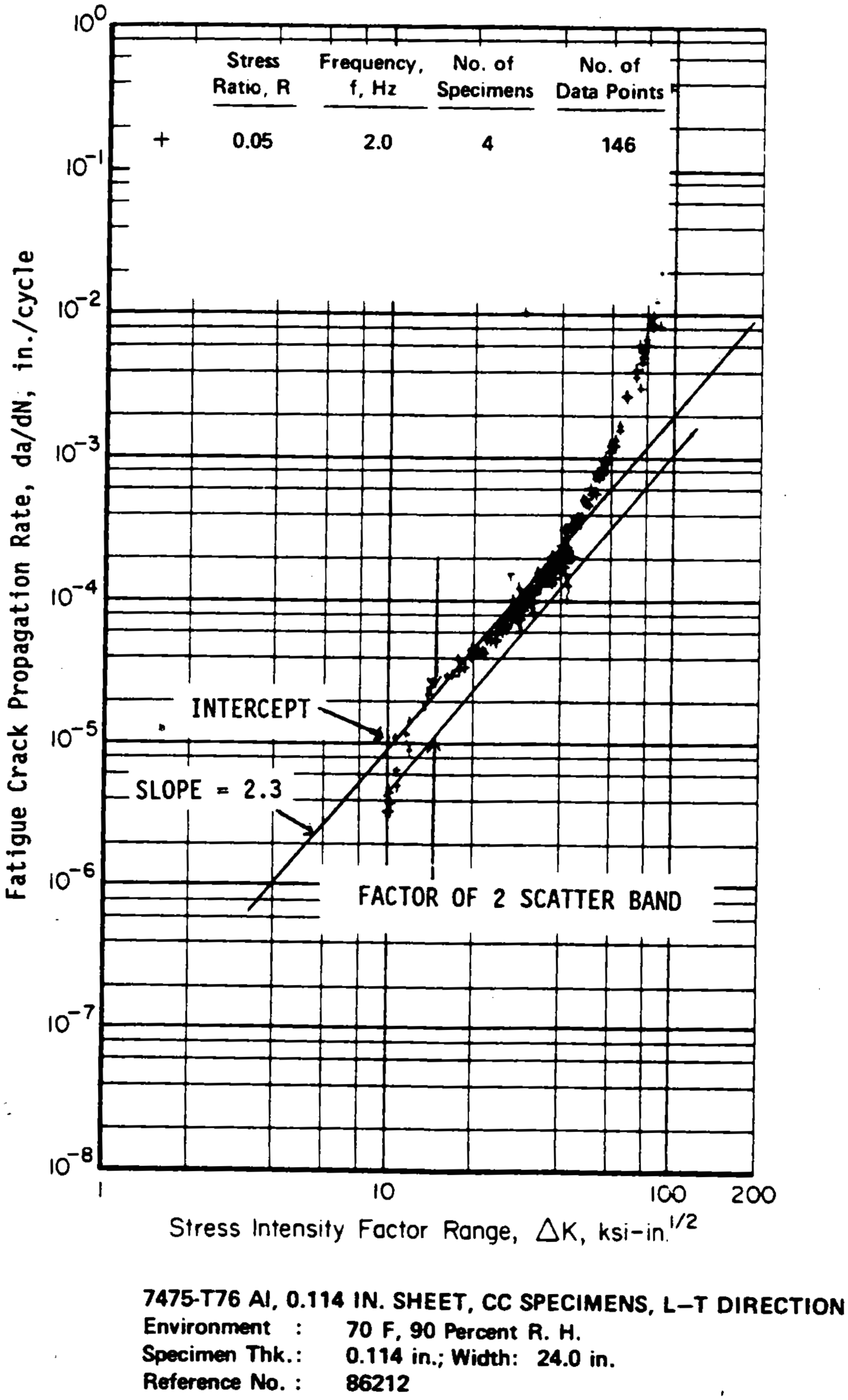

$INTERCEPT = 10^{-5}$
$AT \;\; \Delta K = 10$

$$C = \frac{10^{-5}}{10^{2.3}} = 5x10^{-8}$$

Figure 3-4. Crack growth rate in 7475-T6 aluminum.

[Reprinted from Damage Tolerant Design Handbook, 1975, Fig. NAW28, by permission of Battelle, Columbus, Ohio.] [3-12]

would expect an R-curve asymptote of roughly 100 ksi $\sqrt{in}$, i.e., at about the right position to be an asymptote for the accelerated crack growth rate trend.[8]

Figure 3-5 illustrates the effect of stress ratio on the crack growth rates in 7075-T6 specimens. It is evident that increasing the stress ratio makes the crack growth rate increase, an effect generally found in aluminum alloys. The ΔK axis in this plot is linear, so the rate exponent m cannot be conveniently determined. When such data is plotted on the common format using logarithmic scales on both axes, it is usually found that increasing the stress ratio: (1) increases the crack growth rate constant C but does not change the rate exponent m; (2) decreases the threshold stress intensity factor K_{TH}; and (3) decreases the ΔK value of the accelerated crack growth rate asymptote.

When the stress ratio has a significant effect on crack growth rate, the effect is commonly represented by modifying the Paris equation to the form:

$$\frac{da}{dN} = \frac{C(\Delta K)^m}{(1 - R)} \tag{3-6}$$

Equation (3-6) is often called a Walker equation, after the author who originally proposed the form [3-4]. For example, taking account of the actual test conditions $R = 0.05$ for the data shown in Figure 3-4, one might choose to represent those results by the Walker equation.

$$\frac{da}{dN} = \frac{4.76 \times 10^{-8}(\Delta K)^{2.3}}{(1 - R)} \tag{3-7}$$

instead of equation (3-5).

When a Walker equation is used to represent the data near the threshold region, the 1-R factor is also used to modify the threshold stress intensity factor if it has not been measured at different stress ratios. The estimated threshold value is given by $(1\text{-}R)K_{TH}$, where K_{TH} is the value of the

---

[8] A similar test of a thicker specimen with a higher R-curve asymptote would be expected to have a slow growth region extending to higher ΔK values.

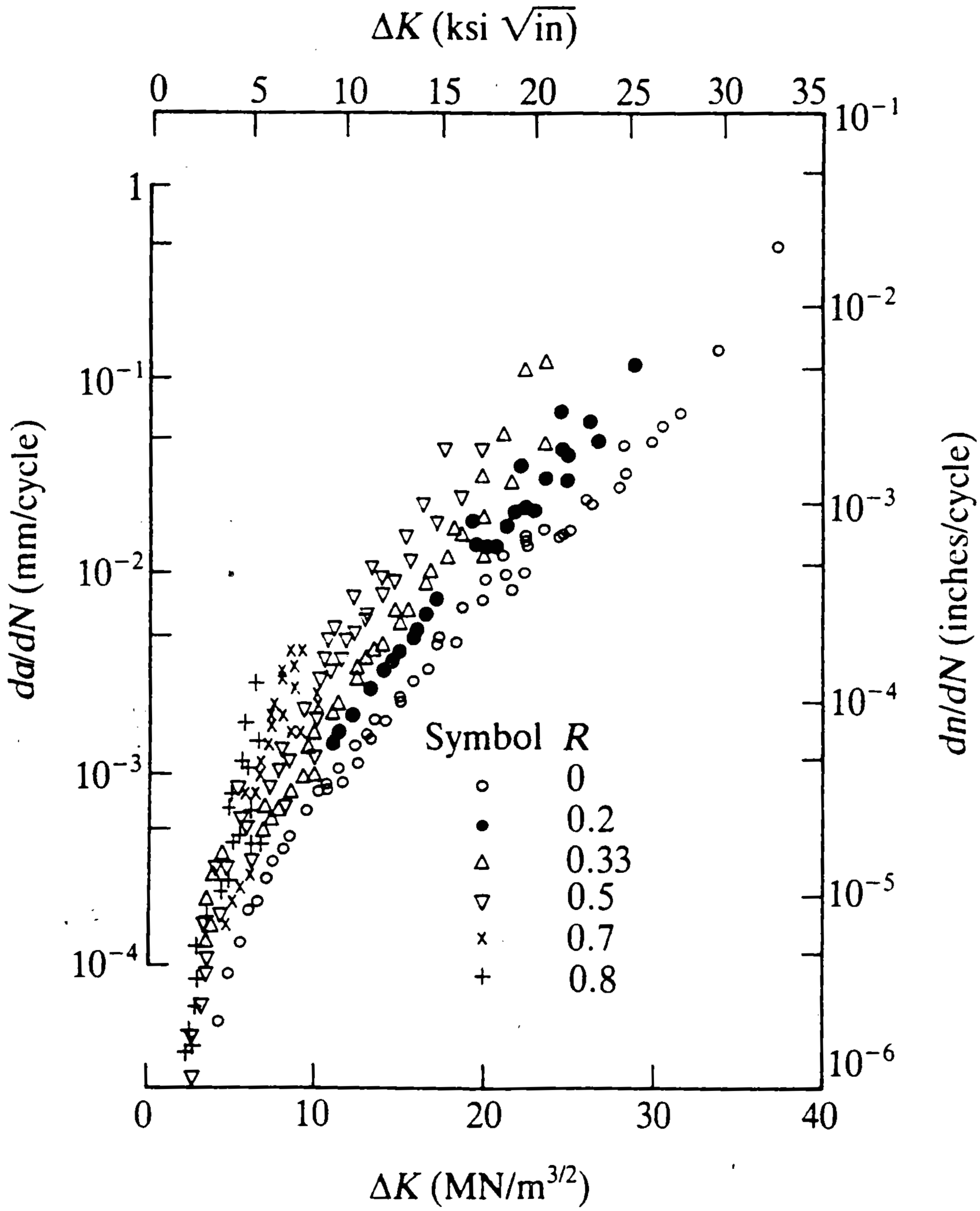

Figure 3-5. Effect of stress ratio on 7075-T6 aluminum crack growth rate.

[Reprinted from T.H. Courtney, Mechanical Behavior of Materials, 1e, © 1990, Fig. 12.17, by permission of McGraw-Hill, New York, N.Y.] [3-13]

threshold stress intensity factor at $R = 0$. This formula is based on the assumption that the maximum stress intensity factor controls the threshold phenomenon.

One other useful form is the modified Walker equation [3-5]:

$$\frac{da}{dN} = \frac{C(\Delta K)^m}{(1 - R)^p} \tag{3-8}$$

where p is another empirical constant. This form is particularly useful for representing data from tests with a wide variation of stress ratios.

Literally dozens of empirical equations have been proposed for the purpose of fitting the da/dN - ΔK plot. Many of these equations are elaborate attempts to fit the entire plot (threshold, slow growth, and accelerated regions), in spite of the fact that most crack growth analyses require consideration of only one (or at most two) of the three behavior regions.

In addition to the Paris and Walker equations, the following equation proposed by Forman [3-6] is often used to fit the slow and accelerated crack growth regions:

$$\frac{da}{dN} = \frac{C(\Delta K)^m}{(1 - R)K_c - \Delta K} \tag{3-9}$$

where K_c represents the accelerated crack growth asymptote.

In Forman's equation the constants C and m are determined by fitting the data at one R, usually at $R = 0$. Hence, the curves generated by the equation may not fit the experimental data well for all other R ratios.

None of the models just described account for the threshold effect. While some of the more elaborate equations do so, the common practice is to combine one of the above equations with the so-called sharp cutoff threshold model:

$$\frac{da}{dN} = 0 \; for \; \Delta K \; < \; (1 - R)K_{TH} \tag{3-10}$$

This procedure conservatively overestimates the crack growth rate at ΔK values above but close to the threshold.

Other empirical models have been proposed to represent the $\frac{da}{dN}$ *versus* ΔK relation. The modified Forman's equation

$$\frac{da}{dN} = \frac{C[(1-R)^{n-1}\,\Delta K]^m}{[(1-R)^n K_c - (1-R)^{n-1}\,\Delta K]^L} \tag{3-11a}$$

or

$$\frac{da}{dN} = C(1-R)^{(n-1)(m-L)}\,\frac{(\Delta K)^m}{[(1-R)K_c \, - \, \Delta K]^{\,L}} \tag{3-11b}$$

was proposed [3.7] to better control the spread of crack growth rate curves by introducing two additional constants n and L.

Collipriest et al. proposed an inverse hyperbolic tangent equation to represent the sigmoidal character of the crack growth rate curve [3.8 and 3.9]

$$\log \frac{da}{dN} = C_1 + C_2 \; \tanh^{-1} \left[\frac{\log\left\{\dfrac{\Delta K^2}{K_o K_c (1-R)^2}\right\}}{\log \; K_c / K_o} \right] \tag{3-12}$$

where K_o is the threshold stress intensity factor and C_1, C_2 are constants.

However, with the introduction of new and powerful computers, tabular simulation of *da/dN* data is being used more frequently instead of a mathematical expression such as the models described above.

A comprehensive treatment of crack growth rate equations is given by Swift [3-10].

3.3 CORRELATION WITH MATERIAL PROPERTIES

Applicable data must first be correlated to establish the parameters of a *da/dN* equation before it can be used in a damage tolerance analysis. Applicability means testing with cracks oriented the same way relative to the material microstructure (Figure 2-14) as expected for the crack orientation in the actual structure. Applicability also means test specimens of a thickness similar to that of the structure or, if the structure is a heavy forging, specimens at least thick enough to qualify as valid for plane strain fracture toughness testing.

When data correlations are presented, the reviewer should pay attention to repeatability in the slow crack growth regime and sample size. The calculation of rates from actual test data involves finding a small number (the crack extension over perhaps a few hundred cycles) by taking the difference of two large numbers (crack length at the first and last cycles). Any error measuring crack length will be amplified by the difference procedure and may distort the results. Measurement error should be suspected if data in the slow or accelerated growth regions is spread over a scatter factor much greater than 2.

Single specimen tests may be influenced by other types of inadvertent error, thus giving an inaccurate picture of the material behavior. Small sample size is an indication that only one or two tests have been performed. The best way to make an initial assessment of such data is to compare its *da/dN* equation parameters with the range of values expected for the alloy class to which the material belongs. Some examples [3-11] which are useful for such comparisons are presented in the next three figures.

Figure 3-6 presents a summary of data from six different aluminum alloys with yield strengths from 34 to 55 ksi. The dashed lines define the scatter band, which has a factor of 3 in the lower, slow growth half of the figure. For many aluminum alloys, including some of those in the figure, the slow growth region is well represented by the rate exponent $m = 4$ with the rate constants C between 10^{-9} and 10^{-10}, as indicated by the solid lines which have been superimposed on the plot. The alloys well represented by $m = 4$ include most of the older aircraft structural alloys.

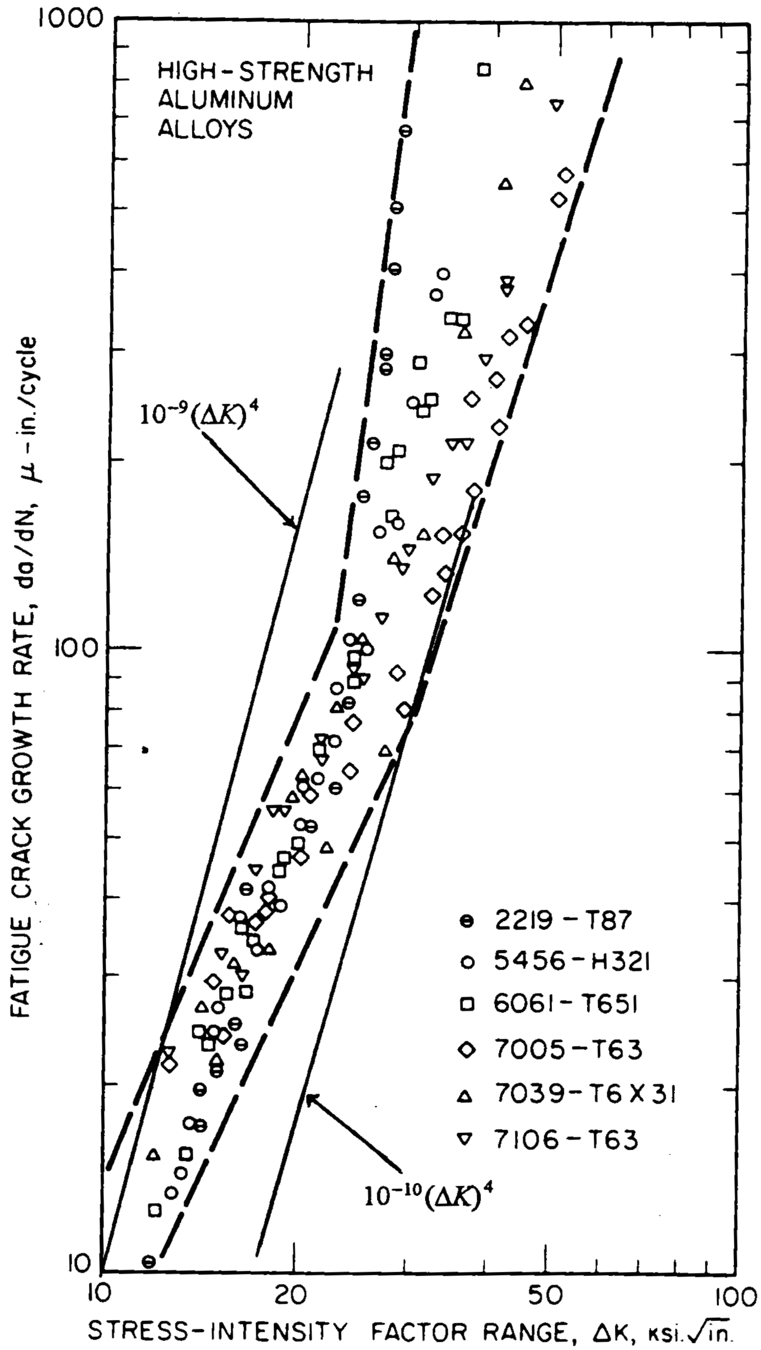

Figure 3-6. Summary plot of *da/dN* versus ΔK for six aluminum alloys.

[Reprinted from John M. Barsom and Stanley T. Rolfe, Fracture and Fatigue Control in Structures : Applications of Fracture Mechanics, 2e, © 1987, Fig. 8.13, by permission of Prentice Hall, Englewood Cliffs, N.J.] [3-11]

Figure 3-7 presents three Paris equations derived by Barsom and Rolfe [3-11] to represent the three major classes of steel alloys. These alloys generally have low sensitivity to the stress ratio effect. Martensitic alloys (quenched and tempered ferritic steels) are generally found in specialized parts requiring very high strength, such as landing gear struts.

Figure 3-8 summarizes the data for five titanium alloys with yield strengths from 110 to 150 ksi. Titanium alloys are usually well represented by the rate exponent $m = 5$ with the rate constants C between 10^{-12} and 10^{-13}, as indicated by the superimposed solid lines. (The very large scatter band in this figure is an artifact of the high slope in a plot of alloys having different rate constants.)

The following groups of plots have been reproduced from reference [3-12] to provide some typical examples of test results for individual alloys. All of these examples deal with aluminum, the major material component of airframe structure. The process of establishing *da/dN* equation parameters is discussed in relation to each group, and some of the typical problems encountered in data reduction are illustrated.

Figure 3-9(a), (b) and (c) shows the results of tests on 7075-T6 thin sheet at five different stress ratios. Note that these results are presented in terms of total crack growth rate *d(2a)/dN*.[9] Therefore, the rate constant C must be divided by a factor of 2 to obtain the correct value for the *da/dN* equation. In Figure 3-9(a), the data for $R = 0.0$ and $R = 0.2$ appear to lie within the same scatter band, so a single line with rate exponent $m = 4$ has been drawn through the average. This line is associated with the majority of the data ($R = 0$). From the intercept at $\Delta K = 10$ ksi $\sqrt{in}$, a rate constant of 5 x 10^{-10} is obtained. Thus the correct rate constant for the da/dN equation is:

$$C = \frac{5x10^{-10}}{2} = 2.5x10^{-10} \tag{3-13}$$

[9] In the plots, the customary symbol a is used in place of c to denote the crack length.

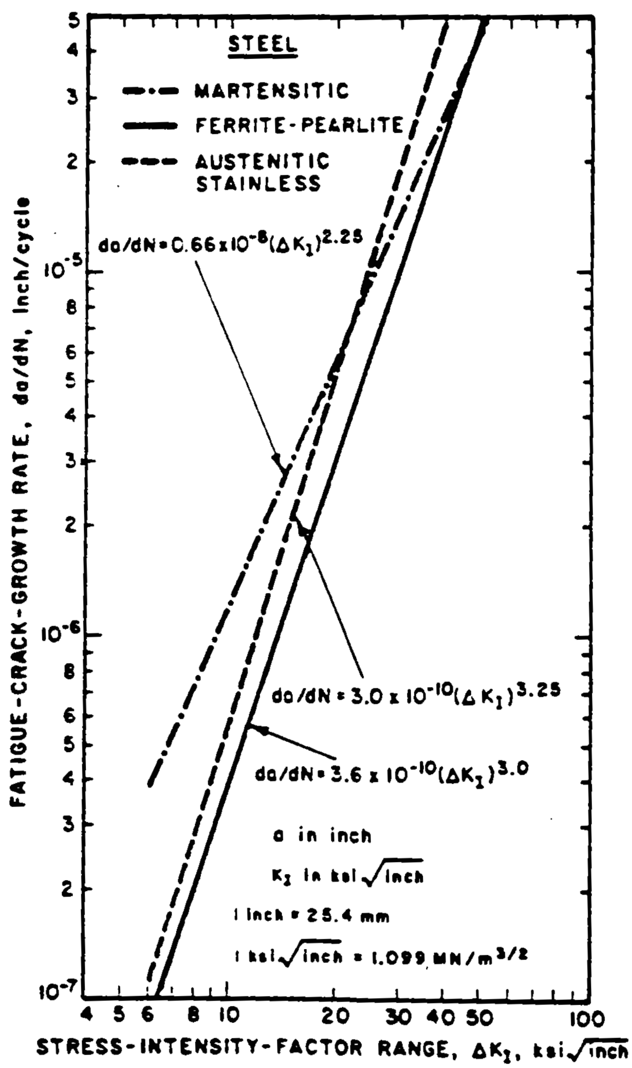

Figure 3-7. Summary plot of *da/dN* versus ΔK for various steel alloys.

[Reprinted from John M. Barsom and Stanley T. Rolfe, Fracture and Fatigue Control in Structures : Applications of Fracture Mechanics, 2e, © 1987, Fig. 8.12, by permission of Prentice Hall, Englewood Cliffs, N.J.] [3-11].

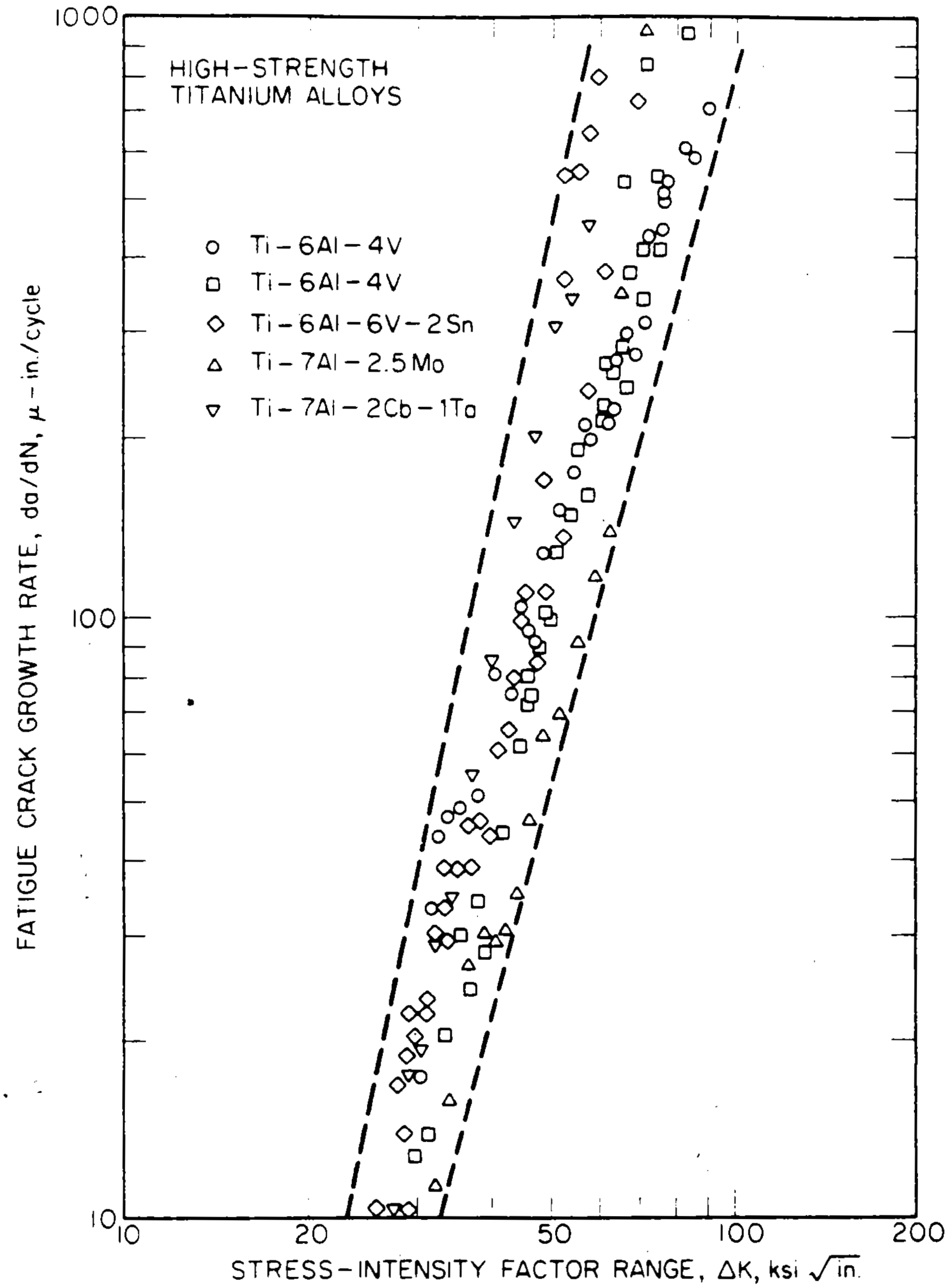

Figure 3-8. Summary plot of *da/dN* versus ΔK for five titanium alloys.

[Reprinted from John M. Barsom and Stanley T. Rolfe, Fracture and Fatigue Control in Structures : Applications of Fracture Mechanics, 2e, ©1987, Fig. 8.14, by permission of Prentice Hall, Englewood Cliffs, N.J.][3-11]

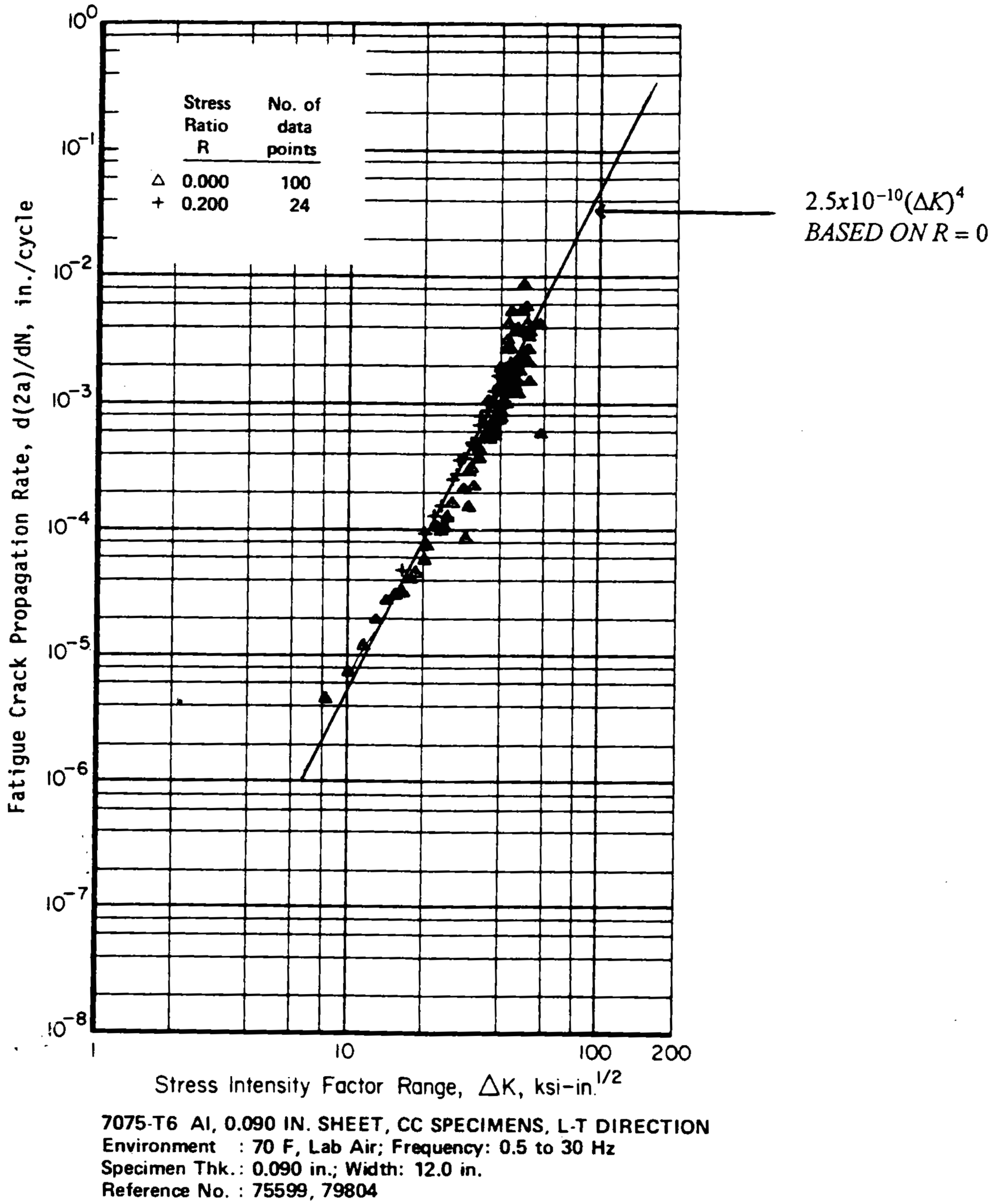

(a) Results for R = 0 and R = 0.2.

Figure 3-9. 7075-T6 aluminum (0.09 in. thick) crack growth rate properties.

[Reprinted from Damage Tolerant Design Handbook, 1975, Fig. NAR4, by permission of Battelle, Columbus, Ohio.] [3-12]

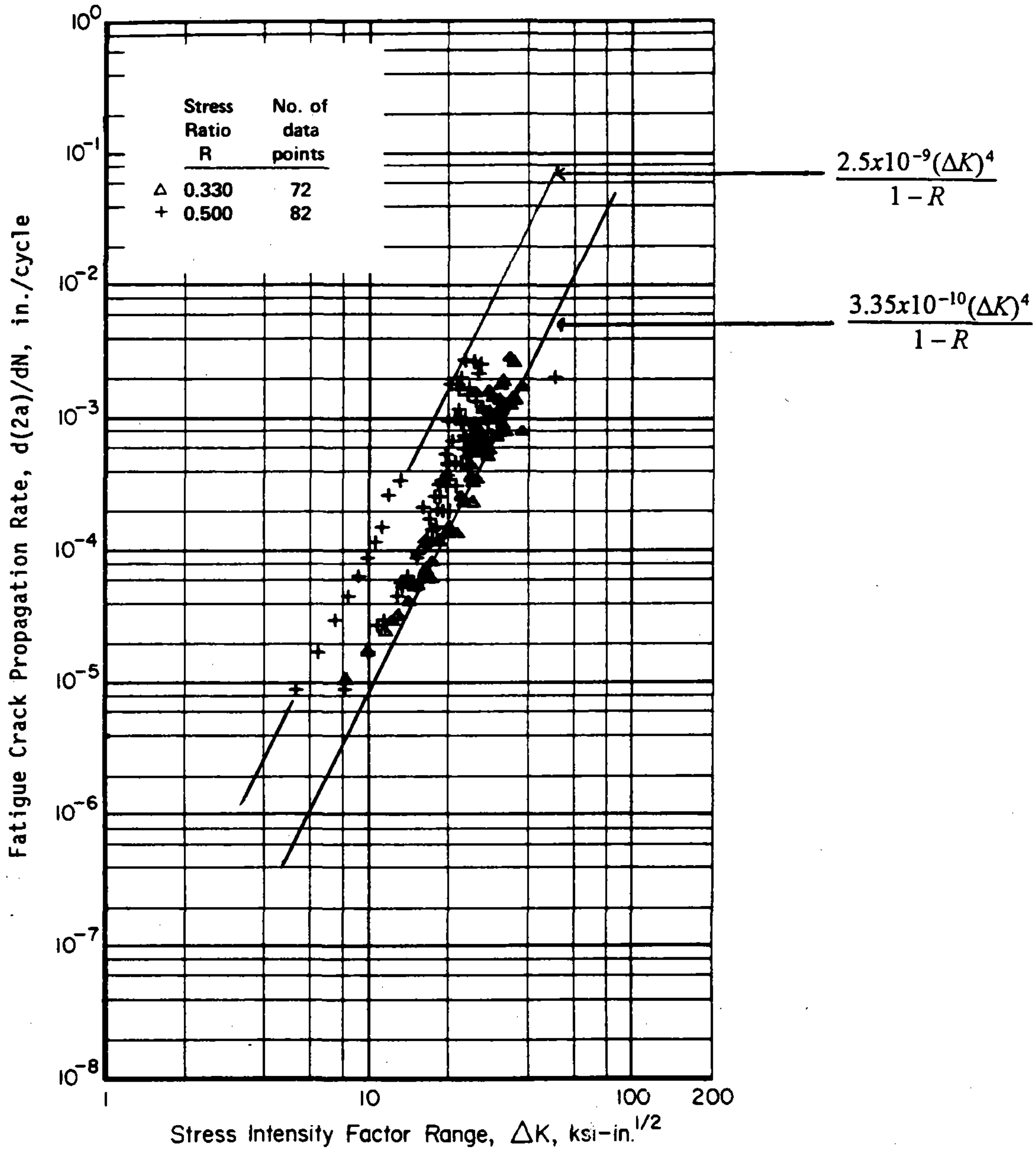

7075-T6 Al, 0.090 IN. SHEET, CC SPECIMENS, L-T DIRECTION
Environment : 70 F, Lab Air; Frequency: 0.5 to 30 Hz
Specimen Thk.: 0.090 in.; Width: 12.0 in.
Reference No. : 75599. 79804

(b) Results for R = 0.33 and R = 0.5.

Figure 3-9 (continued). 7075-T6 aluminum (0.09 in. thick) crack growth rate properties.

[Reprinted from Damage Tolerant Design Handbook, 1975, Fig. NAR5, by permission of Battelle, Columbus, Ohio.] [3-12]

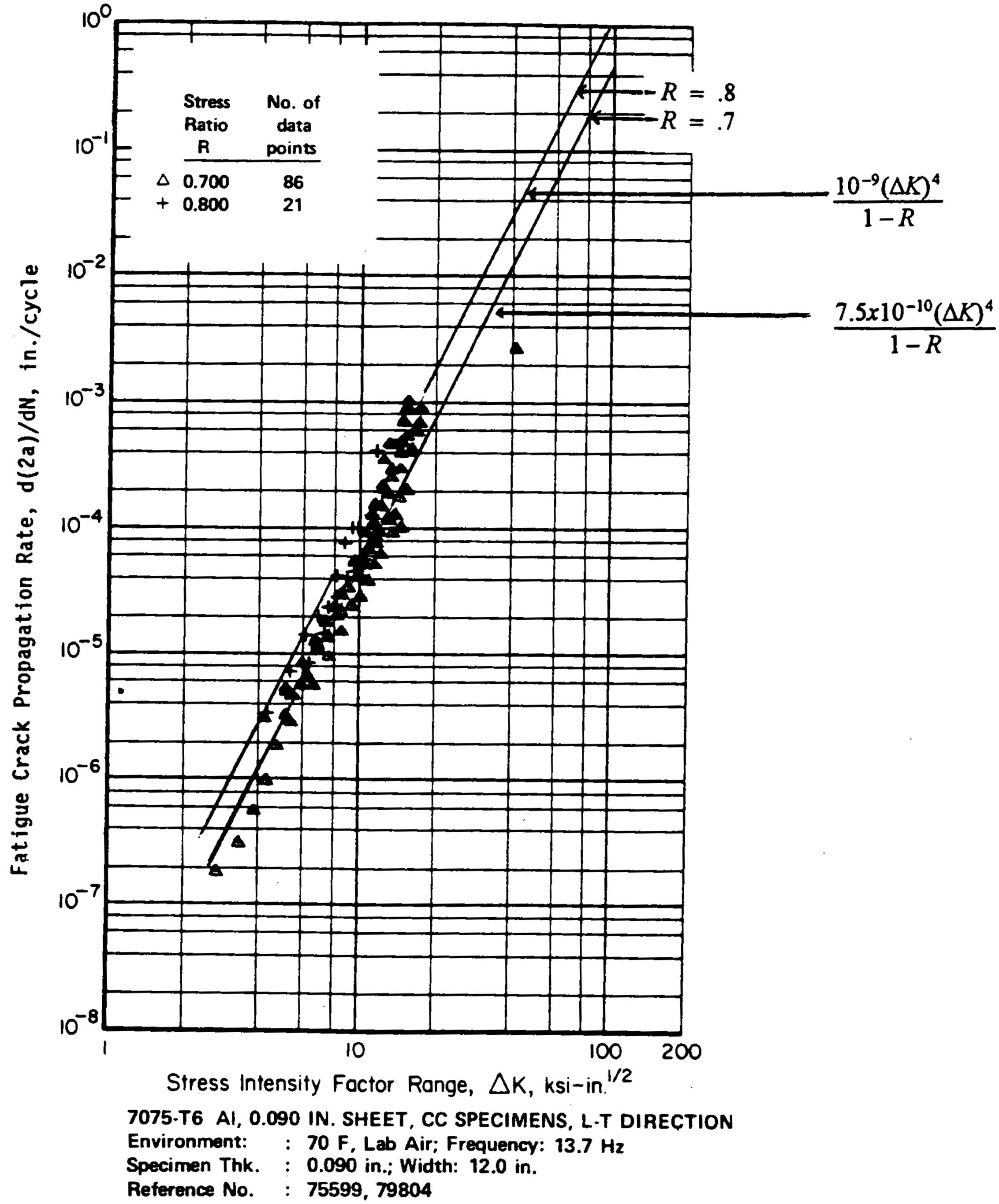

(c) Results for R = 0.7 and R = 0.8.

Figure 3-9 (continued). 7075-T6 aluminum (0.09 in. thick) crack growth rate properties.

[Reprinted from Damage Tolerant Design Handbook, 1975, Fig. NAR6, by permission of Battelle, Columbus, Ohio.] [3-12]

Similar procedures have been followed in Figure 3-9(b) and (c), except that the Walker 1-R factor has also been used to correct the raw rate constant obtained from the plots:

$$C = \frac{(1-R)(Raw\ \ value)}{2} \tag{3-14}$$

The raw value is the C obtained directly from the intercept as given in equation (3-13). The results shown in the right hand border are for the corrected rate constant C.

The table below compares the results obtained from Figure 3-9 and shows that some anomalies exist. For example, C for $R = 0.5$ is much larger than the rate constant obtained for the other stress ratios. Is this a real effect? Closer examination of Figure 3-9(b) casts some doubt on the validity of the high value. The curve fitter's eye was obviously attracted to the series of data points at $R = 0.5$ between $\Delta K = 5$ and $\Delta K = 15$ ksi $\sqrt{in}$. This group is isolated from the clutter and seems to characterize the $R = 0.5$ behavior. Conversely, upon close examination, one can distinguish many more $R = 0.5$ data points in the $R = 0.33$ scatter band. Therefore, the analyst might reasonably discard the $R = 0.5$ curve fit and work with the results from the other stress ratios.

Summary of results for rate constant C obtained from Figure 3-9.

Stress ratio, R	0	0.33	0.5	0.7	0.8
$10^{10}\,C$	2.5	3.35	25.0	7.5	10.0

Even without the $R = 0.5$ result, the spread in the other values for C shows that the Walker equation does not fit this group of data very well. A good fit should produce C values within 10 percent of each other, in order to allow the use of a group average. Conversely, the spread in the above table is a strong warning against extrapolation. If a Walker equation is used, the rate constant should be selected to match the stress ratios expected in the structure when the equation is applied.

On the other hand, the data group (except for $R = 0.5$) can be reasonably well represented by the modified Walker equation:

$$\frac{da}{dN} = \frac{2.5 \times 10^{-10}(\Delta K)^4}{(1 - R)^{1.86}} \tag{3-15}$$

The value $C = 2.5 \times 10^{-10}$ is obtained in this case by modifying equation (3-14), after trial, to the form:

$$C = \frac{(1 - R)^{1.86}(Raw\ value)}{2} \tag{3-16}$$

with the results shown in the table below.

Result of fit with $(1 - R)^{1.86}$ factor.

Stress ratio, R	0	0.33	0.7	0.8
$10^{10}\, C$	2.5	2.37	2.66	2.51

AVG = 2.5

How reliably can any of the *da/dN* equations derived above represent 7075-T6 thin sheet? Aside from the doubtful curve fit for $R = 0.5$, the results appear to come from two test series, and the number of data points is quite large. On the other hand, Figure 3-10 shows two 7075-T6 data sets for somewhat thicker sheet from a different test series. In this case, the C value based on the $R = 0.2$ data is at least three times the value obtained from the preceding data reduction, and at $R = 0.5$ the results agree with the preceding "anomalous" result! This kind of situation can only be resolved by going back to the data sources to check for errors or procedural differences, or by getting more data. The lesson to learn from this example is to compare crack growth rate data from as many independent sources as possible.

Figure 3-11(a) through (d) presents a series of plots for 2024-T3 thin sheet at four different stress ratios. The plots in Figure 3-11(*a*) come from a different test series than the other plots, and the two values $R = 0.1$ and $R = 0.11$ are considered to represent the single stress ratio $R = 0.1$ for

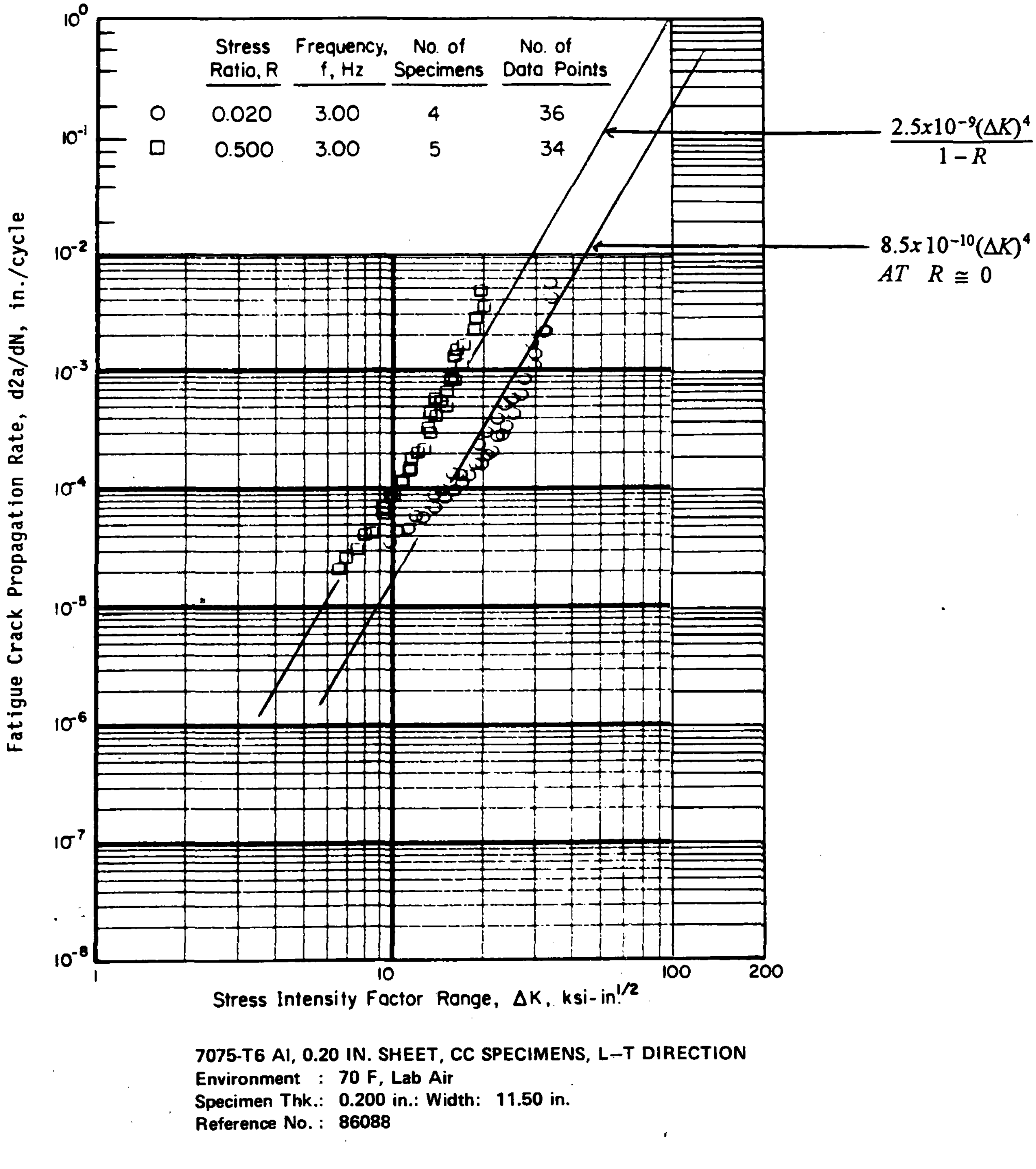

Figure 3-10. 7075-T6 properties (0.2 in. thick) from a different test series.

[Reprinted from Damage Tolerant Design Handbook, 1975, Fig. NAR7, by permission of Battelle, Columbus, Ohio.] [3-12]

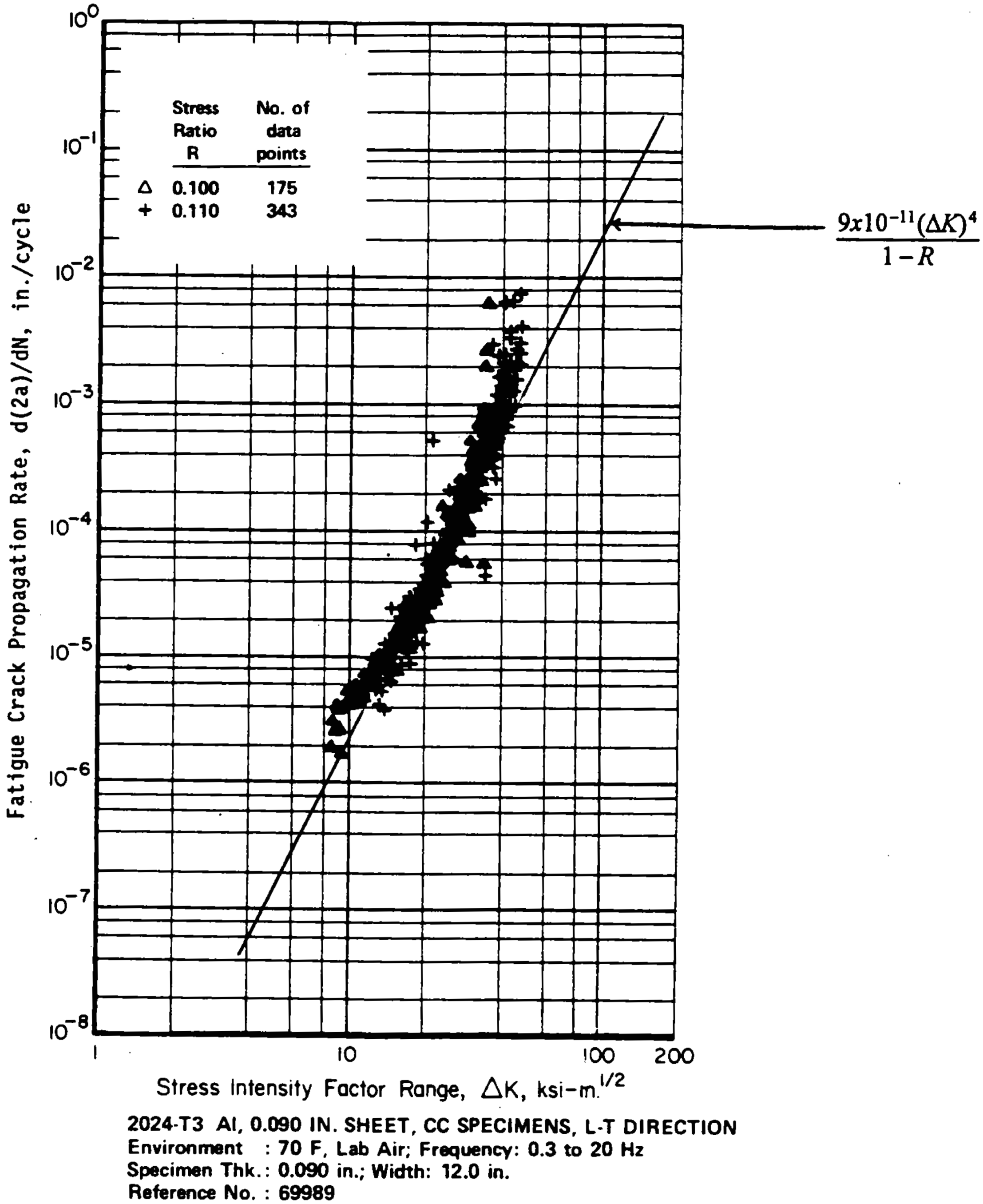

(a) Results for R = 0.1 and R = 0.11 (different test series).

Figure 3-11. 2024-T3 aluminum (0.09 in thick) properties.

[Reprinted from Damage Tolerant Design Handbook, 1975, Fig. NAD6, by permission of Battelle, Columbus, Ohio.] [3-12]

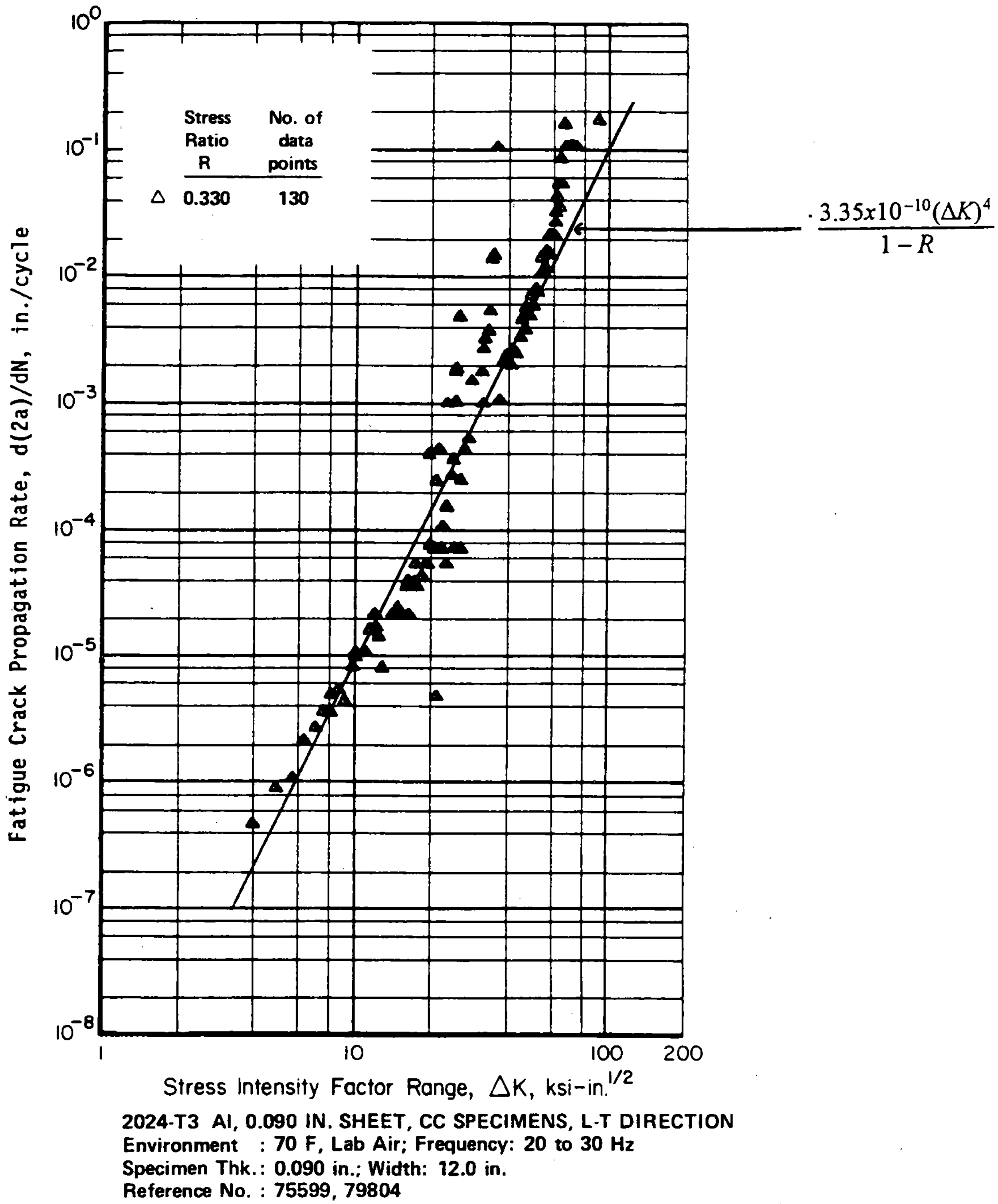

(b) Results for R = 0.33.

Figure 3-11(continued). 2024-T3 aluminum (0.09 in. thick) properties.

[Reprinted from Damage Tolerant Design Handbook, 1975, Fig. NAD7, by permission of Battelle, Columbus, Ohio.] [3-12]

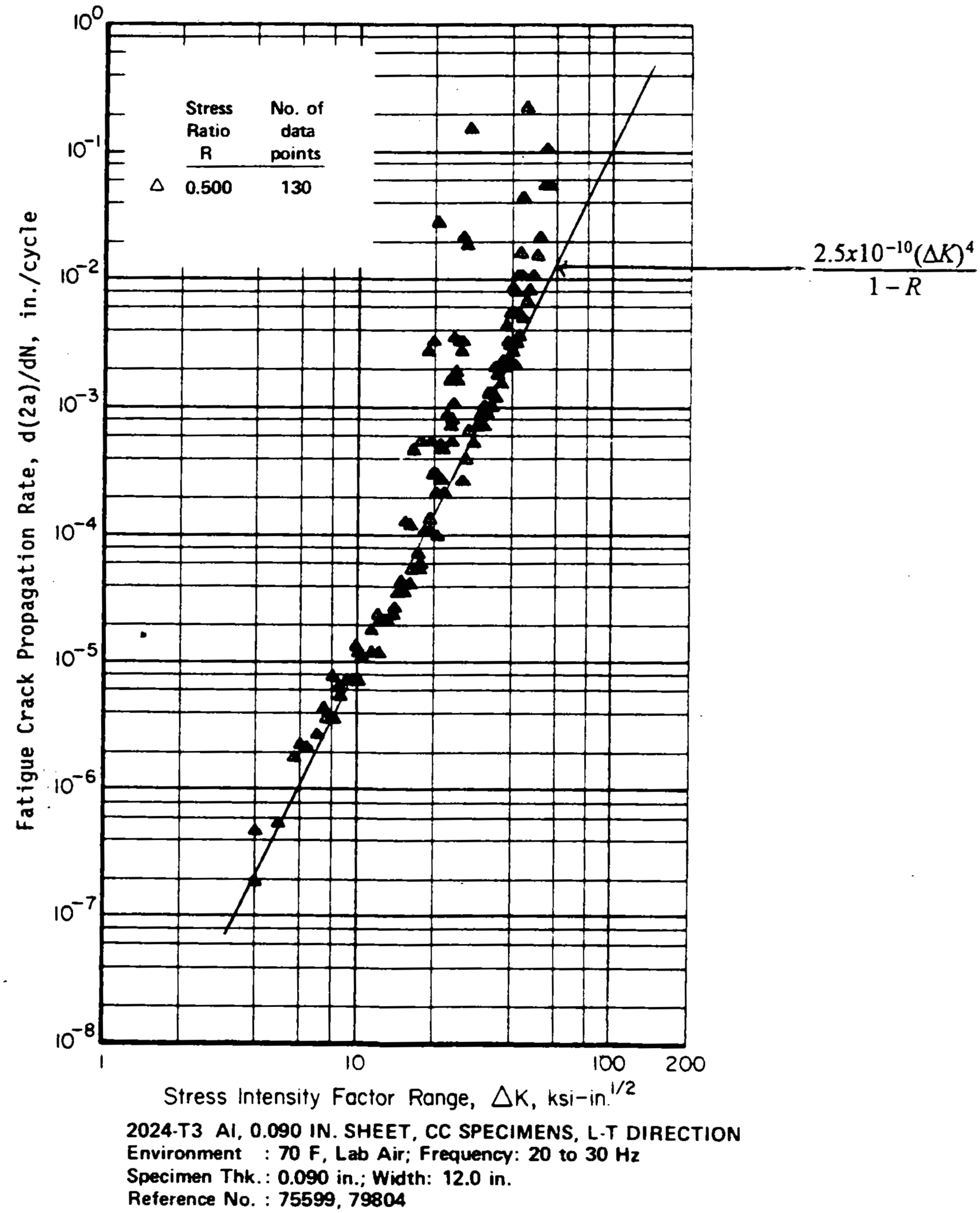

(c) Results for R = 0.5.

Figure 3-11 (continued). 2024-T3 aluminum (0.09 in. thick) properties.

[Reprinted from Damage Tolerant Design Handbook, 1975, Fig. NAD8, by permission of Battelle, Columbus, Ohio.] [3-12]

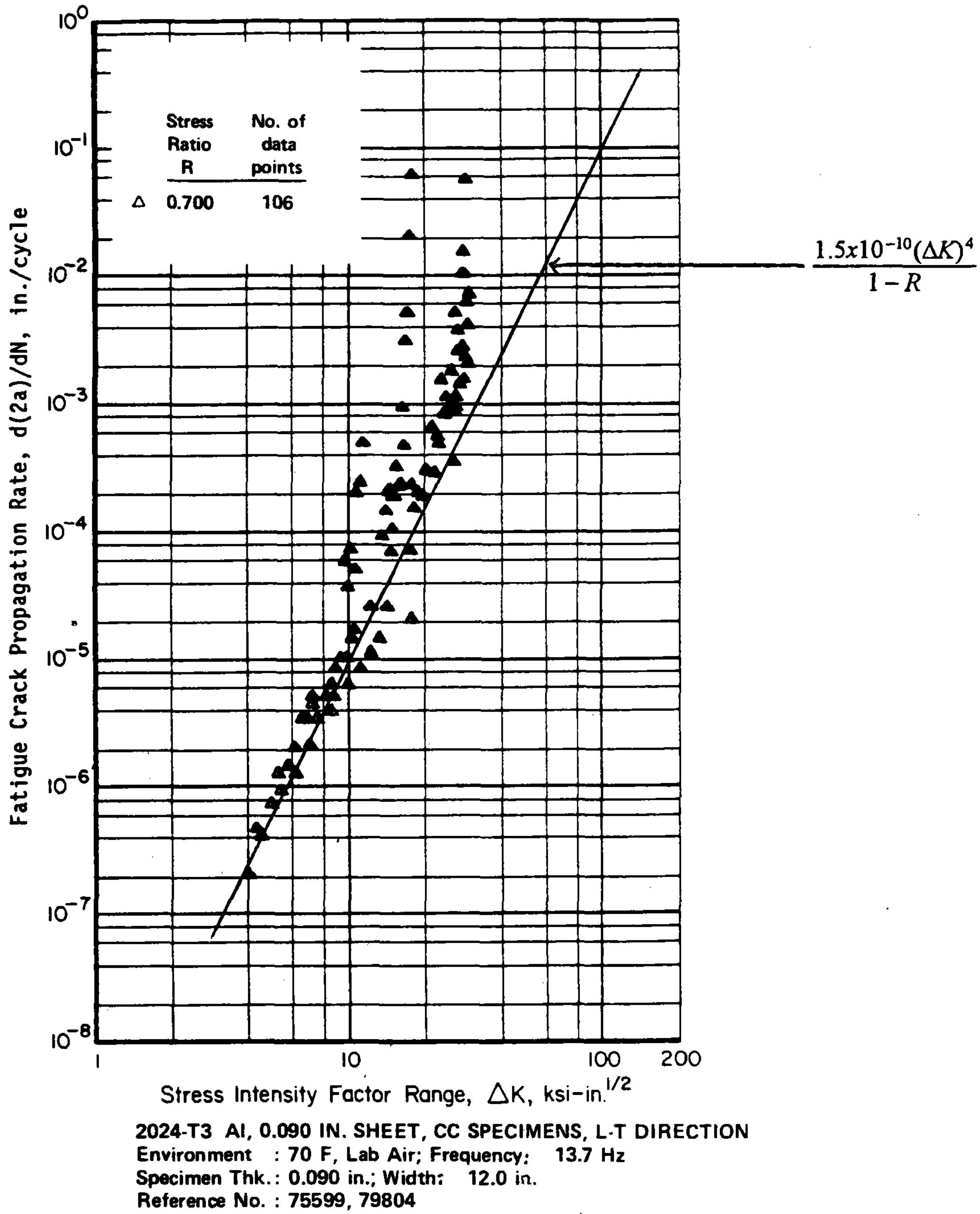

(d) Results for R = 0.7.

Figure 3-11 (continued). 2024-T3 aluminum (0.09 in. thick) properties.

[Reprinted from Damage Tolerant Design Handbook, 1975, Fig. NAD9, by permission of Battelle, Columbus, Ohio.] [3-12]

practical purposes. Again, lines with the rate exponent $m = 4$ have been drawn on each plot, and the table below summarizes the corresponding rate constants C for a Walker equation. In this case, there is no trend which could be used to fit the data with a modified Walker equation, and the values spread too much to justify a group average. In the absence of additional independent data, one might make a conservative judgment by choosing a value between 2.5×10^{-10} and 3×10^{-10} for C.

Summary of rate constants obtained from Figure 3-11.

Stress ratio, R	0.1	0.33	0.5	0.7
$10^{10}C$	9	3.35	2.5	1.5

Another important feature of the data in Figure 3-11(c) through (d) is the appearance of wide scatter bands in the accelerated growth region. If a Forman equation is needed to represent this region for damage tolerance analysis, the curve fit will be unreliable, and the only reasonable choice would be to adopt a very conservative (i.e., low) value for the K_c parameter. This is another example where it would be better to recheck the data source and seek additional independent data.

Figure 3-12 shows a plot of data at $R = 0$ for 1/4-inch thick 2014-T6 sheet from a single test series. Note that there are very few points in the slow growth region, making it difficult to fit the data properly. Two possible lines have been drawn on the plot:[10]

$$\frac{da}{dN} = 5 \times 10^{-12}(\Delta K)^{5.3} \tag{3-17}$$

$$\frac{da}{dN} = 6 \times 10^{-10}(\Delta K)^{4} \tag{3-18}$$

Either equation represents the data well in the region where the data points lie, but either equation can also give unconservative (low) rates outside that region, depending on whether extrapolation is made toward higher or lower ΔK.

[10]Note also that the da/dN rates are plotted, i.e., the correction factor of 2 is not required here.

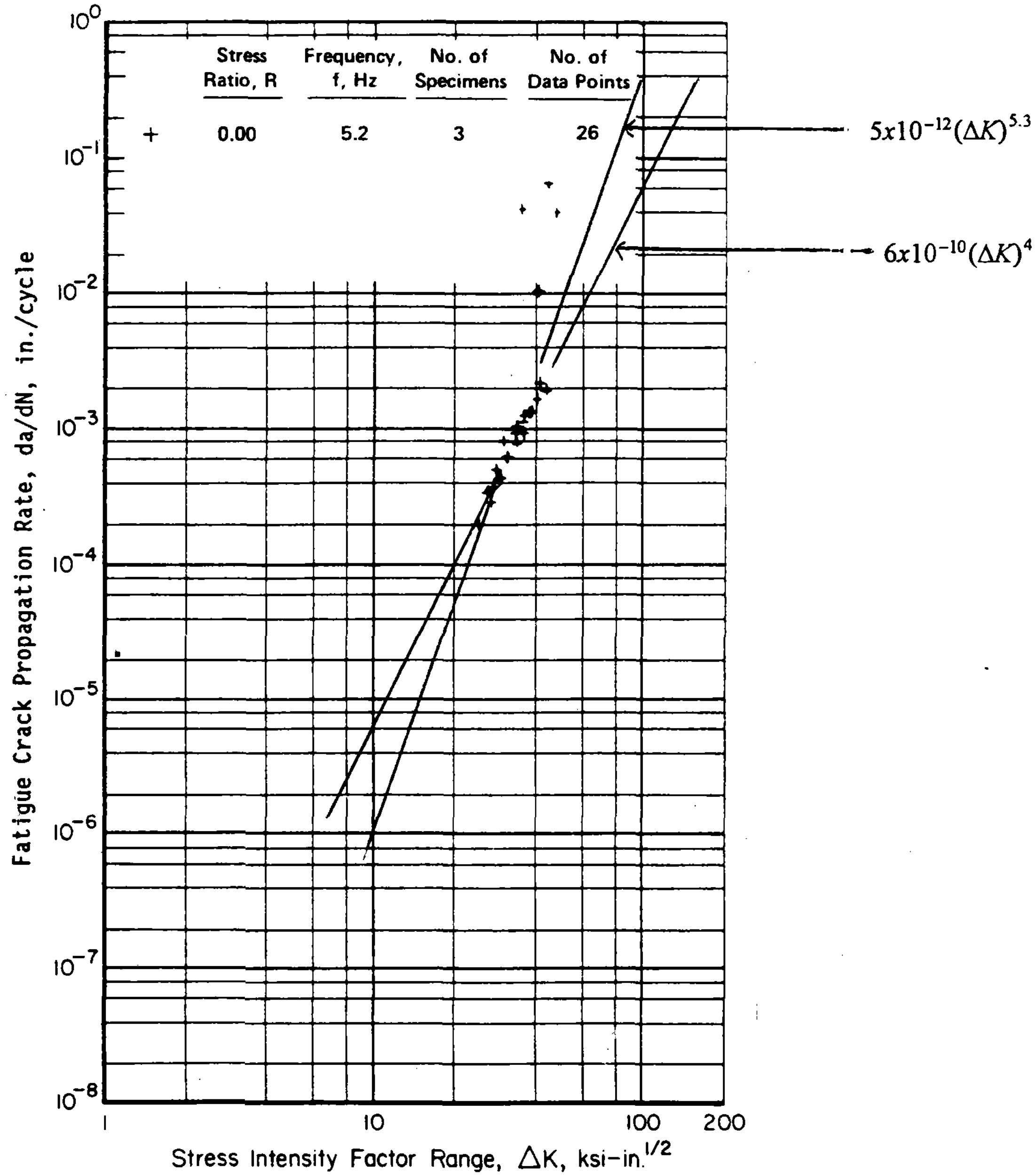

2014-T6 Al, 1.00 IN. ROLLED BAR, CC SPECIMENS, L–T DIRECTION
Environment : 70 F, Lab Air
Specimen Thk.: 0.25 in.; Width: 7.50 in.
Reference No. : 86213

Figure 3-12. 2014-T6 aluminum (0.25 in. thick) properties at R = 0.

[Reprinted from Damage Tolerant Design Handbook, 1975, Fig. NAA5, by permission of Battelle, Columbus, Ohio.] [3-12]

This example shows why it is important to be aware of the general properties expected for an alloy class. Based on aluminum alloys as a class, one would tend to suspect the validity of equation (3-17) because of its abnormal m value. Indeed, comparison with independent data for a different thickness supports the selection of the curve fit based on $m = 4$ (see Figure 3-13).

In the preceding examples, it has sometimes been necessary to compare data from tests of specimens having different thickness in order to expand the base of independent results. Such comparisons are most useful for the purpose of establishing a reliable m value. Conversely, considerable care should be exercised in comparing C values. In particular, one should not attempt to establish C based on a group average from tests of different thickness if the individual values are spread out, since the spread may reflect an actual trend.

Figure 3-14(*a*) illustrates the thickness effect trend in 7475-T651 plate. The rate constant C increases as the thickness increases, until the plate is thick enough to be valid for plane strain fracture. The transition from thin-sheet properties to plane strain properties is reflected by a factor of 3 in the rate constant.

Figure 3-14(*b*) illustrates another important effect: corrosive environments. The dry air test condition (slightly more favorable than ambient or high-humidity air) is generally used as a baseline for comparing environmental effects. The 3.5% salt solution is a generally accepted representation for saltwater and moisture trapped from marine environments. For the alloys shown in the figure, the corrosive medium increases the rate constant by a factor of 2 to 3, relative to the baseline condition. This phenomenon is called corrosion fatigue or environmentally accelerated crack growth. The severity of corrosion fatigue depends strongly on the alloy composition and temper,[11] and tests are essential to establish the magnitude of the effect for a specific alloy. In order to operate, the corrosion fatigue mechanism requires a steady circulation of the fluid medium near the crack tip to replenish the chemicals consumed by environmental

[11] Newer aluminum alloys such as 7175-T73 have been adopted for aircraft construction in part because they are less prone to corrosion fatigue than older alloys such as 7075-T6.

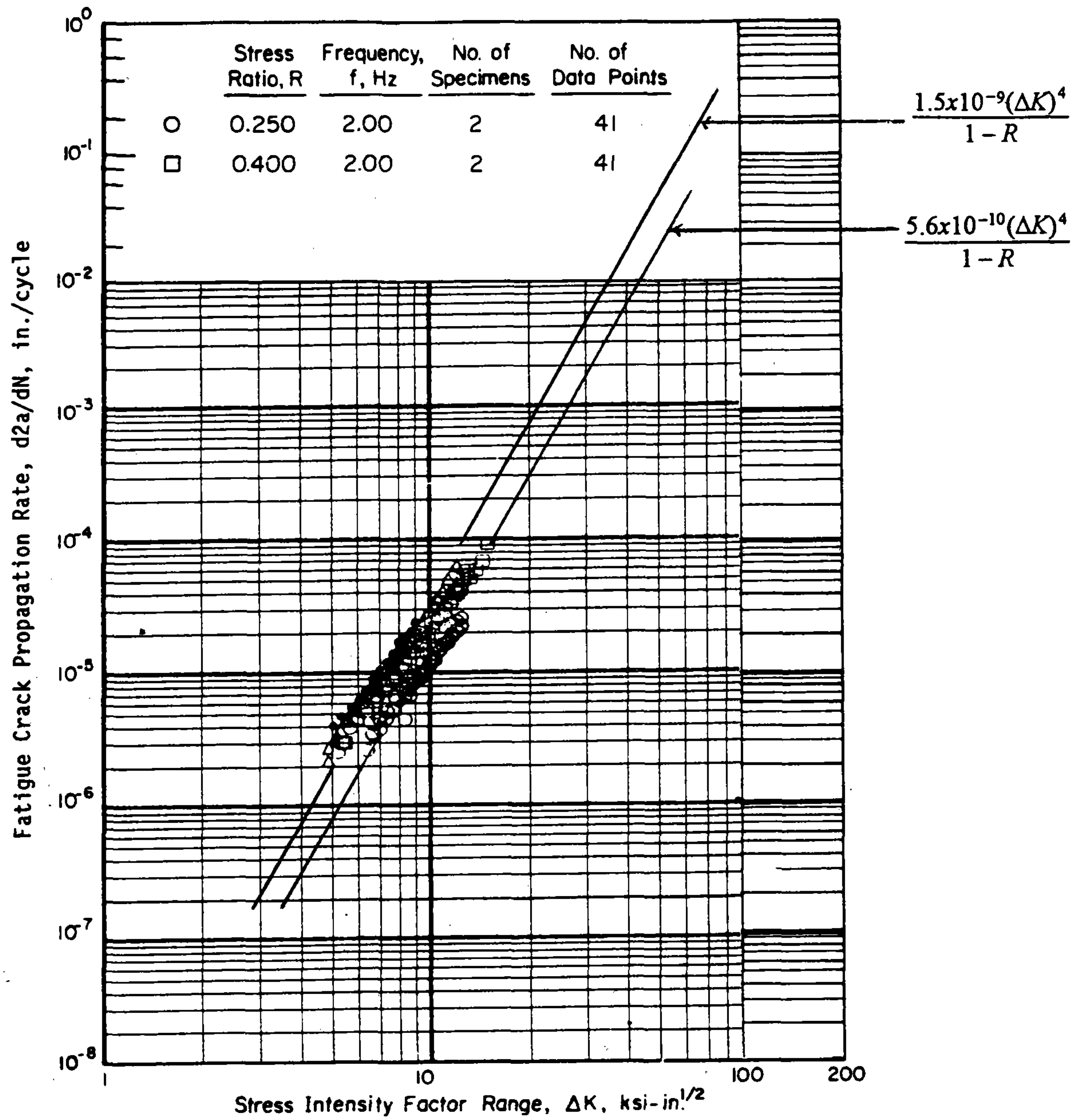

2014-T6 Al, 0.063 IN. SHEET, CC SPECIMEN, L–T DIRECTION
Environment : 70 F, Lab Air
Specimen Thk.: 0.063 in.; Width: 6.00 in.
Reference No. : 86734

Figure 3-13. 2014-T6 aluminum properties for different thickness and stress ratio.

[Reprinted from Damage Tolerant Design Handbook, 1975, Fig. NAA2, by permission of Battelle, Columbus, Ohio.] [3-12]

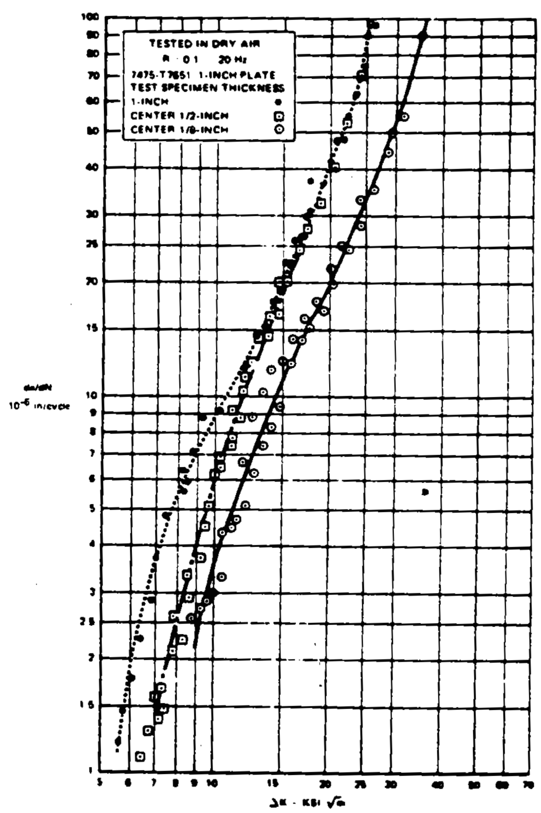

(a) Effect of thickness on FCP behavior of 7475-T651 machined from 1-inch plate and tested in dry air.

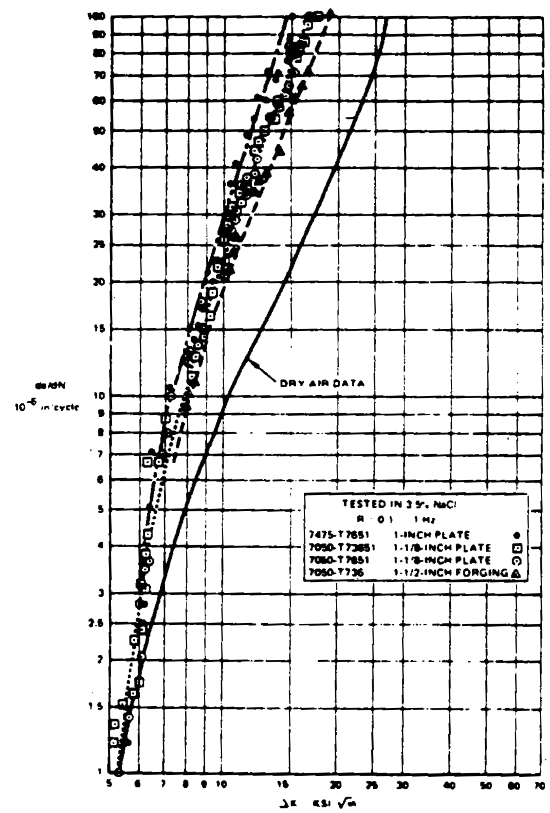

(b) A comparison between the FCP rates in dry air and 3.5% NaC1 solution for aluminum alloys.

FCP: Fatigue Crack Propagation

Figure 3-14. Effects of thickness and environment.

[Reprinted from Damage Tolerant Design Handbook, 1975, Figs. NAW48 and NAW49, by permission of Battelle, Columbus, Ohio.] [3-12]

attack. Thus, corrosion fatigue generally occurs only when the frequency of fatigue loading is below 10 Hz, i.e., when the crack remains open long enough to allow fluid circulation.

All of the examples in this section are based on data plots in English units (in/cycle for crack growth rates and ksi$\sqrt{in}$ for stress intensity factors). However, evaluations in the future may require comparison of English-unit data with results presented in Système Internationale (SI) units. The following conversion factors are useful for this purpose:

Crack growth rate:	1 in/cycle	=	0.0254 m/cycle	
Stress:	1 ksi	=	6.895 MPa	(3-19)
Stress Intensity Factor:	1 ksi $\sqrt{in}$	=	1.099 MPa $\sqrt{m}$	

SI-unit stress intensity factors may also be reported as $MN\text{-}m^{3/2}$, a unit identical to MPa $\sqrt{m}$. Special attention must be paid to conversion of rate constant because the conversion factor depends on the rate exponent m:

$$C\ (\text{English units}) = \frac{(1.099)^m}{0.0254}\, C\ (\text{SI units}) \tag{3-20}$$

3.4 CRACK GROWTH LIFE ESTIMATES

Crack growth life estimates are made for one of two general purposes. Some components are restricted to a single load path for practical design reasons. In such cases, the purpose of the estimate is to demonstrate that the slow crack growth life exceeds the component service life by a suitable factor of safety. Other components have multiple load paths for fail-safety and can tolerate the loss of one path due to fracture. In such cases, estimates are required to establish when to begin periodic inspection and the length of the interval between inspections. Inspection intervals are based on the time required for the largest crack which may escape detection to grow to a size which can be expected to cause a fracture during the next flight. The inspection interval is then established as a fraction of that life, based on a suitable factor of safety. (A companion analysis of fracture resistance is also required to demonstrate that the surrounding structure will be able to contain the failure.) Estimates for the time to first inspection are based on similar calculations except that the initial crack size is based on experience for average production quality. The initial crack size for single-path structure is based on experience for the largest fabrication flaw expected in any one airframe.

Service load and stress spectra must also be defined in order to estimate life. Just as stress spectra are specified in terms of mean and alternating stress pairs for fatigue (see Chapter 1), equivalent spectra for slow crack growth are specified in terms of stress range and ratio pairs (ΔS, R). A complete spectrum for an airframe component usually corresponds to one flight representing a particular mission profile. For convenience, the spectrum may be arranged in "block" form, i.e., with identical pairs ΔS, R grouped together, unless a precise accounting for the effects of cycle order is required. The most widely used procedures for crack growth life estimation are based on direct summing of the crack size increment per cycle or block. The service spectrum is repeated as often as necessary while the calculated crack size is monitored, until the crack has grown from initial to critical size.

The crack size increments are calculated from a *da/dN* equation with parameters chosen to represent the material properties data in the region of values (ΔK, R) contained in the service spectrum. Since the spectrum is specified in terms of (ΔS, R), the ΔK region to be represented must be separately specified, taking into account the stress intensity factor formula(s) used to represent the crack:

$$\Delta K_{\min} = \Delta S_{\min} \sqrt{\pi a_o}\, F(a_o) \tag{3-21}$$

$$\Delta K_{\max} = \Delta S_{\max} \sqrt{\pi a_{cr}}\, F(a_{cr}) \tag{3-22}$$

where $\Delta S_{min}, \Delta S_{max}$ are the minimum and maximum stress ranges in the spectrum, a_o is the initial crack length, and a_{cr} is the critical crack length. The stress intensity factor solutions for various geometries are available in handbooks [2-6 to 2-9]. Some typical examples are also included in Appendix A.

Attention should also be paid to the possibility that the *da/dN* equation might be inadvertently extrapolated beyond its applicable region in the stress ratio variable. If a Walker, modified Walker, Forman or similar equation is used, unconservatively low crack length increments can be projected for cycles that have $R < 0$ (compressive minimum stress), a condition that is not normally tested in the laboratory because of the problems created by grip slack. Spectrum cycles with $R < 0$ should not normally occur except in the ground-air-ground cycle. Nevertheless, it is a good idea to adopt the conservative procedure of preprocessing the spectrum to truncate negative-R cycles to $R = 0$ (and $\Delta S = \Delta S_{max}$ to correspond).[12]

Various procedures with different degrees of numerical approximation are used to calculate spectrum crack growth life. The direct sum (cycle-by-cycle) method has no approximations and serves as a baseline. In this method, the crack length increment Δa is calculated for one stress cycle and the crack length is immediately updated to $a + \Delta a$ for the next cycle. This is also the method most easily adapted to deal with load interaction effects (see Section 3.5).

In the direct sum (block method), the spectrum order is disregarded, and the stress cycles are grouped into blocks $[(n_1, \Delta S_1, R_1); (n_2, \Delta S_2, R_2); \ldots(n_J, \Delta S_J, R_J)]$, i.e., the flight is considered to consist of n_1 cycles with stress range ΔS_1 and stress ratio R_1, etc. Crack length increments Δa_1, Δa_2, etc. are calculated for each block before updating the crack length. Based on the

[12]The pre-processor should also scan for and delete any cycle for which both S_{min} and S_{max} are compressive. Such cycles can occur in taxi loads. They do not actually contribute to crack growth, but leaving them in the spectrum may introduce large errors in calculated crack growth. Compression cycles are insidious because they can have positive R values much greater than 1, leading to an artifact of "negative crack growth."

Walker equation, for example, the sequence of calculations starting from the initial crack length would be as follows:

$$\Delta K_I = \Delta S_1 \sqrt{\pi a_o}\, F(a_o)$$

$$\frac{da}{dN} = \frac{C(\Delta K_I)^m}{1 - R_1}$$

$$a_1 = a_o + n_1\left(\frac{da}{dN}\right) \tag{3-23}$$

$$\Delta K_2 = \Delta S_2 \sqrt{\pi a_1}\, F(a_1)$$

$$\frac{da}{dN} = \frac{C(\Delta K_2)^m}{1 - R_2}$$

$$a_2 = a_1 + n_2\left(\frac{da}{dN}\right)$$

and so forth.

Another variation of this procedure is the direct sum (spectrum) method, in which the crack length is only updated after each full spectrum. In this case, the calculation can be done more efficiently by factoring out the crack length terms as common terms in the expression for Δa for one complete spectrum:

$$\Delta a = C[\sqrt{\pi a}\, F(a)]^m \sum_{j=1}^{J} \frac{n_j(\Delta S_j)^m}{1 - R_j} \tag{3-24}$$

Note that, since the sum of stress spectrum terms does not depend on crack length, it need be calculated only one time.

The direct sum (block) and direct sum (spectrum) methods are prone to lag because the crack growth rate is progressively underestimated in the second and succeeding stress cycles. Updating the crack length at the end of each block or spectrum reduces but does not eliminate the lag. The error may be insignificant over a few flights but may accumulate to an unconservative level if a life in the range of 10^3 to 10^5 flights is being calculated. When these direct sum methods are being used in such applications, the lag error should be evaluated by comparing the results for a typical case with results calculated by the direct sum (cycle-by-cycle) method.

The equivalent S-N curve method is an alternative approach that is useful for checking other results or looking at the effect on life of changes in design or service variables. The basic concept of the method is to use the *da/dN* equation to calculate a constant-amplitude life N_j for each block (n_j, ΔS_j, R_j) in the spectrum. In other words, N_j is the total number of cycles of (ΔS_j, R_j) that would be needed to make the crack grow from the initial length a_o to the critical length a_{cr}, assuming that only (ΔS_j, R_j) cycles are applied. The spectrum crack growth life is then estimated by applying Miner's rule:

$$\text{Life (number of flights)} = \frac{1}{\sum_{j=1}^{J} (n_j/N_j)} \tag{3-25}$$

The equivalent S-N curve method receives its name from its resemblance to the way in which the older safe-life calculations were made, based on S-N fatigue curves. The method was put to widespread use by the Air Force Logistics Command (AFLC) in the 1970s when the Air Force began to apply damage tolerance assessment retrospectively to its existing aircraft fleets. The AFLC adopted the equivalent S-N curve method primarily because it was the easiest way to modify their maintenance scheduling software, which had been based on S-N fatigue life and Miner's rule.

If the constant-amplitude crack growth lives N_j are accurately calculated, then the only numerical error in the equivalent S-N curve method comes from spectrum sequence effects. This source of error can be understood by considering what would happen to a crack subjected to a spectrum consisting of only two stress ranges, one small and one large, with enough cycles of each so that the entire crack growth life only takes one or two spectra. Under these circumstances, that actual crack growth life would be short if the large-amplitude cycles were applied first and long if the small-amplitude cycles were applied first. The equivalent S-N curve method gives an answer between these two extremes. Fortunately, this type of sequence error becomes insignificant in practical cases where the sequence of stress cycles in the spectrum is well mixed and the actual crack growth life ranges from 10^3 to 10^5 flights.

3.4.1 Quick Estimates with Crack Geometry Sums

The equivalent S-N method can also be used to make quick estimates of crack growth life. Estimates are sometimes useful for evaluating the effects of design trade-offs. For example, suppose a crack is modeled by $K = S\sqrt{\pi a}\,F(a)$ and the life to grow the crack from a_1 to a_2 is sought. The material is represented by a Walker equation:

$$\frac{da}{dN} = \frac{C(\Delta K)^m}{1 - R}$$

and the loading is specified as a spectrum $(n_j, \Delta S_j, R_j)$.

Suppose that the total crack growth $a_2 - a_1$ is divided into a large number M of small steps:

$$a_2 - a_1 = M\Delta a$$

The spectrum crack growth rate,

$$\frac{da}{dN} = C\left[\sum_{j=1}^{J} \frac{n_j(\Delta S_j)^m}{1 - R_j}\right][\sqrt{\pi a}\,F(a)]^m = C\Sigma_s[\sqrt{\pi a}\,F(a)]^m$$

can be expressed at each step as follows:

$$\frac{da}{dN} = C\Sigma_S\left[\sqrt{\pi a_1}\,F(a_1)\right]^m \qquad when\ a = a_1$$

$$\frac{da}{dN} = C\Sigma_S\left[\sqrt{\pi(a_1 + \Delta a)}\,F(a_1 + \Delta a)\right]^m \quad when\ a = a_1 + \Delta a$$

$$\frac{da}{dN} = C\,\Sigma_S\left[\sqrt{\pi(a_1 + 2\Delta a)}\,F(a_1 + 2\Delta a)\right]^m \quad when\ a = a_1 + 2\,\Delta\,a$$

and so forth. The time required for each step can then be approximated as Δa divided by the average of the rates at the beginning and end of the step, and the approximate total time is the sum:

$$\text{Life} = \frac{1}{C\Sigma_S}\left[\frac{\Delta a}{2}\left(\frac{1}{\left[\sqrt{\pi a_1}\,F(a_1)\right]^m} + \frac{2}{\left[\sqrt{\pi(a_1 + \Delta a)}\,F(a_1 + \Delta a)\right]^m} + \cdots + \frac{1}{\left[\sqrt{\pi(a_2)}\,F(a_2)\right]^m}\right)\right]$$

The quantity in brackets is called a crack geometry sum, since it contains all of the geometrical effects from the stress intensity factor model, independent of the stress spectrum sum, Σ_S.

3.5 INTERACTION EFFECTS AND RETARDATION MODELS

The cycle order in a stress spectrum can influence crack growth life in a manner similar to its effect on fatigue life. This phenomenon is called load or stress interaction, a term which reflects the fact that the rate of fatigue damage or crack growth during a particular cycle depends not only on the stresses in that cycle, but also on the stresses in earlier cycles. Neither the standard laboratory crack growth rate tests nor the associated rate equations and life estimation methods account for load interaction.

The discovery of load interaction effects in fatigue was quickly followed by a similar finding for crack propagation [3-14, 3-15]. The basic crack growth experiments dealt with the effects of an isolated overload. When an overload was introduced in the midst of a constant-amplitude test, the rate of crack propagation in the succeeding cycles was observed to drop sharply and then to return gradually to the undisturbed value. This particular phenomenon was called retardation; the term was later extended to cover observations of any spectrum crack growth tests in which the measured life was consistently longer than the life estimated by means of one of the basic rate equations.

Retardation models were developed for the adjustment of life estimates to reflect load interaction effects. The first model was based on a purely empirical approach of establishing a scale factor from spectrum test data [3-16]. Since the scale factor was sensitive to changes in the stress spectrum and crack geometry, this model proved to be a poor predictor and soon fell out of favor. It was replaced by the Willenborg model [3-17], in which the first attempt was made to base the retardation adjustment on physical grounds.

The Willenborg model is based on the fact that an isolated overload creates an enlarged plastic zone ahead of the crack tip and the idea that the plastically deformed material reduces the rate of crack growth through the zone. Let S_{OL} denote the peak stress in the overload cycle and define the overload plastic zone size as:

$$r_p = \frac{1}{2\pi}\left(\frac{K_{OL}}{Y}\right)^2 \qquad (3\text{-}26)$$

where K_{OL} is the stress intensity factor corresponding to S_{OL} and Y is the material yield strength. Let Δa be the amount by which the crack has grown from the overload cycle to the current cycle $(S_{\min}, S_{\max})$ and define the effective maximum stress for the current cycle as:

$$S_{\max,\,eff} = S_{\max} - S_{red}\sqrt{1 - (\Delta a/r_p)^2} \qquad (3\text{-}27)$$

where S_{red} is an empirically chosen parameter.[13] The crack length increment for the current cycle is then calculated by substituting the corresponding parameters ΔK_{eff} and R_{eff} in the basic rate equation. This procedure is followed until the crack grows completely through the overload zone ($\Delta a = r_p$) or another overload cycle is encountered. In the second case, a new overload plastic zone is calculated, and the effective stress procedure is restarted.

In spite of its empirical features, the Willenborg model was at least based on a reasonable physical concept, and experience in applying the model showed that it was better able to simulate spectrum retardation than the earlier model. The Willenborg model was also naturally suited for incorporation into computer programs which estimate life by direct summation of crack length increment per cycle or block.

The most realistic retardation model developed to date is the so-called crack closure model proposed by Elber [3-18, 3-19] and further developed by Newman [3-20]. Elber's model is based on the concept of stress reversal in the crack tip plastic zone. Under load, the material in the plastic zone yields in tension and, under some conditions, may reverse its stress state to compression when the load is removed. A residual state of compression near the crack tip can keep the crack closed during the first part of a subsequent loading cycle, until sufficient externally applied tensile stress, S_{OP}, is imposed to re-open the crack. It is then reasonable to argue that the rate of crack growth should be proportional to an effective stress intensity factor range, ΔK_{eff}, associated with the effective stress range $\Delta S_{eff} = S_{\max} - S_{op}$ rather than the nominal range $\Delta S = S_{\max} - S_{\min}$. It can also be argued that Elber's model naturally incorporates the stress ratio effects observed in the standard laboratory tests, and thus, that only a Paris equation need be used to describe basic crack growth rate properties at stress intensities below the accelerated region.

The crack closure model requires a numerical analysis of elastic-plastic stress states in the vicinity of the crack tip. A line-spring model of the plastic zone is used for this purpose, together with the assumption

[13]The reduction stress S_{red} must be specified. It can be established by fitting the model to the results of isolated overload tests.

that the zone is confined to the crack plane [3-20]. The individual spring elements are represented by elastic – perfectly plastic characteristics with a flow stress determined from the material tensile strength properties. The model is subjected to enough cycles to represent the plastic zone residual stress state, and the crack tip is then advanced to represent growth. The spring elements cut by the advancing crack are left in the model to represent the plastic zone wake, and new elements are added to extend the plastic zone itself. Additional cycles are then applied, with the cut elements either in compression or stress-free, to analyze the state of crack closure. At the beginning of each new cycle, a part of the calculation defines the value of S_{OP} for the cycle.

The crack closure model is able to make reasonable predictions of retardation in cracks growing under spectrum loads, but the calculations are much more involved than those required for the Willenborg model. In practice, the computing burden is often reduced by running the crack closure calculation infrequently, on the assumption that any trend of opening stress associated with increasing crack length is slow.

Another practical problem is that the closer calculations are extremely sensitive to small errors in the elastic solution for the distribution of deformations near the crack tip (these deformations control the behavior of the model spring elements). Consequently, good numerical results require either an exact solution or a numerical solution with displacements computed for at least 20 to 30 points within one plastic zone length along the crack surface.

REFERENCES FOR CHAPTER 3

3-1. Paris, P.C. "The Growth of Fatigue Cracks Due to Variation in Load," Ph.D. Thesis, Lehigh University, Bethlehem, PA (1962).

3-2. Clark, W.G., Jr., "Fracture Mechanics in Fatigue," Experimental Mechanics, September, 1971.

3-3. Paris P. and Erdogan, F., "A Critical Analysis of Crack Propagation Laws," Transactions of ASME, p. 528, December 1963.

3-4. Walker, E.K., "The Effect of Stress Ratio During Crack Propagation and Fatigue for 2024-T3 and 7075-T6 Aluminum," Effects of Environment and Complex Load History on Fatigue Life. Spec. Tech. Publ. 462, ASTM (1970), 1-14.

3-5. Orringer, O., Tang, Y.H, Gordon, J.E., Jeong, D.Y., Morris, J.M., and Perlman, A.B. Crack Propagation Life of Detail Fractures in Rails, DOT Transportation Systems Center, Cambridge, MA, DOT/FRA/ORD-88/13, December 1988.

3-6. Forman, R.G., Kearney, V.E. and Engle, R.M., "Numerical Analysis of Crack Propagation in Cyclically Loaded Structures," Trans ASME, J Basic Eng 89, 459-464 (1967).

3-7. Jaske, C.E., Feddersen, C.E., Davies, K.B., Rice, R.C., Analysis of Fatigue, Fatigue-Crack Propagation, and Fracture Data. NASA CR-132332 (November 1973).

3-8. Collipriest, J.E., An Experimentalist's View of the Surface Flaw Problem. North American Rockwell Report SD72-CE-12 (June 1972).

3-9. Collipriest, J.E, and Ehret, R.M., A Generalized Relationship Representing the Sigmoidal Distribution of Fatigue Crack Growth Rates. Rockwell International Report SD74-CE-0001 (March 1974).

3-10. Swift, T., Damage Tolerance Technology , A Course in Stress Analysis Oriented Fracture Mechanics, Phase II, Federal Aviation Administration.

3-11. Rolfe, S.T. and Barsom, J.M., Fracture and Fatigue Control in Structures, Applications of Fracture Mechanics, Prentice Hall, 1987.

3-12. Damage Tolerant Design Handbook, Metals and Ceramics Information Center, Battelle Columbus Laboratories, Columbus, OH. MCIC-HB-01 (1975).

3-13. Courtney, T.H., Mechanical Behavior of Materials, McGraw Hill, 1990 (Data from C.M. Hudson, NASA TN-D5390, 1969).

3-14. Schijve, J., "Effect of Load Sequence on Crack Propagation Under Random and Program Loading," Engineering Fracture Mechanics 5,269-280 (1973).

3-15. Schijve, J.,"Observations on the Prediction of Fatigue Crack Growth Under Variable-Amplitude Loading," Fatigue Crack Growth Under Spectrum Loads, ASTM STP 595, American Society for Testing and Materials, Philadelphia, PA, 1976.

3-16. Wheeler, O.E., "Spectrum Loading and Crack Growth," Transactions of ASME, Journal of Basic Engineering 94, 181-186 (1972).

3-17. Willenborg, J., Engle, R.M., and Wood, H.A., A Crack Growth Retardation Model Using an Effective Stress Concept, AFFDL-TM-71-1-FBR (1971)

3-18. Elber, W., "The Significance of Fatigue Crack Closure," Damage Tolerance in Aircraft Structures, ASTM STP 486, American Society for Testing and Materials, Philadelphia, PA, 1971.

3-19. Elber, W., "Equivalent Constant-Amplitude Concept for Crack Growth Under Spectrum Loading," Fatigue Crack Growth Under Spectrum Loads, ASTM STP 595, American Society for Testing and Materials, Philadelphia, PA, 1976.

3-20. Newman, J.C., Jr., "A Crack Closure Model for Predicting Fatigue Crack Growth Under Aircraft Spectrum Loading," Methods and Models for Predicting Fatigue Crack Growth Under Random Loading, ASTM STP 748 (1981).

☆U.S. GOVERNMENT PRINTING OFFICE:1993-500-428/80041

U.S. DEPARTMENT OF COMMERCE
Technology Administration
National Technical Information Service
Springfield, VA 22161 (703) 487-4650

PB94134335

PO

BIN: M137 10-17-97
INVOICE: 502615
SHIPTO: 1*82522
PAYMENT: CSH*VORNG